Veröffentlichung

MeteoSchweiz
MétéoSuisse
MeteoSvizzera
MeteoSvizra
MeteoSwiss

Autor
Daniel Leuenberger

71 High-Resolution Radar Rainfall Assimilation: Exploratory Studies with Latent Heat Nudging

Veröffentlichung

MeteoSchweiz

Nummer: 71

ISSN: 1422-1381

Autor
Daniel Leuenberger

High-Resolution Radar Rainfall Assimilation: Exploratory Studies with Latent Heat Nudging

Bestelladresse:

Bundesamt für Meteorologie und Klimatologie (MeteoSchweiz)
Office fédéral de météorologie et de climatologie (MétéoSuisse)
Ufficio federale di meteorologia e climatologia (MeteoSvizzera)
Uffizi federal per meteorologia e climatologia (MeteoSvizra)
Federal Office of Meteorology and Climatology (MeteoSwiss)

MeteoSchweiz
Krähbühlstrasse 58
Postfach 514
CH-8044 Zürich

Telefon +41 44 256 91 11
Telefax +41 44 256 92 78
info@meteoschweiz.ch
www.meteoschweiz.ch

Diss. ETH No. 15884

High-resolution Radar Rainfall Assimilation: Exploratory Studies with Latent Heat Nudging

A dissertation submitted to the

Swiss Federal Institute of Technology (ETH) Zürich

for the degree of

Doctor of Sciences

presented by

Daniel Leuenberger

Dipl. Rech. Wiss. ETH
born March 13, 1974
citizen of Bern and Melchnau (BE), Switzerland

accepted on the recommendation of

Prof. Dr. Huw C. Davies, examiner
Dr. Andrea Rossa, co-examiner
Dr. Bruce Macpherson, co-examiner

2005

Dedicated to Petra for letting the sun shine.

Contents

Abstract

Precipitation is certainly one of the most relevant parameters in forecasting the weather, particularly in numerical weather prediction (NWP). Yet, while general NWP has witnessed considerable progress in recent years, quantitative precipitation forecasting (QPF) has shown little to no improvement, especially for the convection-dominated warm season. Reasons for the low performance include model deficiencies, insufficient resolution, and the lack of a properly defined initial model state, particularly related to moisture. Next-generation operational NWP systems will run with grid spacings of around 1 km to circumvent the parametrisation of convection. Such model resolution demands new types of high-resolution observations for initialisation. Doppler radars are able to provide information on precipitation-related phenomena with sufficient spatio-temporal resolution for this purpose. In order to meet the tight time constraints in short-range NWP, very efficient radar assimilation methods will be essential.

Latent Heat Nudging (LHN), a simple scheme for rainfall assimilation, fulfills this requirement. However, despite the LHN's success at larger scales it has not been thoroughly tested in high-resolution applications so far. LHN seeks to adjust the model's buoyancy in order to match the observed precipitation intensity and, therefore, seems to be a natural candidate for the assimilation of convective weather systems. The present thesis attempts to re-evaluate and characterise the LHN scheme within a meso-γ scale NWP model. Emphasis is put on the extent to which LHN can introduce precipitation and small scale flow features into the initial state of a forecast and improve short-range QPF. To this end assimilation simulations of idealised and real severe convective systems are carried out.

In a first study the LHN scheme is applied within the framework of an idealised supercell type storm, providing 'pseudo rainfall observations' for the assimilation simulations. Consideration is given to the model's response to the forcing as well as to the LHN's sensitivity to the uncertainty in the observations and the environment. The scheme is found to successfully capture the dynamical storm structure and reproduce the appropriate rainfall amount in a perfect environment, while a bias in the environmental humidity or wind field can render a successful assimilation difficult. Further, a pronounced sensitivity to the observation insertion frequency points to the need of high update rates for the radar observations, particularly for cases with high propagation velocities.

A second study explores the performance of the LHN scheme in high-resolution simulations of two severe convection cases in Switzerland using rainfall data from the Swiss Radar Network. LHN successfully provides the trigger for convection at the right position and matches the model precipitation closely with that observed during assimilation. A generally realistic response of the model dynamics to the precipitation forcing, such as cold pools and gust fronts, is found during the assimilation period. The performance of free precipitation forecasts strongly varies between the two cases. The stability of the storm environment plays an important role in the evolution of the convection once the LHN forcing is stopped. The LHN scheme appears to be sensitive to the amplitude of the radar-derived precipitation in that it may introduce a too cold and overestimated convective outflow, as well as a phase shift of some 40-50 km of the gustfront during the assimilation period when using rainfall observations with a positive bias of factor 3.

Dividing the observations by that factor partly mitigates these negative effects.

The third study addresses the sensitivity of the LHN scheme to non-rain echoes in the radar data, originating from ground clutter and anomalous propagation of the radar beam. Synthetic non-rain echoes as small as one model pixel can be significantly amplified on a time scale of a few minutes to a couple of hours when assimilated into unstable atmospheres. Non-rain echoes resulting from anomalous propagation of the radar beam in a low-stratus case over Switzerland, by virtue of the usually stable and dry conditions associated, are not conducive to error amplification. However, a strong spurious vertical circulation, along with undesired mixing, may be induced and adversely impact the mesoscale circulation.

Overall, the LHN scheme is found to produce worthwile results on the meso-γ scale. In cases where the model does not develop mesoscale disturbances that lead to the onset of convection, the radar data assimilated with LHN can be of significant value and a positive impact can be observed during the entire lifetime of a convective storm. However, the scheme is found to be vulnerable to errors in the observations, particularly in convective environments, pointing to the need of a careful quality control of the radar data prior to its assimilation.

Zusammenfassung

Niederschlag gehört zu den wichtigsten Elementen der Wetterprognosen, besonders in der numerischen Wettervorhersage. Trotz deren stetigen Verbesserung in den letzten Jahren konnte in der quantitativen Niederschlagsvorhersage (QNV) wenig bis kein Fortschritt verzeichnet werden, insbesondere im Sommer für Niederschläge konvektiver Natur. Gründe für das schlechte Abschneiden der QNV sind unzureichende Modellformulierungen, ungenügende Modellauflösungen und eine mangelhafte Beschreibung des Anfangszustandes, insbesondere der Feuchte. Operationelle numerische Wettermodelle der nächsten Generation werden mit Gitterweiten um 1 km betrieben werden, um eine Parametrisierung der Konvektion zu vermeiden. Für die Initialisierung solcher feinmaschiger Modelle werden zukünftig neue, hochaufgelöste Beobachtungen benötigt. Das Wetterradar liefert Niederschlagsmessungen mit der nötigen zeitlichen und räumlichen Auflösung für diesen Zweck. Da Kürzestfristvorhersagen ausserordentlich zeitkritisch gerechnet werden müssen, sind effiziente Assimilationsschemen für Radardaten absolut unabdingbar.

Latent Heat Nudging (LHN), eine einfache Methode zur Assimilation von Niederschlag, erfüllt diese Anforderung. Trotz der erfolgreichen Anwendung in grösserskaligen Modellen ist die Eignung des Schemas in feinmaschigen Modellen noch nicht genau untersucht worden. LHN wirkt auf den diabatischen Temperaturterm in der prognostischen Modellgleichung und könnte deshalb für die Assimilation von konvektiven Systemen geeignet sein. Ziel der vorliegenden Arbeit ist es, die LHN Methode in einem meso-γ skaligen Wettermodell neu zu evaluieren und zu charakterisieren. Konkret wird untersucht, inwiefern das Schema Niederschlag und feinskalige Strömungsmuster in den Anfangszustand einer Modellvorhersage einbringen und damit die kurzfristige Niederschlagsvorhersage verbessern kann. Zu diesem Zweck werden numerische Assimilations-Simulationen von idealisierten und realen konvektiven Systemen gerechnet.

In einer ersten Studie wird das LHN Schema mit künstlichen Niederschlagsbeobachtungen aus einer Superzellen-Simulation angetrieben. Die Reaktion der Modelldynamik auf die Assimilation und die Anfälligkeit des LHN Schemas auf Fehler in den Beobachtungen und dem atmosphärischen Grundzustand in der Umgebung der Konvektion werden untersucht. Die Resultate zeigen, dass die LHN Methode in einem perfekten Grundzustand die Struktur der Superzelle erfolgreich aufnimmt und den 'beobachteten' Niederschlag mit hoher Genauigkeit wiedergibt. Ein systematischer Fehler in der Feuchte oder dem Wind des Grundzustands kann hingegen zu einer Verschlechterung der Assimilation führen. Weiter zeigt sich, dass die LHN Methode in diesem Beispiel eines schnellen, kohärenten konvektiven Systems, sehr sensitiv auf den zeitlichen Abstand der assimilierten Beobachtungen reagiert.

In einer zweiten Studie wird das LHN Schema in Fallstudien von zwei konvektiven Gewittern in der Schweiz angewendet und mit Niederschlagsbeobachtungen vom Schweizerischen Radarverbund angetrieben. In beiden Fällen löst die Assimilation die Konvektion am richtigen Ort aus und ist in der Lage, den Modellniederschlag in guter Übereinstimmung mit den Beobachtungen anzupassen. Während der Assimilation erzeugt das Modell eine generell realistische bodennahe Strömung, z.B. das Ausfliessen kalter Luft aus der Gewitterzelle oder damit verbundene Windböen. Die Qualität der anschliessenden Niederschlagsvorhersage variert stark zwischen den beiden Fällen, wobei die Stabilität des

Sturmumgebung eine wichtige Rolle für die weitere Sturmentwicklung in der freien Vorhersage spielt. LHN reagiert sensitiv auf Fehler in den Beobachtungen. So kann es einen zu kalten und zu starken Kaltluftausfluss aus der konvektiven Zelle erzeugen, und verschiebt letzteren um etwa 40-50 km stromabwärts, wenn um einen Faktor von drei überschätzte Niederschlagsmessungen assimiliert werden. Eine Korrektur um diesen Faktor vermag diese negativen Erscheinungen teilweise zu beheben.

Die dritte Studie befasst sich mit der Sensitivität des LHN Schemas auf Radarechos, die nicht von Niederschlag erzeugt werden, wie Bodenechos oder Signale von anomaler Propagation des Radarstrahls (Anaprop). Künstlich erzeugte Signale von nur 1x1 Pixel Grösse können während der Assimilation in eine instabile Atmosphäre durch das Modell signifikant verstärkt werden. Dies kann innert weniger Minuten bis ein paar Stunden geschehen. Anaprop Echos treten in der Schweiz vorwiegend in Situationen mit starker thermischer Inversion (Hochnebellagen) auf. Da solche Fälle meistens mit Subsidenz und trockenen oberen Luftschichten verbunden sind, neigen sie nicht zur Verstärkung der Fehler in den Radardaten. Jedoch können in solchen Situationen starke Vertikalwinde auf Gitterpunktskala erzeugt werden, was eine ungewünschte Durchmischung der unteren Luftschichten zur Folge haben kann.

Zusammenfassend kann gesagt werden, dass die LHN Methode auf der meso-γ Skala beachtliche Resultate liefert. In Fällen, in denen das Modell keine mesoskaligen Störungen entwickelt, die zur Auslösung von Konvektion führen, können die mit LHN assimilierten Niederschlagsbeobachtungen von grossem Wert sein und einen positiven Einfluss auf die Niederschlagsvorhersage haben, der über die gesamte Lebensdauer eines konvektiven Systems hinausreicht. LHN scheint jedoch anfällig auf Fehler in den Radardaten zu sein, besonders in instabilen Wetterlagen. Dies deutet auf die Notwendigkeit einer restriktiven Qualitätskontrolle der Daten vor der Assimilation hin.

Résumé

Les précipitations sont parmi les paramètres les plus critiques de la prévision du temps, particulièrement lorsque celle-ci est basée sur la simulation numérique de l'évolution de l'atmosphère. Bien que cet outil aie fait de considérables progrès ces dernières années, la qualité de la prévision quantitative des précipitations (QPF), particulièrement des effets convectifs pendant la saison chaude, n'a elle que peu ou pas évolué. Les déficiences des modèles numériques, une résolution spatiale trop faible, et une connaissance trop imprécise des conditions initiales, en particulier de l'humidité, en sont la cause. Les modèles numériques opérationnels de la prochaine génération seront calculés avec une maille kilométrique afin de contourner le problème de la paramètrisation de la convection. De nouveaux types d'observations, offrant une résolution spatio-temporelle suffisamment élevée, seront requis pour initialiser ces modèles. Le radar doppler est un instrument qui fourni des informations liées aux précipitations satisfaisant ces besoins. Les contraintes temporelles sévères d'un système numérique de prévisions à court terme nécessitent une méthode très efficace pour assimiler ces données radars.

Le Latent Heat Nudging (LHN), une méthode simple permettant d'assimiler les précipitations, satisfait les contraintes précédemment mentionnées. Cependant, malgré les succès enregistrés à grande échelle, une étude systématique à échelle fine n'a encore jamais été entreprise. Cette méthode, qui ajuste la flottabilité du modèle en essayant de reproduire les précipitations observées, est un candidat naturel pour assimiler des systèmes convectifs. L'étude ici présentée cherche à caractériser le LHN dans le cadre d'un modèle numérique à méso- échelle. L'accent est mis sur la capacité de cette méthode à introduire des précipitations et des structures fines du courant atmosphérique dans les conditions initiales, ainsi que sur l'amélioration des prévisions à court terme des précipitations quantitatives. Dans ce but, des simulations de systèmes convectifs sévères, idéalisés et réels, sont effectuées.

Dans une première phase le LHN est appliqué à un orage super cellulaire idéalisé; la simulation de ce phénomène produit des observations virtuelles qui sont utilisées ensuite dans des expériences d'assimilation. La réponse du modèle aux contraintes ainsi introduites et la sensibilité des résultats aux incertitudes des observations et de l'environnement sont analysées. Dans un environnement parfait la méthode est capable de reproduire correctement la structure dynamique de l'orage et la quantité de précipitations, alors qu'un biais du champ de vent ou d'humidité rend difficile une assimilation correcte. En outre, une sensibilité élevée des résultats à la fréquence d'insertion des observations souligne l'importance d'une mise à jour très fréquente des données radars, particulièrement pour des situations où les structures concernées se déplacent rapidement.

Une deuxième phase de cette étude évalue les performances du LHN pour des simulations à échelle fine de deux cas de convection sévère en Suisse, en utilisant les précipitations observées par le réseau radar suisse. En mode assimilation, la méthode est capable de simuler le déclanchement de la convection à l'endroit correct et de bien reproduire les précipitations. De même, une réponse réaliste de la dynamique du modèle est observée, en particulier la création de lacs d'air froid et de lignes de pointes de vent. En mode prévision, la performance des précipitations varie fortement entre les deux cas. La stabilité de l'environnement joue un rôle important dans l'évolution de l'orage une fois que

la contrainte du LHN est relaxée. Le schéma semble aussi être sensible à l'amplitude des précipitations observées; dans le cas d'assimilation d'observations souffrant d'un biais positif élevé, un facteur 3, l'on observe un écoulement convectif exagéré et trop froid, ainsi qu'une erreur de phase de quelques 40-50km de la ligne de pointes de vent. Ces résultats sont améliorés lorsque l'amplitude des observations est corrigée.

Une dernière partie de cette étude se concentre sur la sensibilité du LHN aux échos radars non produits par des précipitations, provenant de la propagation anormale du faisceau ou d'échos fixes. Des échos radars synthétiques, de la taille d'un élément de maille du modèle, peuvent être en l'espace de quelques minutes à quelques heures significativement amplifiés, lorsque assimilés dans une atmosphère instable. Par contre, des échos résultants de la propagation anormale du faisceau dans un cas de stratus sur le Plateau Suisse, du fait de la sécheresse et de la stabilité de l'atmosphère, ne conduisent pas à une amplification des erreurs. Cependant, une forte circulation verticale, associée à un mélange indésirable, peut être induite et affecter de manière négative la circulation à méso échelle.

Globalement cette étude montre que le LHN est une méthode valable à l'échelle méso-γ. Les observations radars assimilées par le LHN peuvent avoir une influence significative, lorsque le modèle numérique ne produit pas les perturbations à méso-γ échelle capables de déclancher la convection, et un impact positif sur tout le cycle de vie d'un système convectif est observé. Cependant cette méthode est vulnérable aux erreurs d'observations, en particulier dans un environnement convectif, soulignant l'importance d'un contrôle soigneux de la qualité des observations radars avant leurs assimilations.

Riassunto

La precipitazione è senz'altro una delle grandezze più rilevanti ai fini della previsione meteorologica ed in particolare della previsione numerica (NWP). Tuttavia, in generale, nonostante negli ultimi anni la previsione numerica abbia compiuto notevoli progressi, la previsione quantitativa della precipitazione non ha registrato grandi miglioramenti, specialmente per quanto riguarda la stagione estiva, dominata dai fenomeni convettivi. Tra i motivi ci sono le carenze e l'insufficiente risoluzione dei modelli nonché il problema della definizione di uno stato iniziale del modello, in particolare per quanto riguarda l'umidità. I futuri sistemi operativi di previsione numerica utilizzeranno griglie con spaziature dell'ordine di 1 km al fine di aggirare il problema della parametrizzazione della convezione. Una tale risoluzione dei modelli richiede, per l'inizializzazione, nuove tipologie di osservazioni ad alta risoluzione. I radar Doppler sono in grado di fornire informazioni sui fenomeni precipitativi con un dettaglio spaziale e temporale adatto a questo scopo. Al fine di soddisfare i vincoli temporali molto stretti della previsione numerica a breve termine, si renderà indispensabile l'approntamento di metodi efficienti di assimilazione dei dati radar.

A questo scopo, il Latent Heat Nudging (LHN), un semplice schema di assimilazione della precipitazione, costituisce un valido strumento. Tuttavia, nonostante il successo dello schema LHN su grande scala, esso non è ancora stato accuratamente testato nelle applicazioni ad alta risoluzione. LHN funziona cercando di aggiustare la "buoyancy" del modello in modo da allinearsi all'intensità di precipitazione osservata e appare pertanto, in definitiva, come il naturale candidato per l'assimilazione dei sistemi convettivi. Lo scopo della presente tesi è quello di ri-valutare e caratterizzare lo schema LHN in un modello numerico a scala meso-γ. Particolare attenzione viene dedicata al modo in cui LHN può introdurre la precipitazione e le caratteristiche del flusso su piccola scala nello stato iniziale di una previsione e migliorare la previsione quantitativa a breve termine. A questo fine si sono eseguite delle simulazioni di assimilazione sia di sistemi convettivi idealizzati che reali.

Nel primo studio lo schema LHN viene applicato nell'ambito di un sistema convettivo idealizzato a supercella, che fornisce le pseudo-osservazioni di precipitazione necessarie per l' assimilazione. Particolare attenzione è dedicata alla risposta del modello alla forzante esterna così come alla sensibilità di LHN all'incertezza delle osservazioni e delle condizioni ambientali. Nel caso di condizioni perfette, si è trovato che lo schema riesce a catturare la struttura dinamica del sistema convettivo e a riprodurre l'effettiva quantità di precipitazione, mentre una deviazione (bias) nell'umidità ambientale o nel campo di vento possono rendere problematica una successiva assimilazione. Inoltre, una pronunciata sensibilità alla frequenza di inserimento delle osservazioni suggerisce la necessità di un aggiornamento frequente delle osservazioni radar, specie nei casi con elevata velocità di propagazione.

Il secondo studio esplora le prestazioni dello schema LHN nella simulazione ad alta risoluzione di due casi di convezione intensa in Svizzera, utilizzando i dati radar di precipitazione della rete nazionale. Lo schema LHN fornisce correttamente la posizione di innesco della convezione e, durante l'assimilazione, allinea la precipitazione del modello a quella osservata. Inoltre si è trovato che durante l'assimilazione, la dinamica del modello

risponde realisticamente, in termini di cold poolsä "gust fronts", alla forzante data dalla precipitazione. La qualità della previsione varia notevolmente da un caso all'altro. Una volta arrestato lo schema LHN, l'evoluzione della convezione dipende fortemente dalla stabilità ambientale. Lo schema LHN si è rivelato essere sensibile all'intensità della precipitazione radar in quanto produttore di un öutflowconvettivo troppo forte e freddo, così come di uno spostamento di circa 40-50 km del "gustfront"durante il periodo di assimilazione in concomitanza con l'utilizzo di osservazioni di precipitazione con un fattore di bias pari a 3. Dividendo le osservazioni per un quantità pari a tale fattore si mitigano parzialmente questi effetti indesiderati.

Il terzo studio investiga la sensibilità dello schema LHN agli echi radar artificiali (cioè non dovuti a precipitazione), prodotti dal clutter di terra e dalla propagazione anomala del fascio radar. Echi di questo tipo della dimensione di un pixel possono essere significativamente amplificati, su una scala temporale che va da pochi minuti a un paio d'ore, se assimilati in condizioni di atmosfera instabile. Gli echi artificiali derivanti invece dalla propagazione anomala, relativi a una situazione con strati nuvolosi bassi sul territorio svizzero, in virtù delle condizioni generalmente stabili e asciutte associate non portano a una amplificazione dell'errore. Tuttavia possono essere indotti una forte circolazione verticale spuria e un rimescolamento indesiderato che vanno ad influenzare negativamente la circolazione a mesoscala.

Nel complesso, si è trovato che lo schema LHN produce dei buoni risultati sulla scala meso-γ. Nei casi in cui il modello non sviluppa dei disturbi a mesoscala che portano all'innesco della convezione, l'assimilazione dei dati radar in LHN può essere di notevole valore e avere un impatto positivo sull'intero tempo di vita del sistema convettivo. Tuttavia lo schema appare vulnerabile agli errori nelle osservazioni, specialmente nelle situazioni favorevoli alla convezione, un fatto che suggerisce la necessità di un accurato controllo di qualità dei dati radar preliminarmente all'assimilazione.

Chapter 1

Introduction

Precipitation constitutes one of the most important meteorological parameters of our habitat and influences life in various ways. As an elementary component of the hydrological cycle it provides fresh water and soil moisture which determines the vegetation cover and thus the basis for agriculture. On the other hand, heavy precipitation events carry the potential for large damage in the form of flash floods, landslides, avalanches, hail and strong wind gusts. An improved understanding and accurate forecasts of precipitating weather systems is thus not only of scientific interest but also of high socio-economic importance. Despite large efforts to improve the skill of quantitative precipitation forecasts (QPF) progress has been slow in recent years, especially for the warm season which is dominated by convection (Ebert et al., 2003; Fritsch and Carbone, 2004; Weckwerth et al., 2004).

1.1 The challenge of QPF

Weather forecasts today are increasingly based on Numerical Weather Prediction (NWP) models which integrate the dynamical and thermo-dynamical atmospheric equations to obtain a future picture of the atmosphere. Precipitation is usually only poorly represented in such models because its formation and evolution is highly complex and nonlinear and occurs on scales that are several orders of magnitude smaller than the size of a numerical grid box. Parametrisation schemes are therefore used to treat subgrid scale processes such as precipitation, but these are somewhat simplified for reasons of computational efficiency or the lack of knowledge about the true characteristics of those processes. A second obstacle to QPF is the difficulty to specify accurate initial conditions of moisture in NWP models. Atmospheric water in all its phases is highly variable in time and space and there is currently a general absence of operational observing systems providing a three-dimensional humidity distribution with sufficient spatial and temporal resolution to capture convection (Weckwerth et al., 2004).

Convective events are particularly challenging to predict because of their small scale, short lifetime and non-linear, chaotic behaviour, inherently limiting their predictability (see e.g. Walser et al., 2004). An example of summertime convection in central Europe is portrayed in Fig. 1.1. Several towers of deep convection formed, both north and south of the Alps. They form seemingly random over structured terrain, as well as over flat regions. Since convection is the dominant form of summer precipitation and carries the potential for large damage, improvements in its prediction are of particular importance.

Convection is governed by mesoscale processes on scales that cannot be properly resolved by today's operational NWP models. Thus, as noted earlier, cumulus parametri-

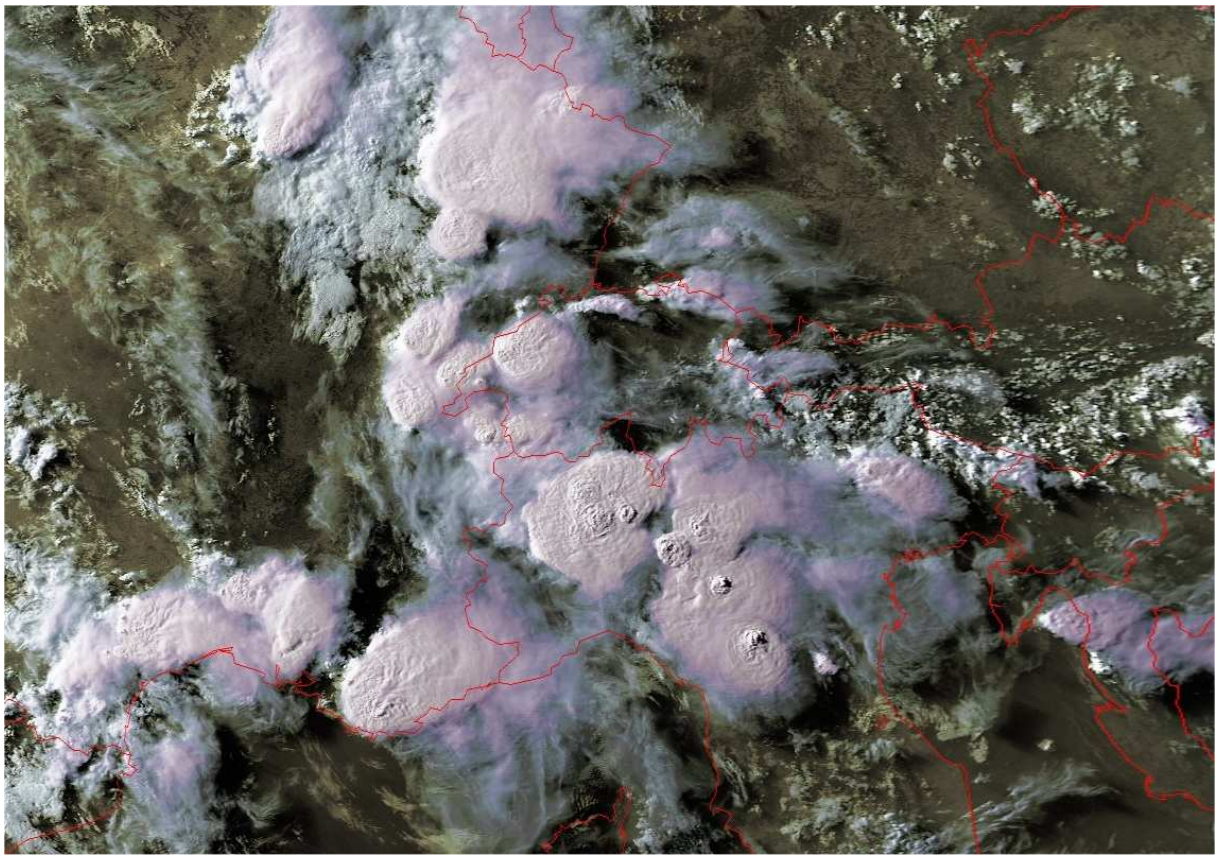

Figure 1.1: Towers of deep convection forming over central Europe on the evening of 3 August 2004, observed by a polar orbiting NOAA satellite. Copyright 2004 RSGB, University of Bern and NOAA.

sation schemes must be used to represent their interaction with the resolvable flow. Such schemes have inherent limitations (Fritsch and Carbone, 2004) and there is growing evidence that QPF skill can be higher with high resolution and without convection parametrisation (e.g. Ducrocq et al., 2002; Zängl, 2004b). Explicit simulation of convection calls for increased model resolution. Weisman et al. (1997) argued that a grid size of 4 km is required to resolve the bulk properties of explicitly simulated organised deep convection, while Bryan et al. (2003) demonstrated that even with a grid spacing of 125 m such simulations do not show convergence. An increase in model resolution is also driven by the need for an accurate representation of the topography, which is crucial for the prediction of the dynamical flow and precipitation in the vicinity of structured terrain (e.g. Benoit et al., 2002; Cosma et al., 2002).

Many National Weather services have recognised that an increased model resolution is a prerequisite for improved QPF and design their next-generation, meso-γ scale[1] NWP systems accordingly (e.g. Doms and Förstner, 2004; Bouttier, 2003; Michalakes et al., 2001). In the next years, computational resources will allow for several very short-range forecasts (up to, say, 18 hours) per day using grid-spacings of O(1 km) . As the forecast range decreases, the importance of well defined initial conditions will increase. They

[1]meso-γ denotes horizontal length scales from $2 - 20$ km, where meso-β scales from $20 - 200$ km, as proposed by Orlanski (1975)

need to properly represent both the large-scale flow and also mesoscale disturbances. The formation and evolution of convection, for example, depends on the interaction between synoptic-scale flow, responsible for the development of an unstable environment and mesoscale processes such as orographic lifting or low-level convergence related to fronts or thunderstorm outflow, acting as a trigger for the convection (e.g Huntrieser, 1995, and references therein). Thus it is clear that both ingredients need to be correctly represented in the model for a successful precipitation forecast.

Increased model resolution calls for new types of high-resolution observations, both for initialisation and verification purposes, since the modelled scales are well below the spatial and temporal scales resolved by conventional observing systems comprising of surface and radiosonde networks. Since the advent of weather radar in the 1950's it is possible to observe precipitation related phenomena within a range of over hundred kilometres and with high spatial (O(1 km)) and temporal (O(1 min)) resolution, unachievable by any other meteorological observing system. Thus, radar has become the most important tool in precipitation research and prediction and is likely to become an important complement to conventional observations in the assimilation into and verification of future NWP models. The effort in bringing together radar and models is reflected in many research actions around the world, one being the COST 717 Action 'On the Use of Radar Information in Hydrological and NWP Models' (Rossa, 2000).

An example where radar data is able to improve upon the simulation of a severe convective event is shown in Fig. 1.2. An intense precipitation cell is observed by the Swiss Radar Network over central Switzerland (panel a). Obviously, this cell is not captured by the Alpine Model of MeteoSwiss in a high-resolution setup (panel b). Previewing the present study, note that radar assimilation, in this case, is able to provide the convection trigger and introduces precipitation well in line with the observations after six hours (panel c). This case will be discussed in more detail in chapter 4 of this thesis. Indeed the potential of using radar data in high-resolution convection simulations for the improvement of short-term QPF will be at the core of the subsequent analyses.

1.2 Recent interest in rainfall and radar assimilation

Assimilation of meteorological observations can be described as the process through which all the available information is used in order to estimate as accurately as possible the state of the atmospheric flow (Talagrand, 1997). Long before the availability of computers, meteorologists had been performing what was called the analysis of the meteorological situation, which consisted in correcting every day, with the new observations, the forecast from the previous day, available as meteorological maps. Richardson (1922), performing the historical first numerical [2] weather forecast, used hand-interpolated analyses as initial conditions. As these were not balanced, fast moving gravity waves introduced a large error in the predicted surface pressure tendency. This example illustrates the importance of well posed initial conditions in NWP. As computers became available the need of automated *objective analyses* was recognised. First algorithms included spatial polynomial interpolation of the available observations to regular grids. Since the number of degrees of freedom of the model is much larger than the available observations, additional information in the form of a *background* (or first guess) had to be supplied for the preparation of the analysis. Typically this background is taken from a short model forecast started

[2] the computations were done by hand, since computers were not available at this time!

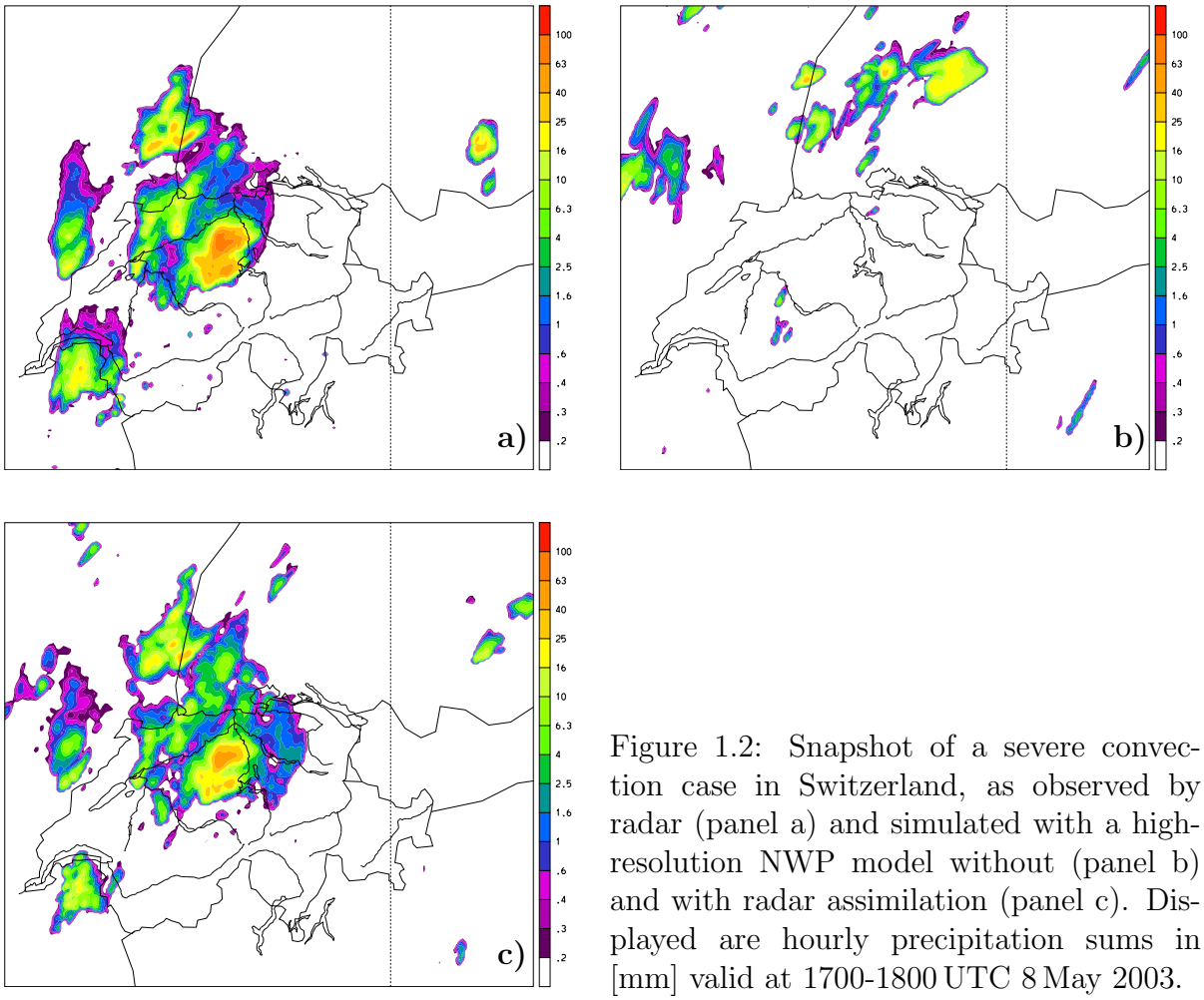

Figure 1.2: Snapshot of a severe convection case in Switzerland, as observed by radar (panel a) and simulated with a high-resolution NWP model without (panel b) and with radar assimilation (panel c). Displayed are hourly precipitation sums in [mm] valid at 1700-1800 UTC 8 May 2003.

from a previous analysis, resulting in the *assimilation cycle*. For a more in-depth review of the history of data assimilation the reader is referred to Daley (1991) or Kalnay (2003).

Research in data assimilation has been primarily concerned with the objective analysis of the dynamic model variables, such as temperature, wind and geopotential, since these are of primary importance for running a numerical forecast. QPF, however, is directly linked to the model's water cycle. Lack of initialisation for the hydrological variables results in the so-called spin-up (spin-down) problem i.e. precipitation is too weak (high) and not in balance with the evaporation during the the first hours (or days) into the forecast. Diabatic heating constitutes a major energy source in the tropics and plays an important role in the intensification of extratropical cyclones (e.g. Rossa, 1995). Therefore, and since temperature (or potential temperature) is a primary model variable, latent heating has been frequently used for the diabatic initialisation.

Global and meso-β scale models

The first attempts to incorporate rainfall observations into a model were undertaken in the tropics where the spin-up problem is particularly serious because of sparse observations. Fiorino and Warner (1981) introduced diabatic temperature tendencies in the model based upon satellite rainrate estimates in a forecast of a tropical cyclone. They made use of the assumption that the surface rainfall rate is proportional to the vertically integrated latent heating. Their method can be regarded as the prototype of **Latent**

Heat Nudging (LHN), though the profiles were not nudged (relaxed) but simply specified in the model. Wang and Warner (1988) used the same method but with rainrates derived from radar and gauges. They reported a dramatic improvement of QPF during the first three to four hours in a case of heavy convective rainfall in the US. Chang and Holt (1994) and Manobianco et al. (1994) using satellite derived rainrates, applied LHN to a case of extratropical cyclogenesis and were able to improve the location and intensity of the cyclone's surface pressure as well as the precipitation forecast. The positive impact was apparent up to 12 hours. Jones and Macpherson (1997) adopted the LHN method for use with radar data and noticed an improvement of the QPF in the first six to nine hours into the forecast. Operational experience revealed cases where the impact lasted up to 18 hours (Macpherson, 2001).

Another early approach to diabatic initialisation is **physical initialisation** (Krishnamurti et al., 1991, 1993). Humidity profiles consistent with satellite-derived rainfall rates were determined by inverting the cumulus parametrisation scheme and nudged during the pre-forecast time. The authors found a large reduction of the spin-up in the model and a positive impact on QPF up to 5 days.

The pioneering studies by Zupanski and Mesinger (1995), Zou and Kuo (1996) and Guo et al. (2000) gave an indication that precipitation data can be assimilated with the four dimensional variational (**4D-Var**) assimilation scheme. Guo et al. (2000) assimilated various types of observations for a squall-line case using the MM5 4D-Var system and found that assimilation of precipitation helped improve the predicted squall-line structure but reported a rapid loss of the assimilated signal in the free forecast. At the European Centre for Medium-Range Weather Forecasts (ECMWF) the aim is to assimilate precipitation via direct satellite radiances of cloud- and rain-affected portions of the atmosphere (Holm et al., 2002). Steps towards this goal include the 4D-Var assimilation of Total Column Water Vapour (TCWV) retrieved from TRMM (Tropical Rainfall Measuring Mission) TMI (TRMM Microwave Imager) surface rainfall estimates using a 1D-Var approach (Marécal and Mahfouf, 2002). This two-step procedure was found to be more robust than a direct assimilation of the rainrates with 4D-Var, partly because of strong non-linearities in the physical parametrisation schemes which are not compatible with the tangent linear model concept used in 4D-Var (Marécal and Mahfouf, 2003). Recently, Moreau et al. (2004) retrieved the TCWV directly from brightness temperatures, which is a further step towards the direct 4D-Var assimilation of the radiances and Benedetti et al. (2004) assimilated three-dimensional reflectivities from the TRMM precipitation radar. All theses studies showed that rainfall assimilation gave a noticeable improvement in the representation of tropical and extratropical large-scale precipitation systems.

Other methods for large-scale precipitation assimilation include the humidity nudging schemes described by Falkovich et al. (2000) and Davolio and Buzzi (2004) or the work of Rogers et al. (2000) who used radar reflectivity as a trigger of the convective cumulus parametrisation scheme to release (parametrised) convection in the model.

Meso-γ scale models

The first three-dimensional cloud-resolving models for the simulation of severe convective storms (Wilhelmson and Klemp, 1978) were typically initialised with a horizontally homogeneous, conditionally unstable atmosphere and convection was triggered using a warm bubble or a low-level pool of cold air. An early attempt to assimilate radar observations was undertaken by Lin et al. (1993) who used winds from multiple Doppler radar and

reflectivities to initialise their model. The temperature and pressure fields were retrieved using the momentum equations (Gal-Chen, 1978) and the rain water was derived from the reflectivity. They found that the radar data was able to introduce fine-scale structures into a supercell storm that could only be obtained with a higher model resolution when starting from a classical warm bubble perturbation. The Center for Analysis and Prediction of Storms (CAPS) developed the ARPS (Advanced Regional Prediction System) Data Analysis (ADAS) taking into account multiple types of data, in particular radar and satellite data, in order to obtain a three-dimensional representation of clouds and precipitation (Brewster, 1996; Zhang, 1999). Xue et al. (1998) applied this scheme to a squall line case and identified radar data as the observation with the largest positive impact for the storm assimilation. Ducrocq et al. (2000) developed a similar method and applied it successfully on a number of heavy precipitation events in France (Ducrocq et al., 2002). In the absence of large-scale forcing, the introduction of mesoscale flow patterns in the model's initial state turned out to be crucial, i.e. the combination of both surface, and radar and satellite observations, was found to be critical for a successful initialisation and subsequent forecast of the storm. Haase et al. (2000) developed a physical initialisation scheme based on the idea of Krishnamurti et al. (1991) but for radar derived surface rain rates and tuned for high-resolution application. More recently, Klink and Stephan (2004) reported encouraging results of rainfall assimilation with LHN in a case of summer convection in Germany. The positive impact was found to last up to six hours into the free forecast.

The applicability of 4D-Var at the storm scale was explored by Sun and Crook (1997, 1998) who assimilated 3D radial Doppler winds and reflectivity into a cloud-resolving model. They reported technical feasibility of the method, when tested on a single cell cumulus with a lifetime of 30 min. Wu et al. (2000) applied the method to a convective system where the ice phase played an important role and reported convergence problems in the 4D-Var minimisation procedure due to the complex microphysical parametrisation schemes.

Ensemble Kalman Filter (EnKF) methods (Evensen, 1994) introduce an interesting probability aspect into data assimilation by performing a whole ensemble of analyses each with slightly altered observations. Recently the method has been tested on the storm-scale (Snyder and Zhang, 2003; Zhang et al., 2004; Dowell et al., 2004). Open questions here are how to initialise the ensemble members with an adequate spread that is maintained during the assimilation cycle.

For a more detailed review on radar assimilation, see Macpherson et al. (2004) and for a review of storm-scale variational assimilation, Park and Zupanski (2003).

Operational application

Although radar data exist for almost half a century, its operational assimilation has not been introduced widely up to date. Large-scale models had too coarse a resolution and could thus not benefit from the small-scale information provided by radar. Moreover, radar composites large enough to cover the integration domain of operational models are yet to evolve, particularly in Europe. In 1996, the Metoffice (UK) was the first National Weather Service that routinely assimilated radar-derived rainfall rates using LHN. Since 2001, NCEP (National Center for Environmental Prediction) assimilates rainfall using a similar method (Lin et al., 2001). At the Japan Meteorological Agency, a 4D-Var mesoscale system has been implemented operationally in 2002, including assimilation of

hourly precipitation from a synthesis of radar and gauge data (Ishikawa, 2002).

1.3 Aims and outline of the thesis

As pointed out in the previous section, next-generation NWP models will operate with grid-spacings of O(1 km). As the major benefit of using high-resolution models is expected at short ranges (say one hour to one day), timeliness of forecast delivery is essential in operational NWP. Coherent, fast evolving, small-scale precipitation systems have a lifetime of a few hours, thus requiring forecasts to be delivered to the forecasters and customers in no more than an hour after real time and, possibly, updated every one or two hours. In order to meet these time constraints a very efficient observation acquisition and assimilation system is essential. While for large-scale NWP data assimilation systems 4D-Var has proven to be highly effective, there are, at present, no established procedures for assimilating cloud-scale observations (Macpherson et al., 2004; Park and Zupanski, 2003; Fritsch and Carbone, 2004). The deployment of 4D-Var on the storm scale remains questionable in an operational context because of its excessive computational costs. The computational burden is further enhanced when meso-γ scale QPF is considered in a probabilistic framework, where large ensembles need to be generated (Fritsch and Carbone, 2004). For more fundamental reasons, the applicability of 4D-Var is limited by the highly non-linear nature of the microphysical processes, the non-Gaussian error characteristics of precipitation, and non-linear balance relationships, all of which are in contrast to the basic assumptions made in 4D-Var (Bouttier, 2003).

Despite the success at larger scales the simple Latent Heat Nudging scheme has not been thoroughly tested at smaller scales up to now. LHN seeks to adjust the model's buoyancy in order to match the observed precipitation intensity and, therefore, seems to be a natural candidate for the assimilation of convective weather systems. Moreover, it allows for a timely insertion of high-frequency observations at low computational costs, features that are prerequisites for the operational assimilation of convection.

The present thesis attempts to re-evaluate and characterise the LHN scheme within an operational NWP system in a high-resolution configuration similar to that which will be deployed in the near future. It is hoped to gain some insight into the extent to which this simple scheme can introduce precipitation and small scale flow features into the initial state of a forecast and improve short-range QPF. To this end assimilation simulations of idealised and real severe convective systems and free forecasts started therefrom are carried out. The core of the thesis is composed of three inter-related but self-contained articles, set out in chapters 3, 4 and 5:

- In the first study (chapter 3) the LHN scheme is applied within the framework of a simulated supercell type storm, providing 'pseudo rainfall observations' for the assimilation simulations. Consideration is given to the model's response to the forcing as well as to the sensitivity of the LHN to the uncertainty in the observations and the environment.

- The second study (chapter 4) follows the first in that it explores the performance of the LHN scheme in high-resolution simulations of two severe convection cases in Switzerland using rainfall data from the Swiss Radar Network. The LHN analyses and free forecasts started therefrom are validated against independent surface observations which allows a characterisation of the model's dynamical response to

the continuous forcing during the assimilation and the performance of the forecasts. Further, the scheme's sensitivity to the amplitude of the target precipitation is examined. Beside this, a new observation quality control function suited for the application in complex terrain is proposed.

- The third study (chapter 5) addresses the sensitivity of the LHN scheme to non-rain echoes related to ground clutter or anomalous propagation of the radar beam. To this end, a series of experiments are carried out assimilating artificial, localised rainfall of different amplitude into environments of various instability. Consideration is given to the degree to which these non-rain echoes are amplified in the model and contaminate the forecasts.

Further remarks and future perspectives are given in the final chapter 6. As the articles are self-contained, some introductory remarks or methodical descriptions will inevitably exhibit a certain degree of repetition in the respective chapters.

Chapter 2

Methodology and Data

2.1 The numerical model

The numerical model used in this study is the Lokal Modell (LM) developed within the Consortium for Small Scale Modelling (COSMO) and deployed operationally at five European National Weather Services, namely Germany, Switzerland, Italy, Greece and Poland. The model solves the three-dimensional, fully elastic and non-hydrostatic atmospheric equations on an Arakawa-C grid using the split-explicit technique described by Klemp and Wilhelmson (1978). Prognostic variables include the three Cartesian velocity components (u, v and w), temperature (T), pressure perturbation (p') and mass fractions of water vapour (q_v) and cloud water (q_c). The parametrisation for grid-scale precipitation considers four categories of water (water vapour, cloud water, rain and snow). The mass fractions of rain water (q_r) and snow (q_s) are treated diagnostically for reasons of efficiency. A mass flux convection scheme after Tiedke (1989) is available. Shortwave and longwave radiation is parametrised by the Ritter and Geleyn (1992) scheme. Vertical subgrid turbulence is parametrised following Mellor and Yamada (1982) and the surface flux formulation is based on a roughness-length specifying the drag-coefficients for turbulent momentum and heat exchange with the ground. A force-restore soil model using five soil types determines surface temperature and humidity over land. For a more complete description of the model we refer to Doms and Schättler (2002) and Steppeler et al. (2003), see also `http://www.cosmo-model.org`. The detailed configurations used in this study are set out in the respective chapters in sections 3.2.2, 4.2.2 and 5.2.1.

2.2 The assimilation scheme

The Latent Heat Nudging scheme used in this study is based on that developed by Manobianco et al. (1994) for the assimilation of satellite-derived rainfall observations into a large-scale model and adopted by Jones and Macpherson (1997) for the use with radar QPE. The main principle is to correct the model's latent heating at each time step by an amount calculated from the observed and the modeled precipitation, where the assumption is made that the vertically integrated latent heating is proportional to the surface rain rate. This extra heating then acts as a source term in the prognostic model temperature equation and thus introduces changes in the buoyancy which in turn affect the precipitation production processes. The vertical distribution of the forcing is taken from the model, which allows for consistency with the model's parametrisation schemes and

the temporal evolution of the profiles. The basic concept of the LHN in LM is as follows:

- First, the model physics and the dynamic tendencies are derived from the current state of the model atmosphere.
- Then the diabatic temperature tendencies related to phase changes of water for each grid point are calculated (hereafter related to as model latent heating (LH)).
- Finally, the LHN temperature increments for each grid point are calculated by scaling the profile with a factor determined from the radar-derived and the model surface rain rate and are added to the prognostic temperature field at the end of the time step.

These steps are described in more detail in the following subsections.

Calculation of the model latent heating

Contributions to the source/sink of LH are dependent on the precipitation parametrisation scheme in use. For this study we use the one-category ice scheme described in Doms et al. (2004), i.e. snow is the only frozen hydrometor considered. In this case, the discrete LH is calculated from

$$LH = \frac{\Delta T_{LH}^{mod}}{\Delta t} = \frac{L_V}{c_{pd}}\left(S_c - S_{ev}\right) + \frac{L_S}{c_{pd}} S_{dep} + \frac{L_F}{c_{pd}}\left(S_{nuc} + S_{rim} + S_{frz} - S_{melt}\right) \qquad (2.1)$$

where L_V and L_S are, respectively, the latent heat of vapourization and of sublimation and $L_F = L_S - L_V$ is the latent heat of fusion. c_{pd} denotes the specific heat of dry air at constant pressure, Δt is the model time step. The mass transfer rates S_x are listed in Table 2.1.

Symbol	Definition / Description
S_c	Condensation and evaporation of cloud water.
S_{ev}	Evaporation of rain in sub-cloud layers.
S_{dep}	Depositional growth of snow.
S_{nuc}	Initial formation of snow due to nucleation from cloud water.
S_{rim}	Accretion of cloud water by snow (riming), $T < 273.16K$.
S_{frz}	Heterogeneous freezing of rain to from snow, $T < 267.16K$.
S_{melt}	Melting of snow to form rain, $T > 273.16K$.

Table 2.1: Mass transfer rates contributing to the release/absorption of latent heat

If the new two-category ice scheme (see Doms et al., 2004) is applied, additional source/sink terms S_x must be considered. If the convection parametrisation is switched on, an extra convective temperature tendency is added to LH.

Calculation of the temperature increments

The LHN Temperature increments ΔT_{LHN} added to the prognostic temperature field at the end of the time step are now determined from model latent heat tendencies LH, the radar-estimated surface precipitation rate RR_{rad} and the model surface precipitation rate RR_{mod} from

$$\Delta T_{LHN} = (f-1) \cdot \Delta T_{LH}^{mod} , \quad f = RR_{ana}/RR_{mod} \tag{2.2}$$

where f is the scaling factor determined from the ratio of the analysed and the model rain rate. The analysed rain rate RR_{ana} is a weighted sum of the radar-estimated and the model rain rate:

$$RR_{ana} = w \cdot RR_{rad} + (1-w) \cdot RR_{mod}. \tag{2.3}$$

The observation weight $w = w(x, y, t) \in [0, 1]$ allows for a treatment of the radar quality. For $w = 1$ the analysed rain rate is equal to the radar-estimated rain rate, while for $w = 0$ the observations are disregarded and the analysed rain rate equals the model rain rate. Jones and Macpherson (1997) proposed a simple function dependent only on the distance to the next radar station, accounting for the beam broadening error of the radar which increases with distance. Macpherson et al. (2001) improved the weight by additionally considering the time dependent number of radar stations contributing to the composite and, more importantly, the uncertainty of radar measurements extrapolated to the surface from above the freezing level.

As in mountainous terrain shielding and partial shielding by the orography are among the dominant error sources (see section 2.3) we propose a new weighting function based on a visibility map. A good first guess of the radar visibility can be obtained by a geometrical simulation in which the visibility is calculated ray by ray by combining a digital terrain model and the radar beam propagation properties. The height above sea level of the lowest radar measurement contributing the corresponding surface precipitation value is obtained for each radar pixel. Low values mark high surface QPE quality, high values less reliable measurements. Moreover, since a wet observation is more likely to be accurate than a dry observation (in a yes/no sense), wet observations are assigned a higher quality for the same visibility. The visibility values are mapped to the observation weight as follows: Visibility values less than 2000 m result in a maximum weight of 1. Between 2000 m and 4000 m the weight decreases linearly to $w = 0.5$ for wet observations and to $w = 0$ for dry observations. A similar relation was used by Jones and Macpherson (1997) to calculate the weight from the distance to the nearest radar. Figure 4.2 shows the observation weighting function w interpolated to the model grid ($\Delta x = 7$ km) for the SRN composite. Dark shading results in areas of good radar visibility and denotes high quality with associated large weights. On the other hand, bright shading denotes lower quality with correspondingly lower weights, resulting from areas where the radar beam is blocked by elevated terrain (see 1000 m contour) and at long ranges. If just one or two radar stations contribute to the composite, the weight is adjusted accordingly, resulting in a time dependent quality function. This weight could be easily extended to take into account other quality information, like clutter maps or vertical reflectivity profile corrections, once such is available.

If there are large discrepancies between observed and modelled rain rates, the scaling factor f is limited by a factor α, so that there is not too much heat added to or removed from the model. If at a grid point the observed rain rate is much larger than the model rain rate (this includes the case, where the model has no precipitation) no suitable profile

is provided by the model and a nearby grid point is searched within a given range, where the rain rate more closely matches the local observed rain rate. If such a point is found, the nearby profile is scaled. If no nearby point is found, an idealised Latent Heat profile is used for the scaling. In Table 2.2 the possible ranges for the ratio between observed and model rain rates and the corresponding scaling factor and profile are listed.

		scaling factor f	profile to scale
model fair:	$1/\alpha_{down} \leq \frac{RR_{ana}}{RR_{mod}} \leq \alpha_{up}$	$\frac{RR_{ana}}{RR_{mod}}$	local profile
model too wet:	$\frac{RR_{ana}}{RR_{mod}} \leq 1/\alpha_{down}$	$1/\alpha_{down}$	local profile
model too dry:	$\frac{RR_{ana}}{RR_{mod}} \geq \alpha_{up}$	$\frac{RR_{ana}}{RR_{near/ideal}}$	nearby/ideal. profile

Table 2.2: Ratios of observed and model rain rates and corresponding scaling factors and profiles.

Humidity adjustment

The LHN scheme allows, as an option, an adjustment of the humidity in addition to the latent heating. This is accomplished by retaining the relative humidity during the LHN temperature adjustment. At gridpoints where a positive (negative) temperature increment is applied, this results in an increase (decrease) of the water vapour q_v. At locations were $f > 1$ (i.e. where precipitation should be enhanced in the model), q_v is additionally nudged towards saturation. A similar humidity adjustment was proposed by Manobianco et al. (1994). In this study, the humidity adjustment was found to be beneficial and was applied in all simulations.

2.3 Radar data

The Swiss Radar Network (SRN Joss et al., 1998) consists of three C-band Doppler radars of the same type, providing full volume information every five minutes. Figure 2.1 shows the location of the radar sites. The data are preprocessed and made available on a Cartesian grid with a mesh size of $2 \times 2 \times 1\, km^3$ for the network composite. Radar observations, by virtue of their spatial and temporal coherence, open the way for a variety of nowcasting applications, and the initialisation and verification of high-resolution NWP models, tasks for which rain gauge measurements alone would not be sufficient. However, estimating surface rain rates from radar observations, especially in complex terrain, is a challenging task. Radars measure backscattered electromagnetic signals only, giving rise to a number of problems in the quantitative precipitation estimation (QPE) at the surface, notably: strong ground clutter including anomalous propagation, (partial) shielding combined with the vertical reflectivity profile, beam-broadening and partial beam-filling, variations in the reflectivity-rainfall ($Z - R$) relationship and beam attenuation (especially for long ranges

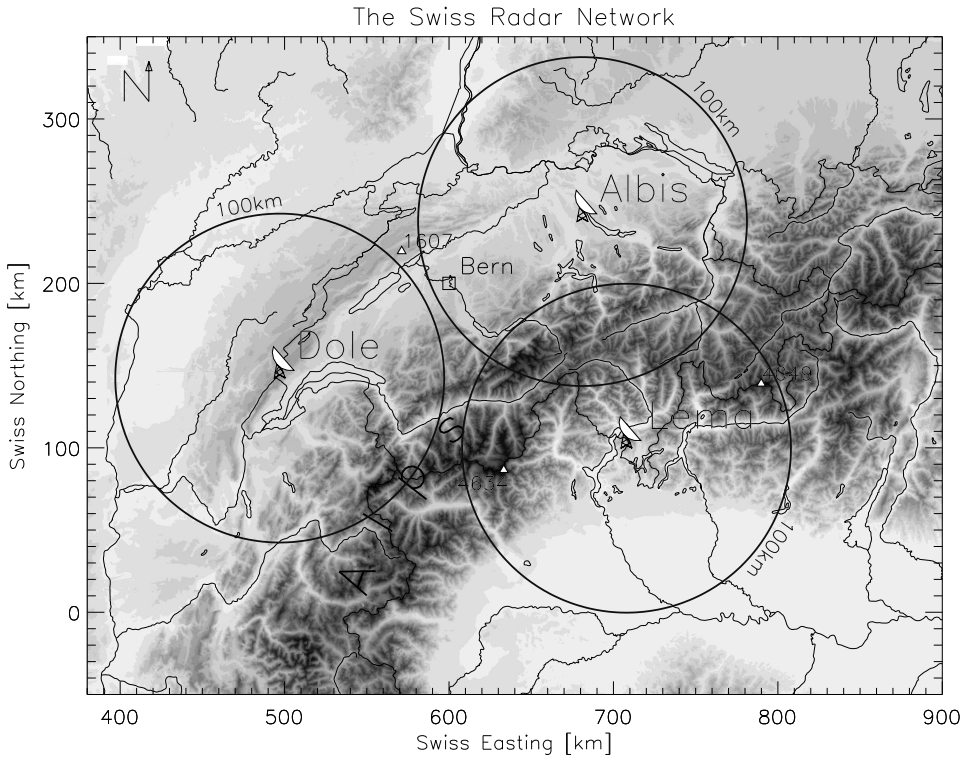

Figure 2.1: Location of the operational MeteoSwiss Radars. The C-Band Doppler radars Albis, La Dole and Lema are located on mountain tops at 925 m, 1675 m and 1625 m ASL, respectively.

and cases of intense precipitation) (Germann and Joss, 2004). Figure 2.2 illustrates the dominant error sources of QPE in mountainous terrain.

At MeteoSwiss, large efforts have been invested into overcoming some of these problems over the past decade, yielding, for example, the operational radar product RAIN, a two-dimensional map with the best surface QPE over Switzerland. The improvement was gradual, i.e. in 1999, a new clutter detection algorithm was implemented, which, on average, removes 98% of the ground clutter. Since 2001, a new vertical profile correction algorithm allows for improved surface QPE in regions where no radar measurements are available near the ground, i.e. in shielded mountain valleys and at far ranges of the radar station, while in early 2003, an adjustment of the radar constants based on a long-term radar-gauge comparison was introduced. As a simple quality measure, the bias of the RAIN product is defined as the total precipitation during a summer half-year as seen by the radar divided by the corresponding measurements from a set of rain gauges. This bias is strongly dependent on the set of gauges considered. For a set of 19 (58) gauges within a distance of 95 km (155 km) the bias could be improved from −49% (−57%) in 2000 to +26% (−2%) in 2003. Moreover the variability of daily radar-gauge ratios between individual stations could be substantially reduced. However, the quality of the radar-derived precipitation is subject to large day-to-day variations. For a more detailed description of the quality evolution of the RAIN product, we refer to Germann et al. (2004). An estimation of the bias on a daily basis is undertaken for the two case studies described in chapter 4 in order to gain insight into the sensitivity of the Latent Heat Nudging scheme to such a bias.

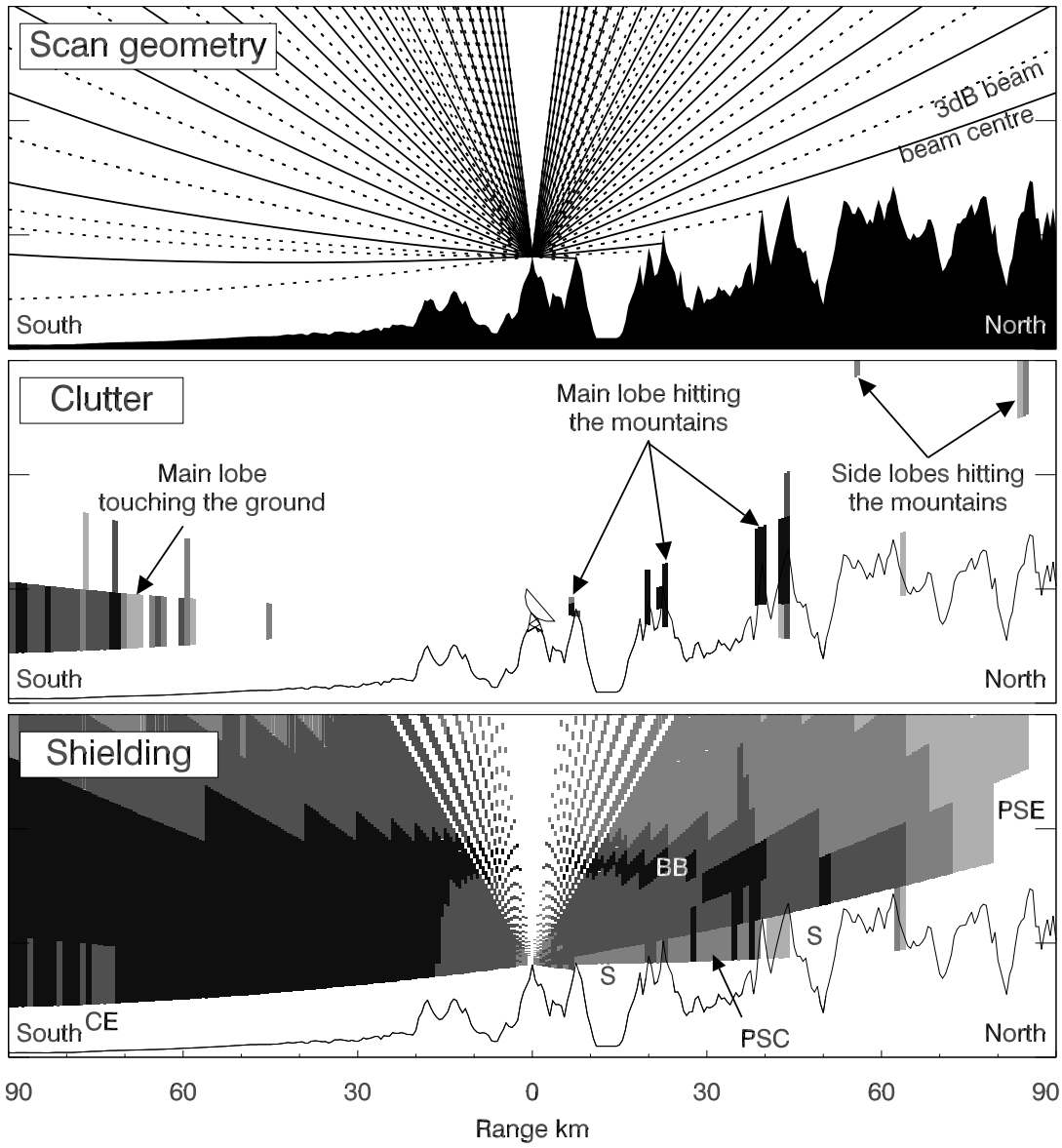

Figure 2.2: The challenge of Radar QPE in the Alps: combination of shielding, partial shielding and ground echoes inhibits direct view of precipitation close to the ground. The three panels show vertical cross sections from 0 to 6 km above sea level of (*top*) scan geometry of the Lema Radar, (*centre*) intensity of ground echoes during fine weather with the clutter elimination algorithm switched off, and (*bottom*) 24-hour accumulation of stratiform precipitation on 3 August 1998 illustrating the problem of shielding. To the north, the lowest two elevations are blocked at a range of 8 and 44 km, respectively. Everything behind is shielded (S). Between 8 and 44 km, the second-lowest elevation is partially shielded and occasionally contaminated by ground clutter not eliminated (PSC). The notch of the third lowest elevation at 80 km north (PSE) is caused by partial shielding, by evaporation, or by a combination of both. To the south beyond 70 km, the lowest elevation shows gaps that result from eliminating frequent ground clutter (CE). The melting layer is at a height of around 3.3 km (BB). This figure is taken from Germann and Joss (2004).

Chapter 3

Idealised Simulation Studies

Abstract

Next-generation, operational, high-resolution numerical weather prediction models require economical assimilation schemes for radar data. In the present study we evaluate and characterise the Latent Heat Nudging (LHN) rainfall assimilation scheme within a meso-γ scale NWP model in the framework of identical twin simulations of an idealised supercell storm. Consideration is given to the model's dynamical response to the forcing as well as to the sensitivity of the LHN scheme to uncertainty in the observations and the environment.

The results indicate that the LHN scheme is well able to capture the dynamical structure and the right rainfall amount of the storm in a perfect environment. This holds true even in degraded environments but a number of important issues arise. In particular, changes in the low-level humidity field are found to affect mainly the precipitation amplitude during the assimilation with a fast adaptation of the storm to the system dynamics determined by the environment during the free forecast. A constant bias in the environmental wind field, on the other hand, has the potential to render a successful assimilation with the LHN scheme difficult, as the velocity of the forcing is not consistent with the system propagation speed determined by the wind. If the rainfall forcing moves too fast, the system propagation is supported and the assimilated storm and forecasts initialised therefrom develop properly. A too slow forcing, on the other hand, can decelerate the system and eventually disturb the system dynamics by decoupling the low-level moisture inflow from the main updrafts during the assimilation. This distortion is sustained in the free forecast. It has further been found that a sufficient temporal resolution of the rainfall input is crucial for the successful assimilation of a fast moving, coherent convective storm and that the LHN scheme, when applied to a convective storm, appears to necessitate a careful tuning.

3.1 Introduction

Since precipitation strongly affects many aspects of our life, large effort has been placed on the improvement of its prediction. Yet, while general Numerical Weather Prediction (NWP) has witnessed considerable progress in recent years, quantitative precipitation forecasting (QPF), particularly in the convection-dominated warm season, is the poorest performance area of NWP forecast systems worldwide (Ebert et al., 2003; Fritsch and Carbone, 2004; Weckwerth et al., 2004). Reasons for this shortcoming include the chaotic nature

of moist convection limiting inherently its predictability (Walser et al., 2004), model deficiencies and/or insufficient resolution and the lack of a properly defined initial model state. Numerous studies have demonstrated the potential of improving QPF using models with increased horizontal resolution (e.g. Mass et al., 2002; Ducrocq et al., 2002; Zängl, 2004b). Next-generation operational NWP systems will cover the meso-γ scale and run with grid spacings around 1 km, with more sophisticated physical parametrisation schemes and thus be able to describe explicitly mesoscale flow features related to convection.

Such model resolution calls for new types of high-resolution observations, both for initialisation and verification purposes, since the modelled scales are well below the spatial and temporal scales resolved by the conventional observing systems comprising of surface or radiosonde networks. Doppler radar networks are able to provide this kind of information and have become an increasingly important complement to conventional observations for these purposes that currently receive much attention in many research actions around the world (e.g. the COST-717 Action 'On the Use of Radar Information in Hydrological and NWP Models', Rossa, 2000). Doppler radar wind and reflectivity information offer spatial resolutions of a few kilometres and temporal resolutions of a few minutes, sufficient to capture precipitation-related, mesoscale phenomena and thus are particularly useful to tackle the the QPF-challenge in NWP models.

New assimilation schemes for Doppler radar data have frequently been tested using simulated radial wind and reflectivity observations from idealised deep convective storms. Gal-Chen (1978), for example, has developed a retrieval method allowing the specification of pressure and temperature fields from simulated radial wind observations with the aid of the momentum equations. Sun and Crook (1997) used radial winds and three-dimensional reflectivity from an idealised single cell storm to test the four dimensional variational (4D-Var) method with radar data. This method has a number of attractive properties like the use of even complex, non-linear observations operators to make use of virtually all types of meteorological observations, a theoretically sound treatment of observation and model uncertainty, or the possibility to find optimal, dynamically consistent initial conditions and boundary conditions (e.g. Zou and Kuo, 1996), making it interesting also for limited-area data assimilation. However, there are theoretical and practical limitations of 4D-Var which have impeded its successful operational application in meso-γ models up to now. Firstly, the strongly nonlinear nature of moist convection, along with the need to parametrise the associated highly complex microphysical processes, aggravates the construction of the tangent linear and adjoint models, and may limit their validity in time. Secondly, meaningful model and observation error characteristics are not well known for cloud-scale processes and thirdly, the weighty computational requirements may prevent the method from operational deployment for high-resolution models covering large domains in foreseeable future (Park and Zupanski, 2003). The computational burden is further enhanced when meso-γ scale QPF is considered in a probabilistic framework, where large ensembles need to be generated (Fritsch and Carbone, 2004). More recently, Snyder and Zhang (2003) and Zhang et al. (2004) explored the use of an Ensemble Kalman Filter (EnKF) method (Evensen, 1994) to assimilate Doppler radial winds extracted from a simulated supercell storm into a storm scale model and Tong and Xue (2004) included also reflectivity observations in the EnKF assimilation. This method generates a whole ensemble of analyses and allows for a flow dependent representation of the model background error. However, it is presently not clear how to initialise the ensemble members and sustain a meaningful spread throughout the assimilation (Snyder and Zhang, 2003; Zhang et al., 2004).

Besides the large efforts invested in the development of statistical data assimilation methods, like 4D-Var or EnKF, simpler and more economical schemes have received notable attention for cloud-scale radar data assimilation. Ducrocq et al. (2000) developed a method which makes use of surface observations to introduce mesoscale boundary layer features related to convection (like cold pools from thunderstorm outflows) in conjunction with satellite and radar observations to adjust humidity and hydrometeors in the initial conditions of a storm scale model. Xue et al. (1998) and Haase et al. (2000) also report a large positive impact on the simulation of convection when using reflectivity data for the derivation of the initial state, sustaining that radar data can indeed be of substantial value even when assimilated using simple schemes.

Latent Heat Nudging (LHN) is an economical four-dimensional data assimilation method for surface rainfall observations. Originally developed for large-scale models and satellite data (Manobianco et al., 1994) it has been adopted for the use with radar-derived precipitation observations (Jones and Macpherson, 1997). Operational experience at the Metoffice (UK) showed a slight overall improvement of QPF with occasional positive impacts up to 15 hours into forecast time (Macpherson, 2001). Lin et al. (2001), using a similar scheme, also reported noticeable improvements in the first 6 hours of the precipitation forecast and a slight overall improvement over 24 hours with NCEP's operational ETA model. The scheme adjusts the buoyancy and therefore seems to be suited for the assimilation of convection. It allows for a timely insertion of high-frequency precipitation observations at a low computational cost, features that are necessary prerequisites for the operational assimilation of convective phenomena. Despite these appealing properties, LHN has not been thoroughly tested in high-resolution applications so far.

The present study aims at evaluating and characterising the LHN scheme at the meso-γ scale in the framework of an idealised supercell type storm. Consideration is given to the model's response to the forcing as well as to the sensitivity of the LHN scheme to uncertainty in the observations and the environment. The LHN scheme, the numerical model and the experimental setup are described in section 3.2, results of the assimilation simulations are presented in section 3.3, while in section 3.4 sensitivities of the scheme are investigated. The results are summarised and discussed in section 3.5.

3.2 Methodology and setup of experiments

3.2.1 Conceptual framework

Supercell storms represent one of the most vigorous types in the palette of convective storms. They occur in environments with high convective available potential energy (CAPE) and moderate to strong wind shear and are characterised by a strong rotating updraft, a propagation direction differing from the mean wind and a life-time of several hours. Browning (1964) presented the first conceptual model explaining the structure of supercells. This model has then been gradually refined with observational studies (e.g. Lemon and Doswell, 1979) and the aid of numerical modelling. Since the pioneering three-dimensional simulations of Klemp and Wilhelmson (1978) supercell type storms have received much attention from the modelling community not only to enhance the understanding of this damaging phenomenon but also to test new models and assimilation schemes (see e.g. Klemp, 1987; Wilhelmson and Wicker, 2001, for reviews). Weisman and Klemp (1982) defined a rough regime diagram in terms of CAPE and vertical wind shear, which

distinguishes simulated supercell storms from other forms of deep convection, namely short-lived single cells (favoured in weak wind shear) and multicells (favoured in low to moderate wind shear). The interfaces between the regimes are dependent on the CAPE and are not sharp, in that e.g. for a given CAPE and wind shear, both multicells and supercells can occur. During its early development (transient phase), the supercell storm

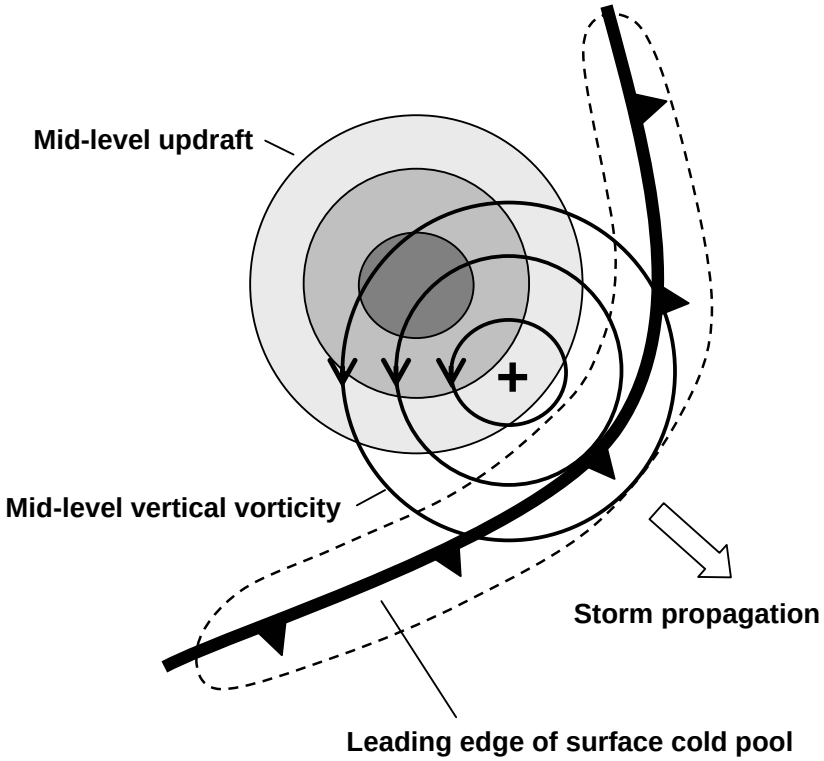

Figure 3.1: Schematic depiction of key processes of a simulated supercell storm. Mid-level updraft (shaded contours) and vorticity (solid contours) are overlayed with the leading edge of the surface cold pool and the associated region of enhanced moisture convergence (dashed contour).

grows as a single cumulus triggered by some perturbation in the boundary layer. As precipitation begins to form inside the cumulus cloud a cold downdraft, enhanced through evaporation, forms a low-level cold pool. Now, two distinct mechanisms, both connected with the strong environmental shear, begin to work enabling the long life of supercell type storms: Firstly, the shear prevents the cold pool from spreading away ahead of the storm so that low-level moist air is continuously fed into the updraft in a region of enhanced moisture convergence. Secondly, the strong updraft tilts the horizontal vortex lines embedded in the shear into the vertical, producing a pair of counterrotating vortices. Connected with these vortices are vertical, non-hydrostatic pressure gradients, reinforcing new updraft growth on the southern and northern flanks of the central updraft. As a result, the central updraft splits into two rotating storms moving each with a transversal velocity component to the mean flow in a quasi-steady manner.

Figure 3.1 presents a schematic depiction of the important dynamic ingredients that enable the long life of supercell storms. A region of enhanced mid-level vorticity is con-

nected with a pressure minimum at its centre (marked with a '+' in Fig. 3.1), resulting from the cyclostrophic effect (e.g. Holton, 1992, section 3.2.4). Since the vorticity is larger at mid-levels than at low levels, also the negative perturbation pressure is larger, resulting in an upward directed, non-hydrostatic pressure gradient force, favouring new updrafts ahead of the storm. The leading edge of the surface cold pool with the associated region of enhanced moisture convergence (contoured with the dashed line) is located in the vicinity of the the updraft region, enabling the continuous supply of moist air.

The strategy for the characterisation of the LHN scheme is to test its performance in a series of assimilation experiments using surface rainfall 'observations' extracted from a reference supercell simulation. This type of convective storm has been selected because of its long lifetime and quasi-steady behaviour. The quality of the analyses and subsequent forecasts started therefrom are judged using the framework described above and by comparing their dynamical and microphysical fields against their reference simulation counterparts. Particularly, the structure and relative position of the mid-level updraft and vorticity and the location of the surface cold pool leading edge as indicators of the balance of the storm are considered. A more quantitative validation is provided by means of vertical velocity root mean square errors (RMSE) computed on a 25×25 km domain centred around and moving with the right part of the reference storm and extending throughout the whole vertical domain. Errors of other model variables like horizontal velocity or temperature have also been calculated but are not discussed, as their qualitative behaviour is similar. The use of RMSE may not be well suited in the presence of phase errors. However, a close inspection revealed a good agreement between the subjective validation and the RMSE, indicating that in this case it can be regarded as a suitable error measure.

3.2.2 Model description and experimental setup

All simulations are undertaken with the Lokal Modell (LM) developed within the Consortium for Small Scale Modelling (COSMO) and used operationally at five European national weather services. The model version used in this study solves the three-dimensional, fully elastic and nonhydrostatic atmospheric equations on an Arakawa-C grid using a two-time-level split-explicit integration scheme introduced by Gassmann (2004). Prognostic variables include the three Cartesian velocity components (u, v and w), temperature (T), pressure perturbation (p'), and mass fractions of water vapour (q_v) and cloud water (q_c). The parametrisation for grid-scale precipitation accounts for four categories of water (water vapour, cloud water, rain and snow). The mass fractions of rain water (q_r) and snow (q_s) are treated diagnostically for reasons of efficiency. This simplification is justified for larger scales but might be less appropriate for storm-scale applications. However, as will be demonstrated in section 3.3.1, even with this simplified scheme, the main characteristics of a supercell type storm can be realistically simulated. Vertical subgrid turbulence is parametrised following Mellor and Yamada (1982), radiative forcings are excluded, the soil model switched off and Coriolis effects neglected. A more complete description of the model can be found in Steppeler et al. (2003) and Doms and Schättler (2002).

The Cartesian computational domain consists of 251×301 gridpoints in the horizontal with a mesh size of 1km. Additional 100 gridpoints at each side are used for the computation in order to minimize disturbing boundary effects in the middle of the domain since the LM does not allow for open (radiating) lateral boundary conditions but uses a Davies-type boundary relaxation scheme (Davies, 1976). In the vertical, a stretched grid

is employed composed of 60 levels and separated by 67 m near the ground and 500 m near the model top at 18000 m. Boundary conditions are rigid and free-slip at the top of the computational domain and above 11000 m a rayleigh damping layer is used to absorb vertically propagating waves. At the surface the drag coefficients for turbulent momentum and heat exchange are set to a small value, resulting in a quasi-free-slip lower boundary condition. In order to damp grid-scale noise, fourth-order numerical diffusion is applied. All simulations are integrated to 180 min with a time step of 5 s.

The atmospheric environment of the simulations is chosen to be supportive for splitting supercell storms as described by Weisman and Klemp (1982). It is characterised by a conditionally unstable thermodynamical profile and a moist, well mixed boundary layer with constant water vapour mixing ratio r. Unless stated otherwise, $r = 12\,\mathrm{g/kg}$, yielding a lifting condensation level of ∼1500 m, a level of free convection of ∼1900 m, a level of neutral buoyancy of ∼10000 m and a CAPE of 1200 J/kg. The environmental wind profile has a vertical shear of 20 m/s over the lowest 4000 m and constant wind aloft. For reasons of simplicity we do not vary the wind direction with height ($V = 0$), therefore the two splitting storms evolve symmetrically with respect to the x-z plane at $y = 50\,\mathrm{km}$ as noted by Wilhelmson and Klemp (1978). The convective system is started by a warm bubble centered at $x = 25\,\mathrm{km}, y = 50\,\mathrm{km}$ and $z = 1400\,\mathrm{m}$ with a horizontal radius of 10 km, a vertical radius of 1400 m and a temperature excess of 2 K. The lateral boundaries are relaxed towards the initial state throughout the whole simulation.

3.2.3 Assimilation method

The LHN scheme used in this study closely follows that of Jones and Macpherson (1997). The main principle is to correct the model's latent heating (LH) at each time step by a factor derived from the ratio of observed and model-estimated surface precipitation. This is accomplished by an extra term in the prognostic temperature equation, resulting in a gradual adjustment of the other fields according to the full, nonlinear model. The introduced change in buoyancy provokes an enhancement or dampening of the vertical velocity and the associated cloud and precipitation processes. The vertical shape of the applied forcing is taken from the model LH, ensuring consistency with the microphysical parametrisation scheme as proposed by Manobianco et al. (1994) and Jones and Macpherson (1997). At gridpoints where the model is too dry (i.e. has less than half the observed precipitation) a 'wetter' LH profile is sought for at surrounding gridpoints. Conversely, for gridpoints that are too wet (i.e. the model shows more than twice the observed precipitation) the scaling of the model profile is limited to a factor of two. These limits have been empirically established from sensitivity studies. For a more complete description of the LHN scheme, see Jones and Macpherson (1997) and Leuenberger and Rossa (2003).

The following changes to the original scheme have been introduced for this study:

- At grid points where no appropriate model profile can be found, a climatological profile deduced from a number of model runs is used for the vertical partitioning of the temperature increment. It has an approximatively parabolic shape with a maximum around 4000 m. The introduction of the climatological profile has proven to be of particular importance for the triggering of convection in model regions without precipitation. In order to avoid that the convection initiation is slowed down, the scaling of the climatological profiles is not limited.

- In order to remove grid-scale noise the model and observed rain rates are filtered at

each time step prior to the computation of the scaling factor and the temperature increments. This has been proposed by Christidis and Macpherson (2004).

- The subcloud evaporation part of the model LH profile is not used for the scaling. This setting has proven to yield better results than using the full profile (see section 3.3.4 for further explanations).

3.3 Results

3.3.1 Reference simulation

The model used for this study (see section 3.2.2) cannot be considered a fully-fledged cloud model so that first its ability to simulate a supercell type storm is investigated by comparing the key storms features with the conceptual model presented in section 3.2.1 and a state-of-the-art simulation described in the literature. The initial updraft of the reference simulation (REF), triggered by the buoyant bubble, exhibits vertical velocities up to 31 m/s (Fig. 3.3a) and tilts the horizontal vortex lines into the vertical, while 10 min into the simulation time, rain builds in the single cumulus cloud, and storm-splitting commences. A snapshot of the quasi-steady right moving storm at $t = 100$ min is presented in Fig. 3.2. Panel b) shows a vertical cross-section of w (shaded) and specific rain content q_r (dashed). Above the freezing level, precipitation forms as snow (not shown). The cloud outline is indicated with a heavy solid line showing the deep cell and its leading anvil. For the sake of a better representation, all fields are averaged over 10 gridpoints in y-direction, centred around the maximum updraft. A horizontal cross-section trough the storm similar to that schematically depicted in Fig. 3.1, is shown in Fig. 3.2c. Shaded contours denote w and thin lines vertical vorticity at $z = 4000$ m. The heavy solid line marks the boundary of the surface cold pool, while dashed lines delineate the associated moisture convergence at $z = 50$ m. The spatial coupling between the updraft and the region of enhanced moist inflow is clearly apparent, a necessary ingredient for the long life of the storm.
Figure 3.2a shows the right moving storm's cumulated rainfall distribution after 180 min, the left part being a mirror image of it. During the transient phase the single storm produces a local accumulation of 22 mm of rain where after the splitting maxima of 16 mm are reached. The total domain-integrated accumulated rainfall (DAR) at the end of the simulation amounts $12 \cdot 10^6$ m^3. The post-transient behaviour is quasi-steady until 130 min as apparent from a time-series of the vertical velocity domain extrema (Fig. 3.3a) and the domain sum of q_r (Fig. 3.3c). After 130 min the storms slowly loose strength but still move with the same propagation velocity (13.5 m/s) on their respective paths.

Environment and model settings for the REF simulation were chosen to allow for a comparison with the work of Seifert (2002) (SE02, hereafter). SE02 tested a new two-moment microphysical scheme including graupel in a state-of-the-art cloud model on the same idealised storm (results are not shown here). This comparison reveals the LM's ability to capture the main features of the storm evolution. The domain maxima of the updrafts are 20% larger in the LM simulation during the transient phase (30 m/s compared to 25 m/s) but slightly lower in the post-transient phase, while the maximum downdrafts compare well. The fluctuations of the w extrema are considerably smaller than in SE02, which might be a result of the missing treatment of horizontal turbulence in the LM. Our storm moves somewhat faster transverse to the mean flow. The DAR of our simulation

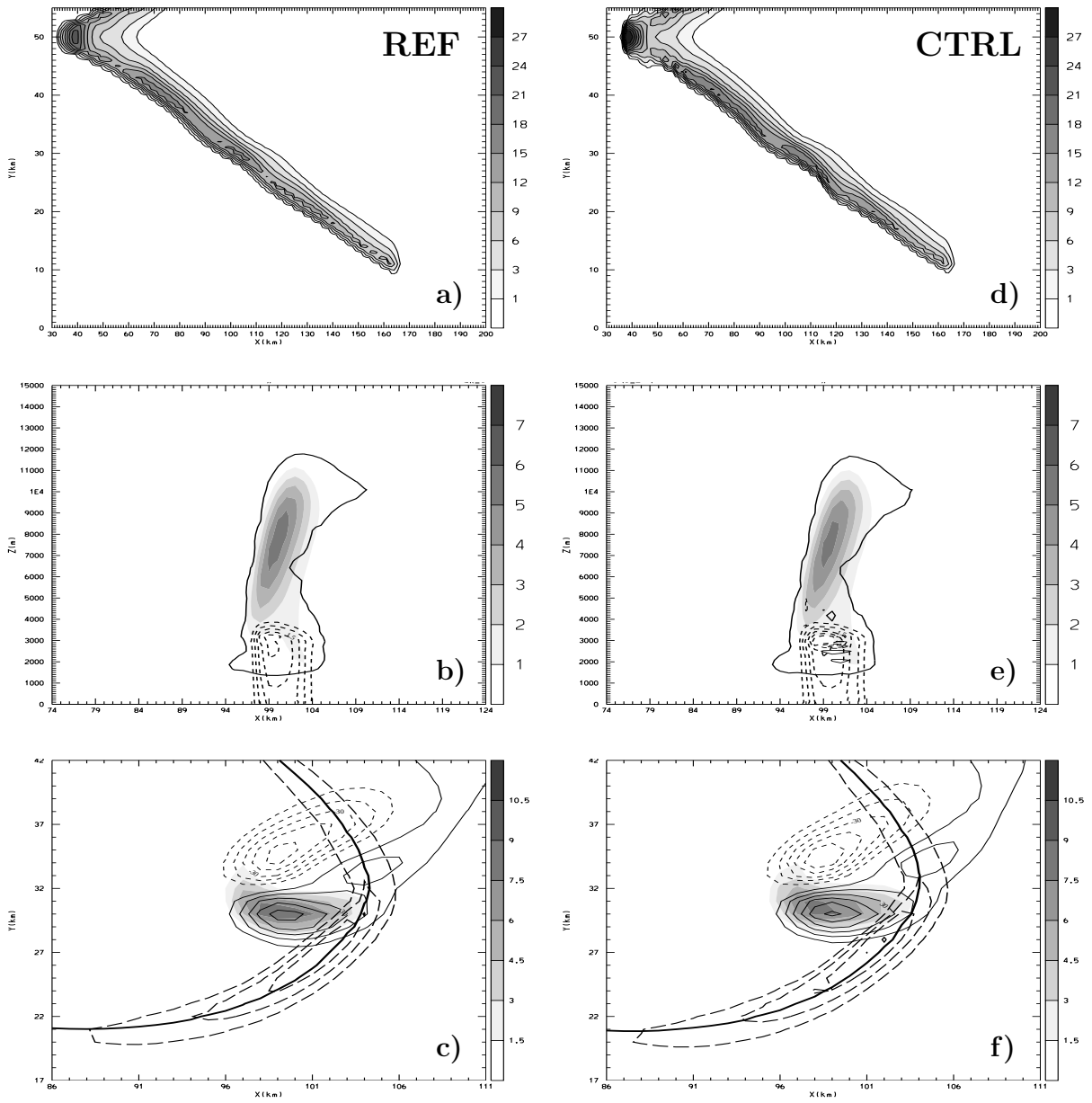

Figure 3.2: Selected results from the reference (REF) and the CTRL assimilation simulations (see Table 3.1 for a description). Upper panels: 3h cumulated surface precipitation (in mm) valid at 180 min. Middle panels: vertical cross-sections of w (in m/s, shaded, only positive values are plotted), nudging temperature increment (0.0015 K contour interval, thin solid lines for positive values, thin dashed lines for negative values), cloud water q_c (0.1 g/kg contour, thick solid line) and rain water q_r (0.5 g/kg contour interval, thick dashed lines) valid at 100 min. All quantities are averaged over 10 grid points. Lower panels: w (in m/s, shaded) and vertical vorticity ($10 \cdot 10^{-4}\,\mathrm{s}^{-1}$ contour interval , thin solid lines for positive values, thin dashed lines for negative values) at $z = 4000$ m, moisture divergence at $z = 50$ m ($2 \cdot 10^{-5}\,\mathrm{s}^{-1}$ contour interval, thick dashed contours, only negative values are plotted), and -0.5 K contour of surface perturbation temperature (thick solid contour) valid at 100 min.

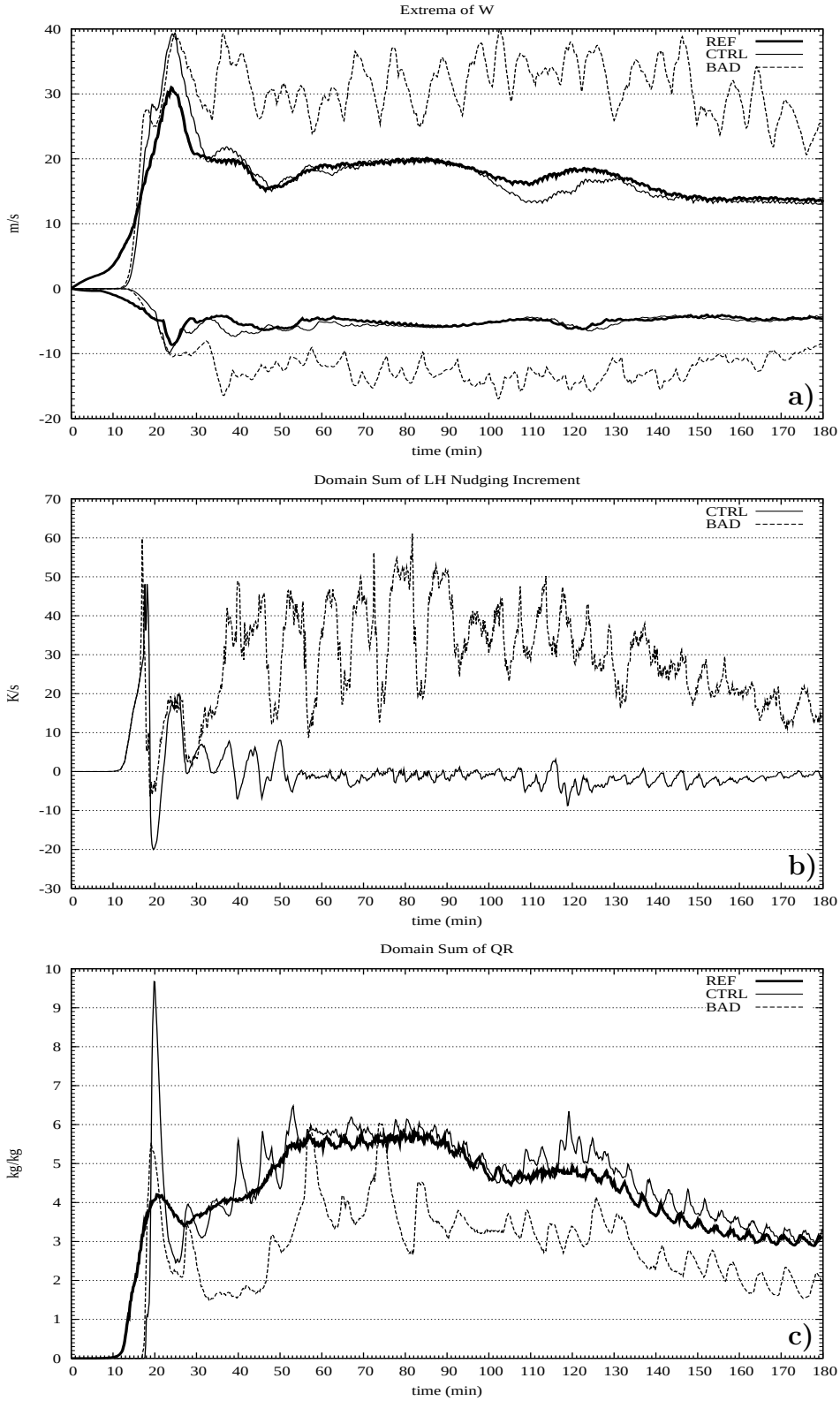

Figure 3.3: Time series of vertical velocity extrema (panel a), domain-integrated assimilation temperature increment (panel b) and rain water (q_r, panel c) from the reference (REF), the CTRL and the BAD assimilation simulation.

at 180 min is 71% larger than the one reported in SE02, probably because of the much simpler microphysical parametrisation scheme used in the LM. Indeed, SE02 reports a 30% increase of DAR for a simulation with a simple Kessler-type precipitation scheme in which rain water is the only treated hydrometeor. Moreover, the rainfall was not only more intense but also started earlier using the simple scheme, which is in agreement with our results. Finally, the rain swath of the LM simulation is slightly narrower due to the missing precipitation transport. Although some important characteristic features, like the hook reflectivity signature apparent in typical supercell radar images (e.g. Cotton and Anthes, 1989) can not be simulated with our model because of the simple representation of the microphysical processes, the LM reference simulation exhibits the main ingredients for a long-lived convective system, on the basis of which a characterisation of the LHN scheme is undertaken.

3.3.2 Assimilation simulation

In order to test the LHN scheme an identical twin experiment (CTRL) is performed, in which the environment and model are exactly the same as in the reference simulation (i.e. assumed perfect), but no triggering thermal is added. Identical twin experiments represent the most basic test for an assimilation scheme in that all hampering effects like observation errors or deficiencies in the model representation are disregarded. Therefore, the focus here is on a proof of concept of the assimilation method applied to a convective storm. Pseudo rainfall observations are extracted from the reference simulation every minute.

After 10 min, when the first rain reaches the surface in the reference run, the LHN scheme triggers the initial cell reaching a first maximum in the temperature increment domain sum at 18 min (Fig. 3.3b). This time lag is inherent to the use of surface rain as assimilated variable. The strong initial forcing results in a fast production of rain, the first maximum exceeding the corresponding value of the reference simulation by a factor of more than 2. The scheme reacts with strong cooling and corresponding suppression of rain production, until the model rain rate drops below the observed rain rate again. This cycle is repeated another four times with diminishing amplitude before a quasi-steady state is reached at 55 min. The duration of this transient phase is dependent on the stability of the environment, the model characteristics, and the settings of the assimilation scheme. The domain sum of the forcing remains small thereafter, suggesting that the assimilated storm is well in phase with the observations. This is confirmed by the temporal evolution of the RMSE showing a saturation at roughly 60 min (Fig. 3.4, heavy line). The error stays below 0.5 m/s for the rest of the assimilation time with an average value of 0.431 m/s. Snyder and Zhang (2003) reported the same error saturation time and a similar magnitude of the RMSE in their EnKF assimilation experiments with simulated radial Doppler winds of a comparable supercell storm. The spatial distribution of the surface precipitation compares well with that of REF, with the exception of the initial overshoot (Fig. 3.2d) and the DAR agrees within 5%. At 100 min the vertical and horizontal structure of the assimilated storm corresponds very well with that of the reference solution and virtually no assimilation increments are applied (Fig. 3.2e,f) giving further evidence of the successful assimilation.

Name	Description	LHN start	LHN end	RMSE (m/s)
REF	Reference simulation			
CTRL	Identical twin simulations	0	180	0.431
BAD	Simulation with varied settings	0	180	1.973
AW1	Assimilation window experiments	0	20	1.319
AW2		0	25	1.224
AW3		0	40	1.043
AW4		0	50	0.720
AW5		0	60	0.676
AW6		60	87	1.212
AW7		60	120	0.987
AW8		60	150	0.872
AW9		60	180	0.853
IF1A	Obs. insertion frequency of 2 min	0	180	0.602
IF2A	Obs. insertion frequency of 4 min	0	180	0.990
IF3A	Obs. insertion frequency of 6 min	0	180	1.246
IF4A	Obs. insertion frequency of 10 min	0	180	1.408
IF4F	Obs. insertion frequency of 10 min	0	60	1.968
O1A	Error in observations (factor 0.5)	0	180	0.889
O2A	Error in observations (factor 2)	0	180	1.777
H1A	Error in PBL humidity ($r = 11.5$ g/kg)	0	180	0.512
H2A	Error in PBL humidity ($r = 12.5$ g/kg)	0	180	0.502
H3A	Error in PBL humidity ($r = 13.0$ g/kg)	0	180	0.637
W1A	Error in wind (-2 m/s)	0	180	0.873
W2A	Error in wind (+2 m/s)	0	180	1.001

Table 3.1: List of idealised assimilation simulations. Indicated are experiment name and description, start and end of the assimilation (in min) and the mean root mean square error (RMSE) of the vertical velocity for a 25×25 km domain centered around and moving with the storm averaged over the whole integration period.

3.3.3 Variation of the assimilation window

The quality of the assimilated storm is further assessed by the quality of forecasts started from the LHN analyses at various times. Two forecasts are chosen to start during the transient phase (at 20 and 25 min, simulations AW1 and AW2) and one at its end (at 40 min, simulations AW3) whereas two other forecasts are initialised at the beginning of

the quasi-steady post-transient phase (at 50 and 60 min, simulations AW4 and AW5). As can be read from Fig. 3.4 the error rapidly grows during the forecast, roughly doubling during the first $20 - 30$ min. For AW3 the main part can be attributed to a phase error, as after one hour the cell is situated 3 km more to the southeast than in the reference run, whereas the structure and amplitude of the vorticity, updraft and moisture convergence , as well as the relative position of the surface gustfront compare well with their reference counterparts (not shown). The surface precipitation structure (Fig. 3.5a) and amount are very close to the 'truth' (cf. Fig. 3.2a), with an error in the DAR of only 2% at the end of the simulation. These results suggest that the analysis at 40 min is well able to initialise a forecast in line with the 'observations'. Even better results are obtained when starting the forecasts at 50 and 60 min.

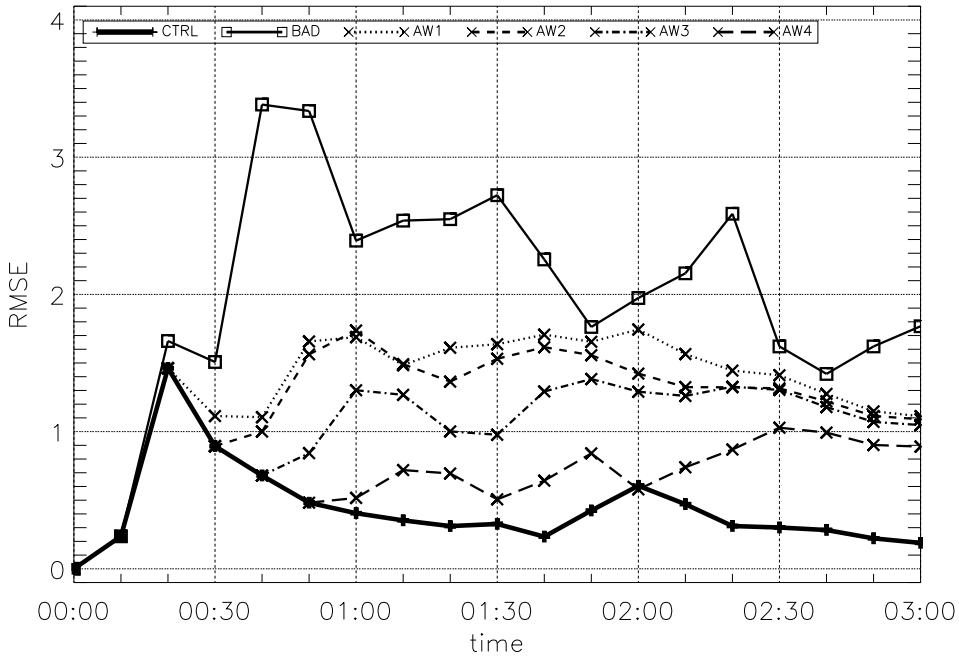

Figure 3.4: Time series of vertical velocity root mean square errors (in m/s) for the CTRL, BAD and the assimilation window simulations starting at $t = 0$.

The forecasts initiated in the transient phase exhibit larger errors during the forecast (up to a factor of 2) than those starting in the post-transient phase, yielding considerably larger average RMSE values (see table 3.1), a behaviour that may be linked to the unsteady nature of the forcing during the transient phase (Fig. 3.3b). Nevertheless, also these forecasts produce storms that are qualitatively similar to the reference storm, with DAR differing by up to 18%.

In a second series of experiments the assimilation is started during the post-transient phase when the splitting of the reference storm has already occurred and two isolated quasi-steady storms must be initialised by the LHN scheme, rather than one cell in its incipient stage. The forcing starts at 60 min and is applied during 27, 60, 90 and 120 min (simulations AW6, AW7, AW8 and AW9). The surface precipitation of simulation AW6 (Fig. 3.5b) shows the swath of the main cell with approximatively the right structure and amplitude, indicating the storms successful initialisation and evolution. Additional rain patterns appear to the north and east of the swath and are related with the forcing of

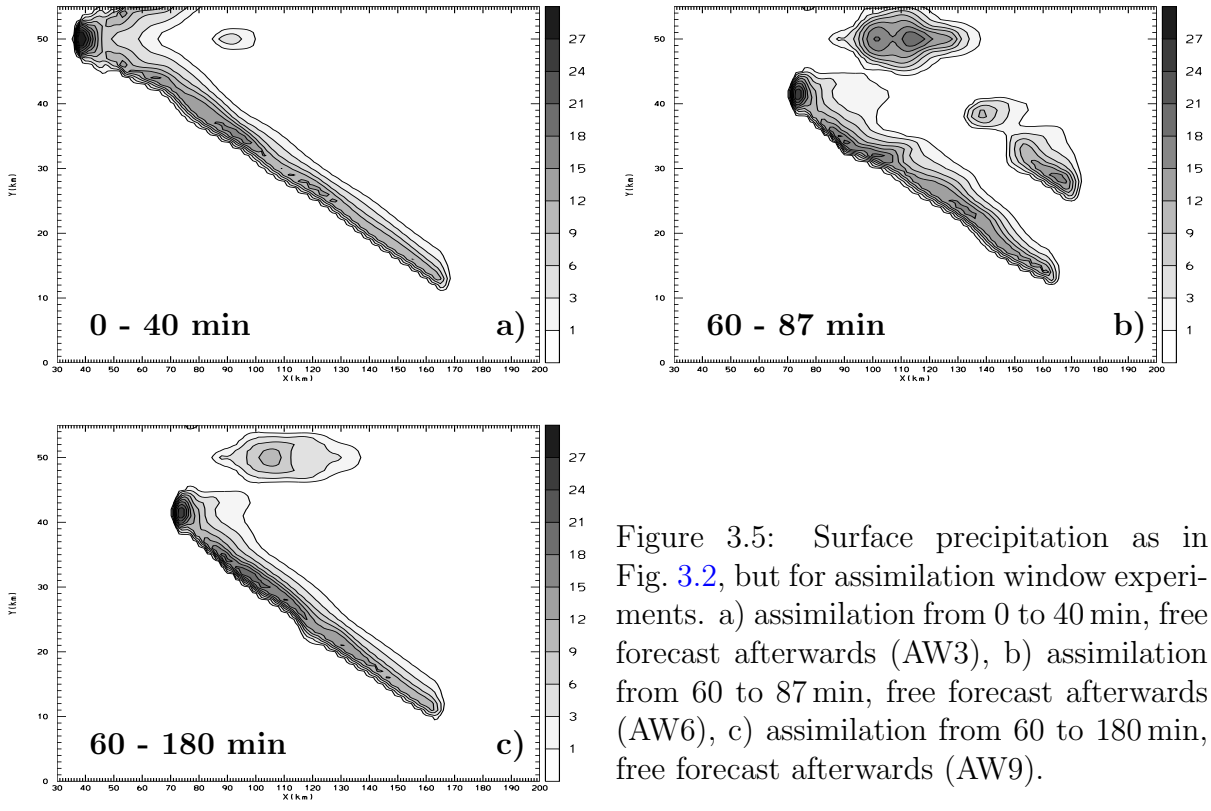

Figure 3.5: Surface precipitation as in Fig. 3.2, but for assimilation window experiments. a) assimilation from 0 to 40 min, free forecast afterwards (AW3), b) assimilation from 60 to 87 min, free forecast afterwards (AW6), c) assimilation from 60 to 180 min, free forecast afterwards (AW9).

the storm initiation at $(x, y) = (75, 40)$ km (and the northern mirror location). Each of the two cells are picked up as primary cells and tend to split in a right moving and a left moving part, one being favoured, the other suppressed by the assimilation scheme. Apparently a forcing period of 27 min is too short to inhibit the misplaced cell while with increased assimilation time these erroneous patterns are significantly reduced, but not completely eliminated, even when the forcing is applied until the end of the simulation (Fig. 3.5c).

If the forcing starts at 60 min, the saturation of the error is estimated 47 min, which is approximatively equal to that in the CTRL simulation, however a slightly larger average cooling is applied afterwards, suggesting that more work is required to suppress rainfall than in the CTRL simulation. This is reflected in larger RMSE than in the simulations where the assimilation starts at $t = 0$ min (Fig. 3.6 and table 3.1)

3.3.4 Variations of the scheme

The LHN scheme has several options and parameters which need to be carefully chosen. In order to demonstrate that a wrong setting of the method can have a serious negative impact on the assimilated storm a sensitivity study has been carried out using the same environment as in the CTRL simulation, but a version of LHN scheme altered as follows:

- numerical filtering of observed and model rainrate at each time step is switched off;
- maximum scaling of the model profile is set to a factor of 3 instead of 2 as proposed by Jones and Macpherson (1997) for a hydrostatic meso-β scale model;

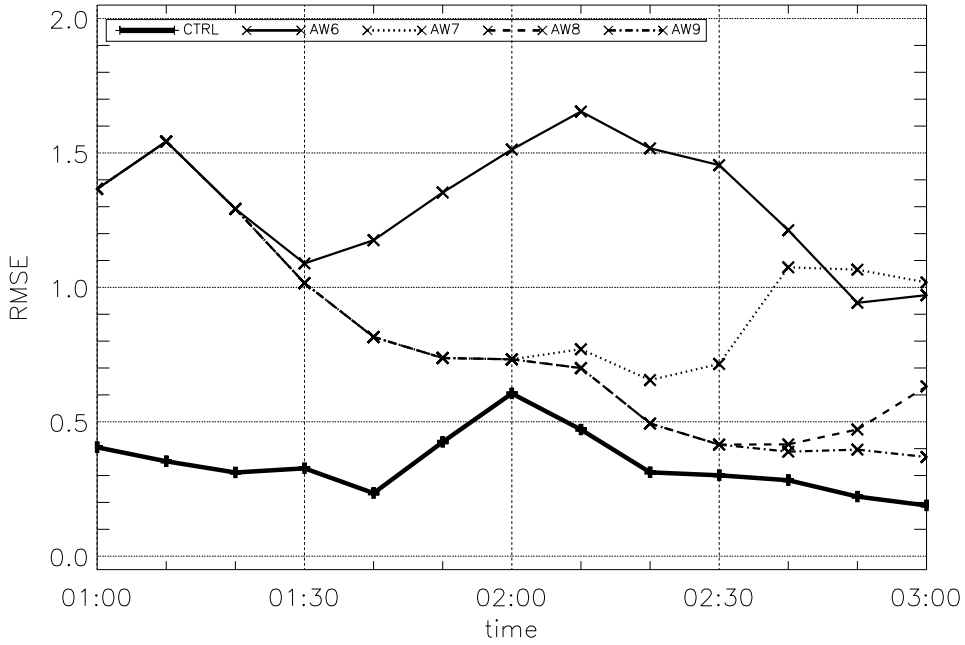

Figure 3.6: Time series of vertical velocity root mean square errors (in m/s) for the CTRL and assimilation window simulations starting at 60 min.

- scaling of the model latent heating profile is extended to the surface including sub-cloud evaporation;
- adjusting the specific humidity towards saturation in case of heating or towards constant relative humidity in case of cooling. A similar adjustment has been proposed by Manobianco et al. (1994).

Results derived from these settings (simulation BAD) reveal that the LHN forcing becomes gradually inconsistent with the dynamical storm structure as obtained in the reference simulation during the assimilation. After $t = 30$ min enhanced cooling in sub-cloud layers due to the negative evaporation part of the model LH profile yields strong downdrafts (Fig. 3.3a). The associated adiabatic drying is supported by additional drying that comes with the negative temperature increments, leading to enhanced precipitation evaporation and a reduction in the surface rainfall. The LHN scheme reacts with an increased forcing of the model LH profile inducing strong heating (Fig. 3.3b) in cloudy regions aloft and cooling at low levels where the model profile exhibits evaporative cooling (Fig. 3.7b). The so induced strong up- and downdrafts reach up to 14 km and may transport stratospheric air down into the troposphere which in turn may influence the accuracy of the analysis outside the convective region. Eventually, the strong cool and dry downdrafts lead to a spatial decoupling of the low-level moisture inflow from the main updraft (Fig. 3.7c) so that precipitation is further weakened (Fig. 3.7a). The DAR of the BAD simulation at 180 min amounts to just 40% of the CTRL simulation. Apparently, the LHN method can produce different dynamical forcings dependent on the scheme settings, leading to a well behaved (CTRL) or distorted (BAD) storm assimilation.

Further simulations (not shown) indicate, that the above mentioned changes to the scheme do not have a negative impact on the assimilation if applied each on its own,

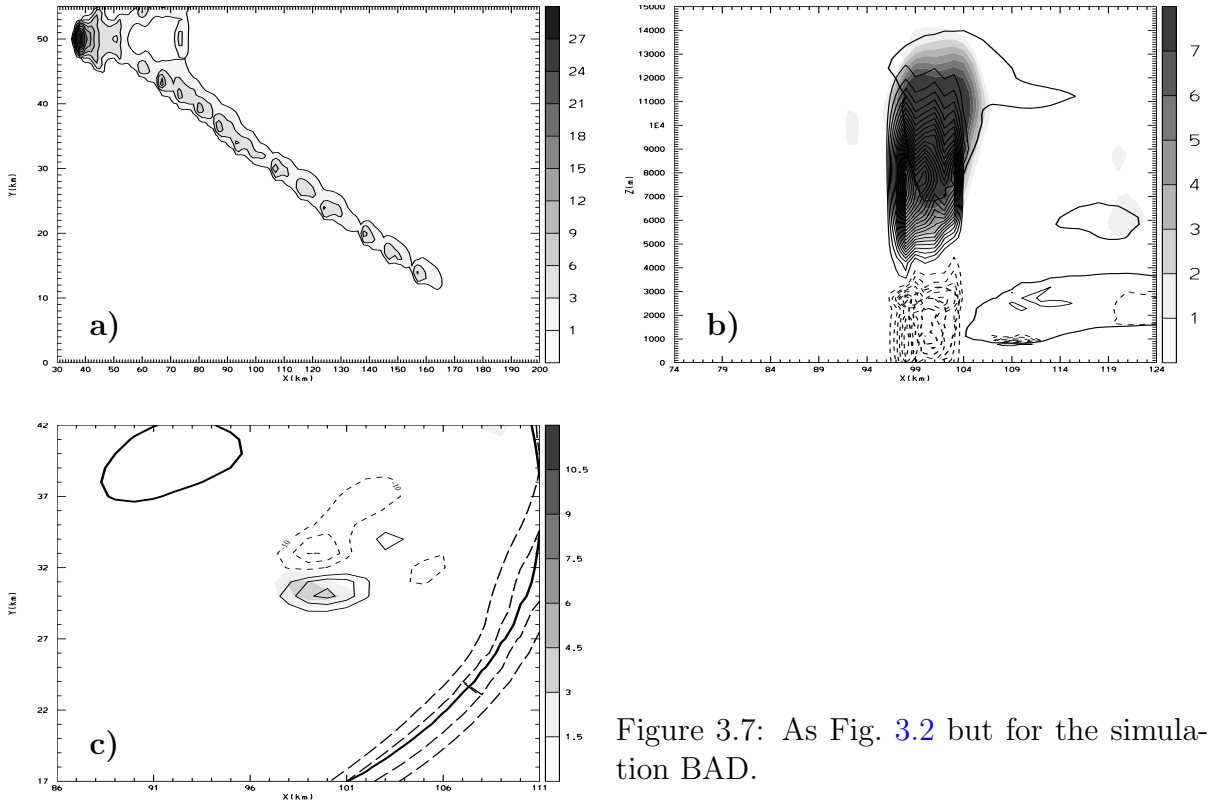

Figure 3.7: As Fig. 3.2 but for the simulation BAD.

but rather can lead to the described amplifying feedback when used in combination. For example the inclusion of the subcloud part of the profile for the scaling does not have a strong negative impact if the rain rates are filtered and the scaling factor is limited to a value of 2. The best results are obtained with the filter, a limiting factor of 2, the omittance of the subcloud part of the profile and without moisture adjustment. Therefore the remaining simulations in this study are performed using these settings.

3.4 Sensitivity experiments

Since in real-life applications neither a perfect model nor a perfect environment is available, it is necessary to evaluate the performance of the LHN scheme under non-perfect conditions. Simulations are carried out where the rainfall observations are degraded or biases are introduced into the storm environment.

3.4.1 Sensitivity to observation uncertainty

Observation amplitude

In order to simulate the effect of observation amplitude errors, two assimilation experiments are made in which the pseudo observations extracted from the reference simulation are multiplied by a factor of 0.5 (underestimation, simulation O1A) and 2.0 (overestimation, O2A). These factors can be taken as a very rough estimate of the radar rainfall accuracy over well observable terrain (Germann et al., 2004). The cumulated rain of the assimilated storms is not halved (doubled), as could be expected, but amounts to 88%

(133%) of the CTRL experiment. This indicates that in this case, the LHN scheme, combined with a perfect model and a perfect environment, is able to dampen an amplitude error in the assimilated precipitation. The spatial pattern of the rainfall distribution does not differ much from that of the CTRL experiment (not shown), but the vertical storm extent, updrafts and assimilation temperature increments are reduced (increased) (Fig. 3.8a,c). In the case of underestimation (O1A) (overestimation, O2A) the cloud top is 3000 m lower (2000 m higher) and the mean updraft is 40% weaker (160% stronger) than in the reference simulation. Negative (positive) temperature increments reveal that the assimilation scheme dampens (intensifies) the convective activity of the system. This is reflected in weaker (stronger) rotation, cold pool and moisture inflow (Fig. 3.8b,d).

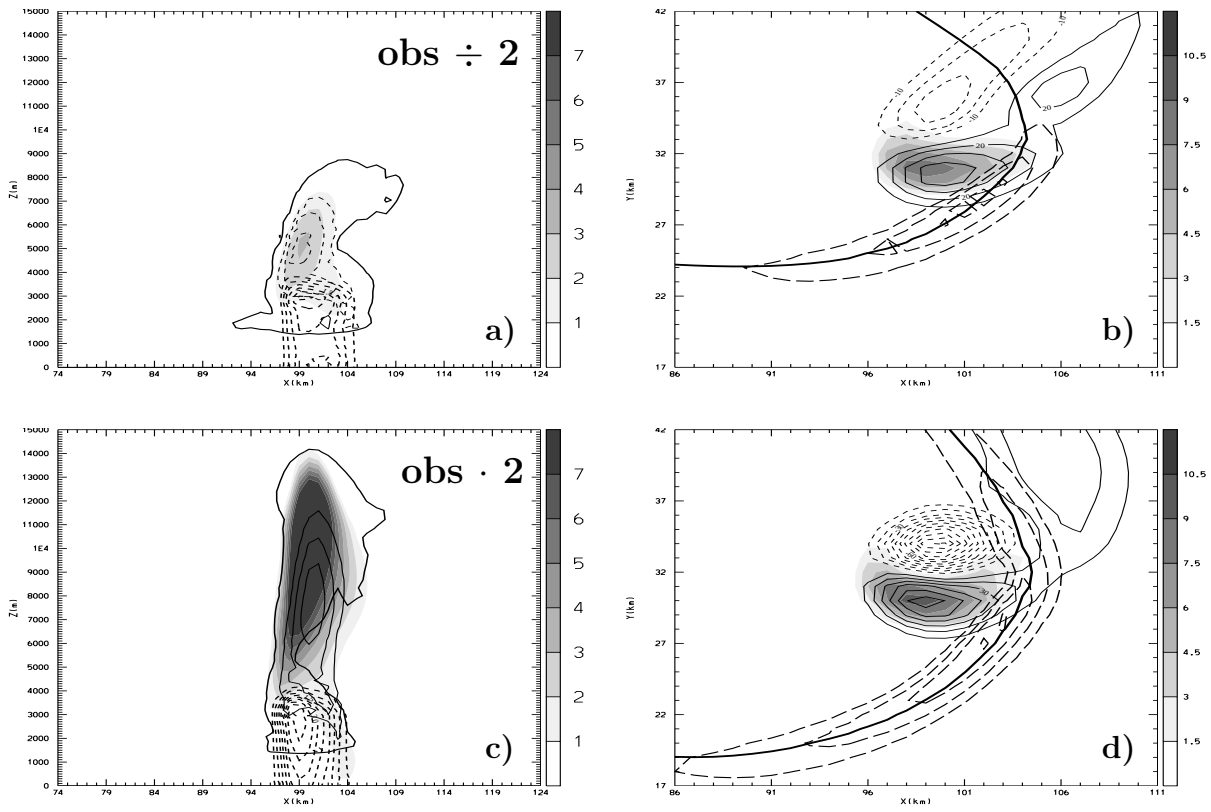

Figure 3.8: Vertical cross-sections of microphysical parameters and horizontal cross-sections of dynamical fields as in Fig. 3.2, but for amplitude error simulations. a,b) underestimated precipitation observations (O1A), c,d) overestimated observations (O2A)

A forecast started from the O2A analysis at 60 min (not shown) rapidly adjusts to the reference solution (i.e. error decreases) after the forcing is switched off, but one starting from the O1A analysis shows an error increase and eventually triggers multiple cells. A possible explanation for this behaviour is the dampened forcing in the O1A simulation which reduces the downdraft and thus the extent of the cold pool. At 60 min its leading edge is much closer to the updraft than in the reference run, enabling the inflow of more moisture and a subsequent storm intensification in the free forecast.

In previous studies, amplitude errors were found to be of minor importance for the assimilation results (Manobianco et al., 1994; Chang and Holt, 1994). Our results suggest that for the LHN assimilation of an idealised convective storm amplitude errors in the

rainfall input can have a negative impact and even lead to position errors, e.g. support of multiple cells during the forecast.

Insertion frequency

In this section the sensitivity of the LHN scheme to the temporal resolution of the observations is investigated. Macpherson (2001) reported a worthwhile improvement of the precipitation forecast in the first six hours when assimilating hourly data instead of three-hourly. For small-scale and fast moving convective systems the sensitivity is anticipated to be of different nature than for large scale frontal systems. Here we test the sensitivity by increasing the sampling interval of the pseudo observations to 2, 4, 6 and 10 min (simulations IF1A, IF2A, IF3A and IF4A). Typical radar systems provide observations every 5 to 15 min. As the LHN scheme interpolates the observations linearly between two subsequent observation times the area of the assimilated signal between two observation times increases with larger intervals (or decreasing insertion frequency). This can be regarded as a combined amplitude and position error. The resulting effect on the storm assimilation is negative and can be quite serious. The enlarged forcing area causes DAR amounts of 110%, 143%, 180% and 280% of that found in the REF simulation for sampling intervals of 2, 4, 6 and 10 min. As an example, the IF4A precipitation (interval of 10 min) distribution (Fig. 3.9a) shows a swath with a width more than doubled compared to the REF simulation. The dynamical structure of the storm at 100 min is highly degraded: the area of mid-level ascent and rotation and the surface moisture convergence are much larger than those in the reference simulation (Fig. 3.9b). The RMSE are enhanced up to a factor of 6 (Fig. 3.10 and table 3.1).

A forecast started from the IF4A analysis at 60 min produces even larger amounts of precipitation and clearly shows that the distorted structure at the initial time can not be corrected during the forecast. Multiple cells are triggered yielding a storm evolution which differs substantially from that of the reference storm (Fig. 3.9c,d).

These results confirm the findings of previous studies that position and structure errors in the observations are more serious than amplitude errors and degrade the assimilation. The sensitivity is larger than reported by Macpherson (2001), probably because of the faster propagation speed of the system. Furthermore, these results suggest that a simple linear interpolation between subsequent observations may not be suited for fast moving, coherent systems if the sample frequency is not sufficient. For the present case the assimilation suffers already when increasing the sampling interval from 1 min (CTRL) to 2 min (IF1A). The interpolation of the precipitation field could be improved by calculating a deformation vector field optimally shifting and distorting the precipitation at one observing time to match that at the next observation time, similar to a method proposed by Brewster (2003). This deformation field could then be used to estimate the rain field at any time step between the two observing times.

3.4.2 Sensitivity to environment uncertainty

One of the major difficulties in storm-scale analysis is the representation of the mesoscale environment into which the convective system is to be assimilated (e.g. Ducrocq et al., 2002). In this section we present a number of assimilation experiments in which biases are applied to the environment in terms of boundary layer humidity or the ambient wind. 'Observations' are taken as perfect like in the CTRL run.

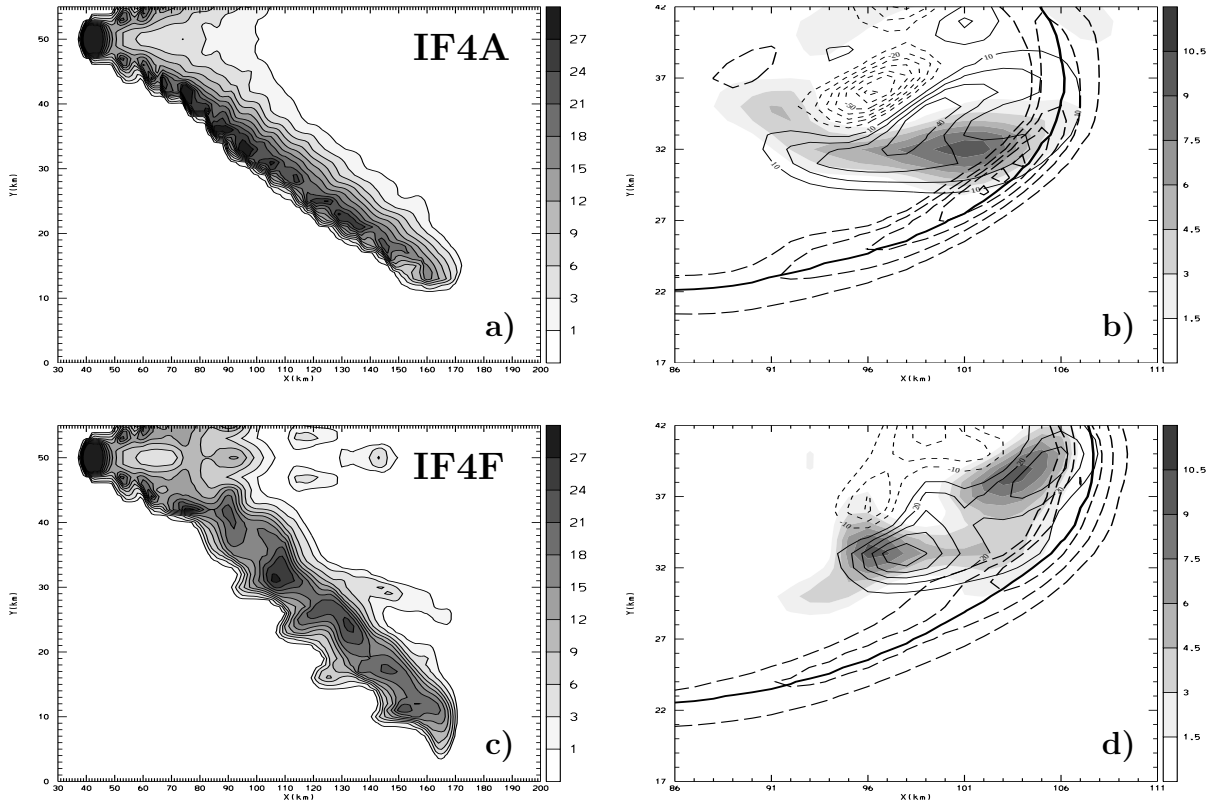

Figure 3.9: Surface precipitation and horizontal cross-sections of dynamical fields as in Fig. 3.2, but for insertion frequency simulations (sampling interval of 10 min). Upper panels: assimilation during the whole simulation (IF4A), lower panels: assimilation from 0 to 60 min, free forecast afterwards (IF4F).

Degraded low-level humidity

The amount and distribution of atmospheric humidity is crucial in the precipitation building process, but is poorly represented in today's NWP systems. Typical mean errors in relative humidity (as compared against radiosonde measurements) reach values up to 10% but can be considerably larger in single cases. Park (1999) reported that simulated supercells are sensitive to low level humidity: even small changes can lead to different storm developments, particularly in environments classified at the transition between different storm regimes according to Weisman and Klemp (1982). Three experiments are carried out to test the sensitivity of the assimilated storms to changes in the boundary layer humidity. The mixing ratio of water vapour (r) is set to values of 11.5 g/kg (simulation H1A), 12.5 g/kg (H2A) and 13 g/kg (H3A). These values reflect errors in the mixing ratio of -4%, +4% and 8% respectively. With a value of 11 g/kg the environment has not enough CAPE for the evolution of a long lived storm (in agreement with the findings of Weisman and Klemp (1982)) and is not examined therefore. The LHN scheme is able to assimilate the storm into the different environments. The spatial patterns of cumulated precipitation compare well with the reference simulation (Fig. 3.11a,c), but deviations of the DAR amount -14% for experiment H1A, 11% for H2A and 29% for H3A, compared to the CTRL. In the drier (moister) environment the assimilation scheme on average

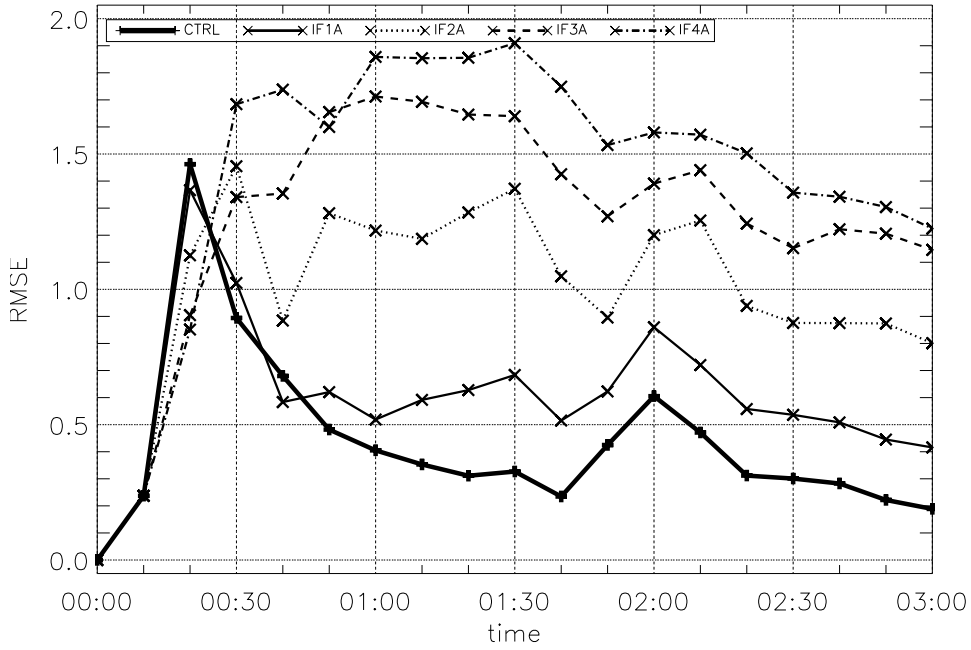

Figure 3.10: Same as Fig. 3.4, but for insertion frequency experiments.

generates positive (negative) temperature increments in order to match the observations, yielding stronger (weaker) updrafts and a higher (lower) cloud top (Fig. 3.11b,d). The RMSE of the experiments with ±4% humidity error is about 20% higher on average, while a 8% humidity error causes roughly an increase of 50% as compared to the CTRL (Table 3.1 and Fig. 3.12).

When the forcing is switched off after 60 min the storms rapidly change to the regime determined by the environment. While the storm in the drier environment gradually diminishes, the storms in the moister environments gain strength and develop multiple cells, as is expected according to the regime diagram of Weisman and Klemp (1982).

Degraded environmental wind

The ambient wind field is another key variable determining the evolution of convective systems. A constant bias of −2 m/s (simulation W1A) and +2 m/s (W2A) is added to the wind field of the assimilation environment, corresponding to an error of 15% with respect to the upper-level environmental wind speed. This value is comparable with the typical uncertainty in an operational NWP model at analysis time. A constant wind bias does not alter the vertical shear and the storm dynamics but changes the propagation speed of the cell. The rainfall forcing propagation velocity is therefore higher (lower) compared to the propagation velocity determined by the environmental wind of simulation W1A (W2A) and the resulting phase shift between the observations and the storm can be interpreted as a constant observation position error. If the forcing moves faster than the storm the scheme forces new updrafts ahead of the system, but is not able to suppress those downwind of the system, thus enlarging the updraft area. Since this forcing is in phase with the storm propagation dynamics the structure of the assimilated system is similar to that of the CTRL experiment (Fig. 3.13a-c), but with a 26% higher DAR

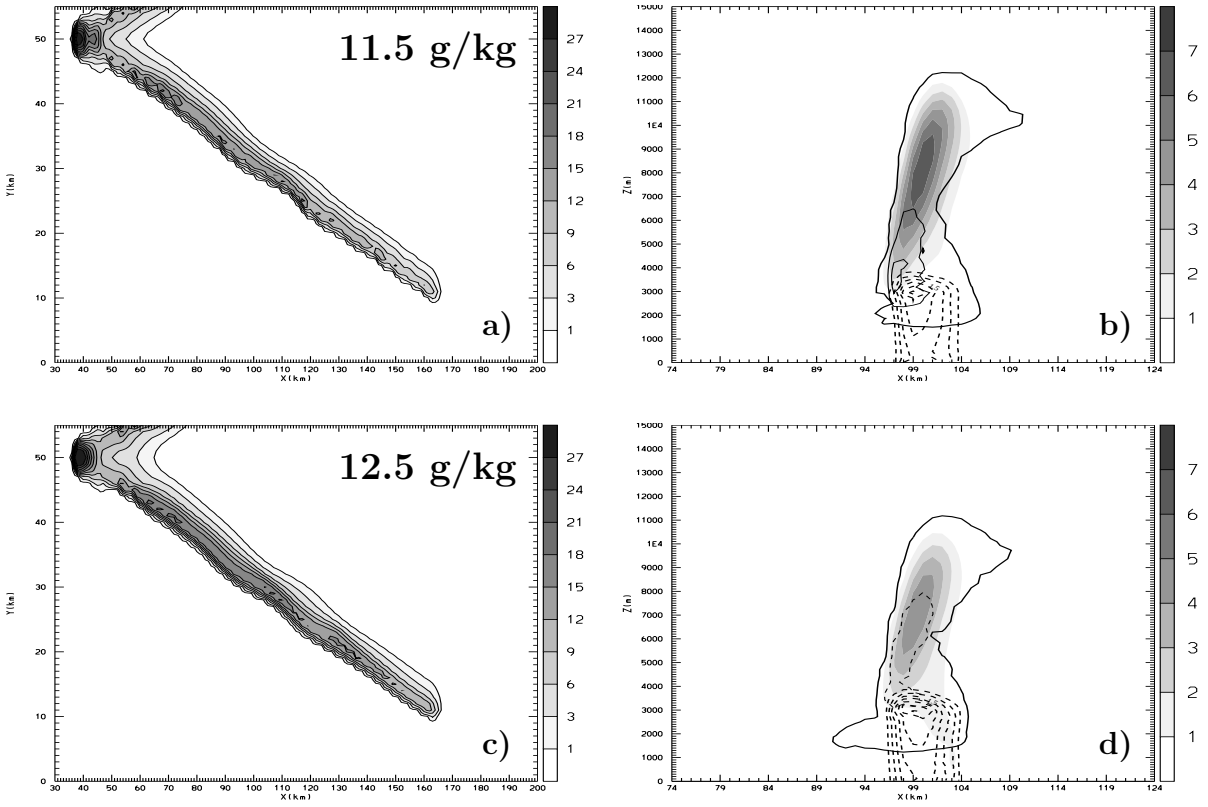

Figure 3.11: Surface precipitation and vertical cross-sections of microphysical parameters as in Fig. 3.2, but for environment error simulations. a,b) too dry boundary layer (11.5 g/kg, H1A). c,d) too moist boundary layer (12.5 g/kg, H2A).

due to the enlarged updraft area. The RMSE is three times larger than in the CTRL simulation, partly due to phase errors. A forecast initialised at 60 min from the W1A experiment yields a storm with the same structure as the reference simulation, but a slower propagation speed relative to the ground, as is consistent with the reduced wind speed of the environment.

The slower moving forcing, on the other hand, causes the LHN to decelerate the storm by cooling (heating) ahead of (behind) the storm (Fig. 3.13e). As this works against the propagation of the system interferences between the forcing and the model storm dynamics arise and cause a distorted evolution of the assimilated cell. Particularly, the surface outflow boundary is gradually decoupled from the updraft and the low-level moisture supply is cut off (Fig. 3.13f), yielding a gradual decrease in rainfall intensity (Fig. 3.13d). These effects combine to lift the level of the LH to drier regions and increase the vertical velocity without producing the required rain intensity and consequently distort the dynamical fields in this region (Fig. 3.13e). The RMSE is 5 times larger than in the CTRL simulation. In a free forecast started from the W2A experiment at 60 min the distorted storm dynamics is sustained, giving further evidence that the W2A simulation is not well balanced.

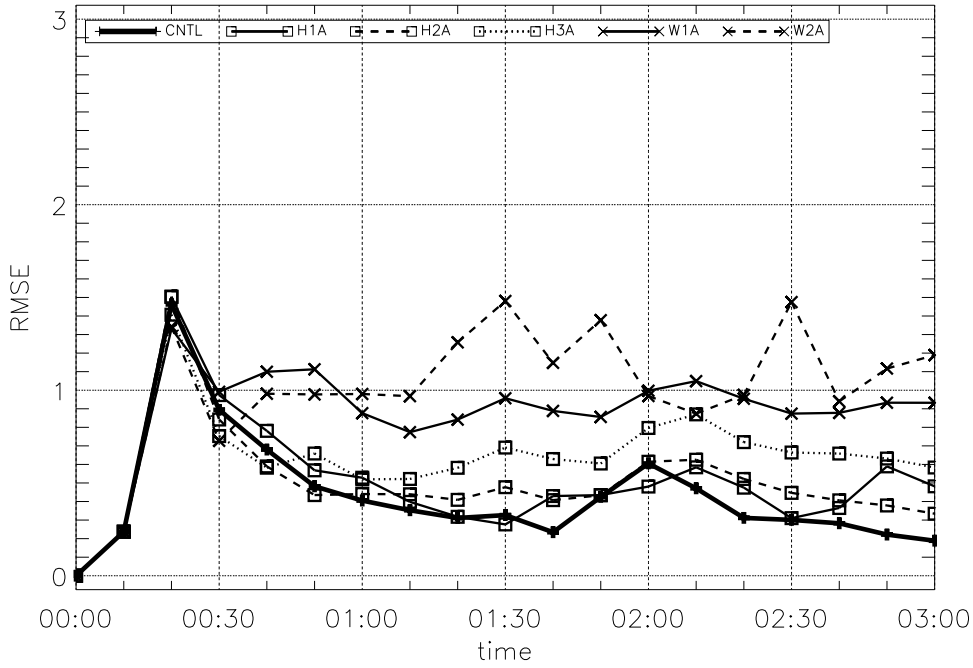

Figure 3.12: Same as Fig. 3.4, but for environment error simulations.

3.5 Summary and discussion

In this study, an attempt was made to characterise the Latent Heat Nudging (LHN) rainfall assimilation scheme within a meso-γ scale NWP model in the framework of an idealised supercell storm. The focus of this evaluation has been placed on the dynamical structure of and the rainfall produced by the assimilated system and forecasts started therefrom.

A set of identical twin simulations have demonstrated that the scheme is well able to assimilate the dynamical storm structure and reproduce the appropriate total rainfall amount in a perfect environment within a few percent. However, a time lag in the initiation of the system inherent to the use of surface rain as observation yields a transient period during which the assimilated storm differs from the reference solution. This time lag could be reduced if cloud observations (e.g. from satellites) would be assimilated instead of latent heating derived from rain observations. Forecasts started during this phase are clearly inferior to those initialised after the transient period. The duration of this period depends on the atmospheric environment and the type of convection connected to it, the model characteristics (e.g. the microphysical treatment of precipitation) and the nudging constant of the LHN scheme. The quality of the analysis seemed to be superior if the onset of the convection occurred during the assimilation period as compared to a start of the assimilation during the steady state of the storm. This result points to the need of a large radar composite capturing the onset of convection in as large an area as possible.

The LHN scheme, when applied to severe convection, appears to necessitate a careful tuning. Even in a perfect environment and assuming a perfect model the assimilated storm may differ considerably from the reference counterpart for a certain combination of scheme settings. Observation filtering and a limitation of the latent heating scaling

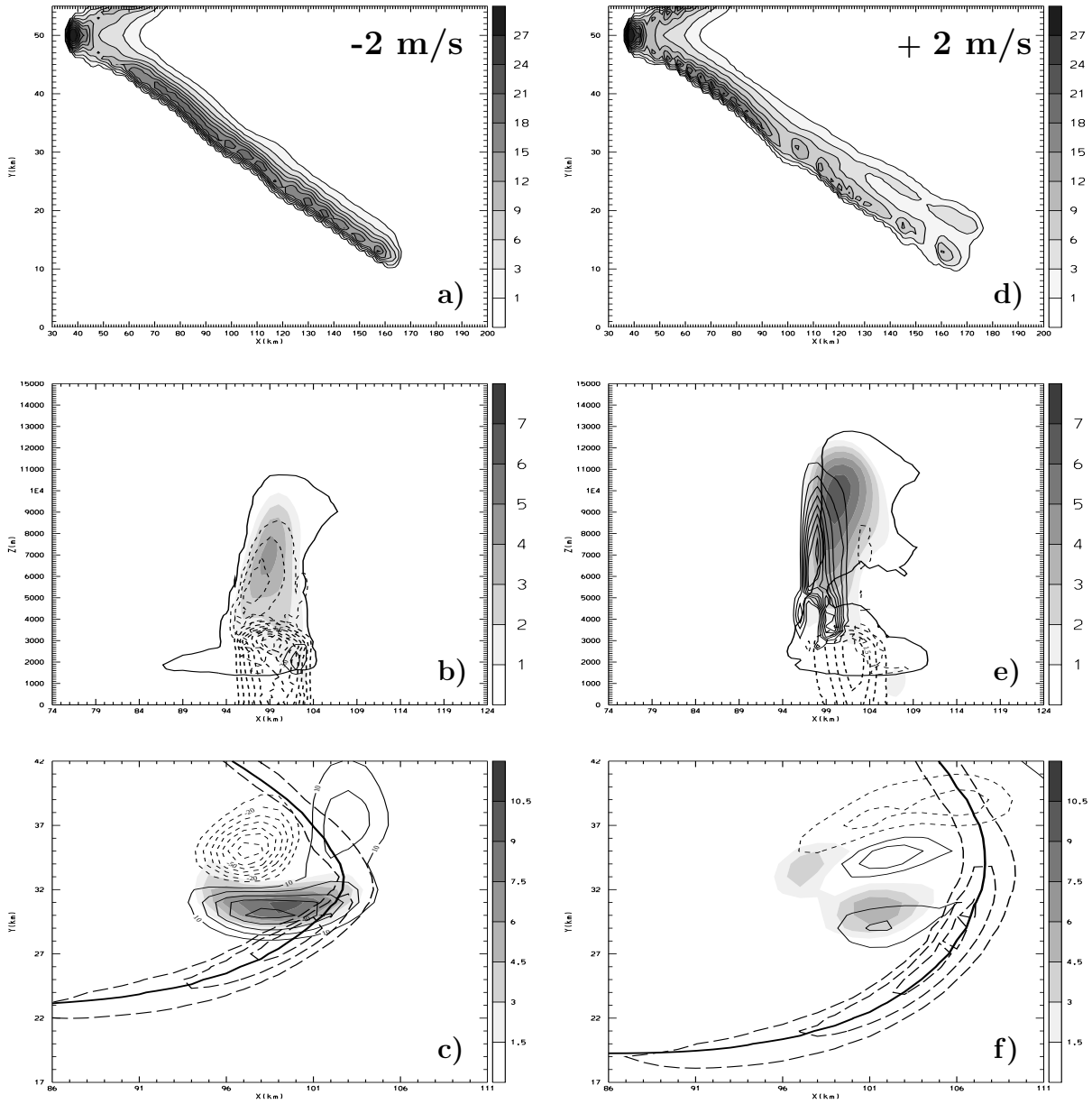

Figure 3.13: Same as Fig. 3.2, but for environment error simulations. a-c) negative bias in environmental wind (W1A). d-f) positive bias in environmental wind (W2A).

factor to a value of 2 turned out to be crucial for a successful assimilation. Identical twin experiments proved to be a useful test bed for tuning the LHN scheme.

Since real surface rainfall observations derived from radar are far from perfect, we have explored the scheme's sensitivity to observation uncertainty in a number of experiments using a perfect environment but a degraded rainfall input. In contrast to previous studies where LHN has been applied to larger scale rain systems (Manobianco et al., 1994; Chang and Holt, 1994) our results have shown that an observation amplitude error can have a negative impact in the assimilated storm and forecasts initialised therefrom in that the latter can develop multiple cells. An even higher sensitivity has been observed related to observation insertion frequency. A simple linear interpolation between subsequent observations may not be suited for fast moving and coherent signals. An enlarged

forcing region at time steps between two observation times resulting from the inappropriate interpolation has proven to trigger widespread convection and thus storms which differ substantially from the 'truth'. This result confirms previous findings that position and structure errors in the observations constitute a serious problem in rainfall assimilation and points to the need of improved interpolation techniques and/or observations with a sufficient temporal resolution.

The evolution of convective storms is strongly dependent on the atmospheric environment in which they are embedded. A series of experiments using perfect observations but degraded low-level humidity or a bias in the wind field have been performed in order to learn about the LHN scheme's sensitivity related to the uncertainty in the environment. Changes in the low-level humidity field have been found to affect mainly the precipitation amplitude but not the dynamical structure of the assimilated storm with a fast adaptation to the system dynamics determined by the environment during the free forecast.
A constant bias in the environmental wind field, on the other hand, has the potential to render a successful assimilation with the LHN scheme difficult, as the velocity of the forcing is not consistent with the system propagation speed determined by the wind. If the rainfall forcing moves too fast, the system propagation is supported and the assimilated storm and forecasts initialised therefrom develop properly. A too slow forcing, on the other hand, decelerates the system and eventually disturbs the system dynamics by decoupling the low-level moisture inflow from the main updrafts. This distortion is sustained in the free forecast.

The results obtained in this study are not comprehensive, but represent a first step towards determining the characteristics of the LHN scheme at the storm scale, revealing a number of important issues and problems. Moreover the present study is subject to the following limitations, in that the model used in this study does not account for the advection of precipitation. The advection of precipitation is in contrast with one of the approximations used in the LHN scheme, i.e. that the vertically integrated latent heating is proportional to the surface rain rate at each grid point, and needs further addressing. Secondly we have only considered an idealised, severe convective system which is strongly governed by vorticity dynamics. The scheme should be tested on other idealised, more microphysically driven types of convection, such as squall lines. Characterisation of the LHN scheme is further complicated in real cases of convection, but evaluation on a set of convective events is necessary to test the scheme's suitability for operational use in a next-generation NWP context.

Chapter 4

Case Studies

Abstract

In this paper the performance of the Latent Heat Nudging (LHN) scheme for high-resolution radar rainfall assimilation is investigated with meso-γ scale simulations of two severe cases of convection in Switzerland . Consideration is given to the model's ability to reproduce the precipitation and the response of the model dynamics to the continuous forcing during the assimilation as well as to the skill of free forecasts started from the LHN analyses. Further, the scheme's sensitivity to the amplitude of the assimilated precipitation is examined. The simulations are validated with radar-estimated precipitation and surface observations.

CASE 1 was characterised by a multicell storm, accompanied by damaging hail while the convective system of CASE 2 produced violent wind gusts. In both cases the LHN method is able to capture detailed precipitation structures of the convective storms, matching the model precipitation closely with the radar-estimated precipitation during the assimilation, with low amplitudes better reproduced than high amplitudes. Comparison of simulated surface variables with observations demonstrate that the low-level mesoscale structure of the atmosphere can be significantly improved with radar assimilation. In CASE 2 the severe wind gusts, entirely missed without LHN, are well captured, both in timing and amplitude at most of the stations. This holds true even for a 1h free forecast started from the LHN analysis. In CASE 1 the benefit of LHN in simulating the low-level structure of the convective system is found to be dependent on the location. While the impact is clearly positive at some stations in simulating the convective outflow structure (i.e. propagation and intensity of the cold pool and the associated gust front), other stations show an overestimation of the cold pool and the introduction of a position error in the low-level convergence connected with the main convective cell.

The performance of the free forecasts started from the LHN analyses are found to be different for the two cases. In CASE 1 the instability of the environment supports the evolution of the storm, while in CASE 2, characterised by only weak instability, the convective system rapidly ceases. Thus, if the model environment exhibits the needed instability but does not contain the trigger, as in the simulations driven by downscaled global analyses, the benefit of the LHN assimilation can last over the whole lifetime of the system. These results confirm findings of previous studies, in that the success of radar assimilation depends on the environment into which the convection is assimilated and points to the need of accurate analyses of the parameters which determine this environment.

The LHN scheme is further found to be sensitive to the amplitude of the assimilated

precipitation in that an overestimated input can lead to a too cold and overestimated outflow which in turn introduces a phase shift in the precipitation position during the free forecast. A simple bias correction can partly mitigate this problem.

4.1 Introduction

Severe precipitating weather systems carry the potential for flooding, hail, and vigorous wind gusts, thus having an immediate societal impact in that they influence our daily life on a broad range of activities as, for instance, agriculture, construction, or traffic. As such precipitation is certainly one of the most relevant parameters in forecasting the weather, and in numerical weather prediction (NWP) in particular. Yet, while general NWP has witnessed considerable progress in recent years, quantitative precipitation forecasting (QPF), especially in the convection-dominated warm season, has shown little to no improvement for many years, despite large research efforts in this field (Ebert et al., 2003; Fritsch and Carbone, 2004; Weckwerth et al., 2004). As an example, Fig. 4.1 shows the evolution of QPF skill at MeteoSwiss, the Swiss National Weather Service, during the last 10 years. The scores show large year-to-year variability while no clear trend is evident. Moreover, the skill for the summer period (red curve) is clearly lower than for the rest of the year. Also, to date a finer resolution non-hydrostatic model (dashed lines) does not perform better than its hydrostatic predecessor (solid lines). Reasons for the low summer QPF performance include the chaotic nature of moist convection inherently limiting its predictability (see e.g. Walser et al., 2004), model deficiencies, and/or insufficient resolution, and the lack of a properly defined initial model state.

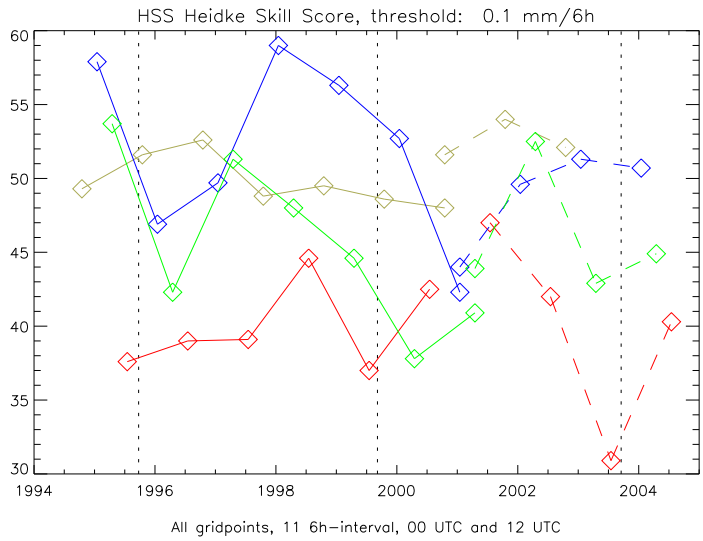

Figure 4.1: Seasonally averaged QPF performance of the operational MeteoSwiss NWP model. Green lines denote spring seasons, red summer, brown autumn, and blue winter. Solid lines denote the former hydrostatic Swiss Model ($\Delta x = 14\,\mathrm{km}$), dashed lines the current non-hydrostatic Alpine Model ($\Delta x = 7\,\mathrm{km}$).

However, numerous studies have demonstrated the potential of improving QPF using models with increased horizontal resolution (e.g. Mass et al., 2002; Ducrocq et al., 2002;

Zängl, 2004b). Next-generation operational NWP systems will run with grid spacings around 1 km and more sophisticated physical parametrisation schemes and so be able to cover the meso-γ scale, i.e. explicitly describe mesoscale flow features related to convection (e.g. Bouttier, 2003; Doms and Förstner, 2004; Michalakes et al., 2001). Such model resolution demands new, adequate types of high-resolution observations, both for initialisation and verification purposes, since the modelled scales are well below what is resolved by conventional observing systems such as surface or radiosonde networks. Doppler radar are able to provide this kind of information and have become an increasingly important complement to conventional observations for these purposes, and currently receive much attention in many research actions around the world (e.g. the COST-717 Action 'On the Use of Radar Information in Hydrological and NWP Models', Rossa, 2000). Doppler radar wind and reflectivity information offer spatial resolutions of a few kilometres and temporal resolutions of a few minutes, sufficient to capture convective scale precipitation-related phenomena and thus are particularly useful to tackle the QPF-challenge.

As the major benefit of using high-resolution models is expected at short ranges (say one hour to one day), timeliness of forecast delivery is essential in operational NWP. Coherent, fast evolving, small-scale precipitation systems have a lifetime of a few hours, thus requiring forecasts to be delivered to the forecasters and customers in no more than an hour after real time and, possibly, updated every one or two hours. In order to meet these time constraints a very efficient observation acquisition and assimilation system is essential.

While for large-scale NWP data assimilation systems four-dimensional variational (4D-Var) methods have proven to be highly effective, there are, at present, no established procedures for assimilating cloud-scale observations (Macpherson et al., 2004; Park and Zupanski, 2003; Fritsch and Carbone, 2004). There are some successful experiences with 4D-Var at the mesoscale. Guo et al. (2000) assimilated various types of observations for a squall-line case using the MM5 4D-Var system (20 km grid spacing) and found that assimilation of precipitation helped improving the predicted squall-line structure but reported a rapid loss of the assimilated signal in the free forecast. 4D-Var has further been found to successfully capture the important mesoscale precursors of a tornadic storm, such as the wind field and instability (Zupanski et al., 2002). The applicability of 4D-Var at the storm scale was explored by Sun and Crook (1997, 1998) who assimilated 3D radial Doppler winds and reflectivity into a cloud-resolving model.

Furthermore, although they reported general success, the deployment of 4D-Var on the storm scale remains questionable in an operational context because of its excessive computational costs. For more fundamental reasons, its applicability is limited by the highly non-linear nature of the microphysical processes (e.g. Wu et al., 2000), the non-Gaussian error characteristics of precipitation, and non-linear balance relationships, all of which is in contrast to the basic assumptions made in 4D-Var (Bouttier, 2003). The computational burden is further enhanced when meso-γ scale QPF is considered in a probabilistic framework, where large ensembles need to be generated (Fritsch and Carbone, 2004). Ensemble Kalman Filter (EnKF) methods, recently tested on the storm-scale (Snyder and Zhang, 2003; Zhang et al., 2004; Dowell et al., 2004), could provide this probabilistic component in theory, but initialising the ensemble members with an adequate spread that is maintained during the assimilation cycle is still a subject of current research.

Besides the very substantial efforts invested in the development of statistical data assimilation methods, like 4D-Var or EnKF, simpler and more economical schemes for cloud-scale radar data assimilation have recently received notable attention. The ARPS

(Advanced Regional Prediction System) Data Analysis System (ADAS) of the Center for Analysis and Prediction of Storms (CAPS) combines the assimilation of surface observations and a cloud analysis scheme (Zhang, 1999) including radar and satellite data to obtain a 3D representation of moisture and cloud water. Xue et al. (1998) applied this scheme to a squall-line case and identified radar data as the observation with the largest positive impact for the storm assimilation. Ducrocq et al. (2000), developed a similar method and applied it successfully on a number of heavy precipitation events in France (Ducrocq et al., 2002). In the absence of large-scale forcing, the introduction of mesoscale flow patterns in the model's initial state turned out to be crucial, i.e. the combination of both surface, and radar and satellite observations, was found to be critical for a successful initialisation and subsequent forecast of the storm.

Operational experience at the Met Office with radar data assimilation in the regional forecast model using the Latent Heat Nudging (LHN) method (Jones and Macpherson, 1997) revealed a clear positive impact on QPF in the first 18 hours (Macpherson, 2001). Moreover, in a data denial experiment, radar data was found to have the largest impact on QPF of all observations assimilated in the model (Anderson, 2001). Lin et al. (2001), using a similar scheme, also reported noticeable improvements in the first 6 hours of the precipitation forecast and a slight overall improvement over 24 hours with NCEP's operational ETA model. These results confirm that radar data can indeed be of substantial value, even when assimilated using simple schemes, both for model grids O(1 km) and O(10 km).

LHN seeks to adjusts the model's buoyancy in order to match the observed precipitation intensity and, therefore, seems to be a natural candidate for the assimilation of convective weather systems. Moreover, it allows for a timely insertion of high-frequency observations at low computational costs, features that are prerequisites for the operational assimilation of convection. Despite these appealing properties and the success of the LHN method at the meso-β scale, it has not yet been thoroughly tested at smaller scales. Leuenberger and Rossa (2005a) (LR05 hereafter) re-evaluated the LHN within the framework of a simulated supercell storm. LHN was found to have potential at the convective scale in that it successfully initialised the storm in a perfect environment and - to a lesser extent - in non-perfect environments with altered low-level humidity or wind fields.

This paper follows LR05 in that it explores the performance of the LHN in high-resolution simulations of two severe cases of convection in Switzerland. Consideration is given to the response of the model dynamics to the continuous forcing during assimilation time, and to the performance of free forecasts started from the LHN analyses. Further, the sensitivity of the scheme to the amplitude of the target precipitation is examined. To this end the simulations are validated against independent surface observations of MeteoSwiss' surface observing network. The radar data, the numerical model and assimilation scheme as well as the evaluation methods used in this study are set out in section 4.2 while the case studies are introduced in section 4.3. The results of the simulations are presented in section 4.4 and discussed in the final section 4.5.

4.2 Methodology

4.2.1 Radar Data

The Swiss Radar Network (SRN Joss et al., 1998) consists of three C-band Doppler radars of the same type, providing full volume information every five minutes. The data are preprocessed and made available on a Cartesian grid with a mesh size of $2 \times 2 \times 1\,km^3$ for the network composite. Radar observations, by virtue of their spatial and temporal coherence, open the way for a variety of nowcasting applications, and the initialisation and verification of high-resolution NWP models, tasks for which rain gauge measurements alone would not be sufficient.

However, estimating surface rain rates from radar observations, especially in complex terrain, is a challenging task. Radars measure backscattered electromagnetic signals only, giving rise to a number of problems in the quantitative precipitation estimation (QPE) at the surface, notably: strong ground clutter including anomalous propagation, (partial) shielding combined with the vertical reflectivity profile, beam-broadening and partial beam-filling, variations in the reflectivity-rainfall ($Z - R$) relationship and beam attenuation (especially for long ranges and cases of intense precipitation) (Germann and Joss, 2004). At MeteoSwiss, large efforts have been invested into overcoming some of these problems over the past decade, yielding, for example, the operational radar product RAIN, a two-dimensional map with the best surface QPE over Switzerland. For an overview of the quality of the RAIN product, see (Germann et al., 2004).

For the purposes of this study the QPE quality of RAIN has been assessed on a daily basis with a set of 58 rain gauges within a distance of 155 km. On 21 August 2000 an underestimation of approximately 30% has been found for the Swiss Plateau, with better quality in the northern and eastern part and worse in the western part and towards the foothill of the Alps. On 8 May 2003 the quality assessment was more difficult, as the radar-gauge ratios were very variable in space. The radar showed a general overestimation by a factor of 3 with ratios up to 10. The change from underestimation in 2000 to an overestimation in 2003 can be partly explained with an increase of the radar constant in 2003 (see Germann et al., 2004). Since this event was characterised by severe hail which cannot be measured accurately either by the gauges or by the radar, the radar-gauge ratios have to be taken with great care. Therefore, the large discrepancy on the 8th May 2003 provided motivation to test the sensitivity of the LHN scheme to precipitation amplitude by assimilating uniformly scaled radar-derived QPEs (see section 4.4.1).

4.2.2 The numerical model

Numerical simulations are conducted with the Lokal Modell (LM) developed within the Consortium for Small Scale Modelling (COSMO) and deployed operationally at five European National Weather Services. The model solves the three-dimensional, fully elastic and non-hydrostatic atmospheric equations on an Arakawa-C grid using the split-explicit technique described by Klemp and Wilhelmson (1978). Prognostic variables include the three Cartesian velocity components (u, v and w), temperature (T), pressure perturbation (p') and mass fractions of water vapour (q_v) and cloud water (q_c). The parametrisation for grid-scale precipitation considers four categories of water (water vapour, cloud water, rain and snow). The mass fractions of rain water (q_r) and snow (q_s) are treated diagnostically for reasons of efficiency. A mass flux convection scheme after Tiedke (1989) is

available. Shortwave and longwave radiation is parametrised by the Ritter and Geleyn (1992) scheme. Vertical subgrid turbulence is parametrised following Mellor and Yamada (1982) and the surface flux formulation is based on a roughness-length specifying the drag-coefficients for turbulent momentum and heat exchange with the ground. A force-restore soil model using five soil types determines surface temperature and humidity over land. For a more complete description of the model we refer to Doms and Schättler (2002) and Steppeler et al. (2003).

In the vertical, a stretched, terrain-following grid after Gal-Chen and Sommerville (1975) is employed composed of 45 levels and separated by 67 m near the ground and 2000 m near the model top at 23500 m. Above 11000 m a Rayleigh damping layer is used to absorb vertically propagating waves. In order to damp grid-scale noise, fourth-order numerical diffusion is applied.

4.2.3 Assimilation method

The Latent Heat Nudging scheme used in this study is based on that developed by Manobianco et al. (1994) for the assimilation of satellite-derived rainfall observations into a large-scale model and adopted by Jones and Macpherson (1997) for the use with radar QPE. The main principle is to correct the model's latent heating at each time step by an amount calculated from the observed and the modeled precipitation, where the assumption is made that the vertically integrated latent heating is proportional to the surface rain rate. This extra heating then acts as a source term in the prognostic model temperature equation and thus introduces changes in the buoyancy which in turn affects the precipitation building processes. The vertical distribution of the forcing is taken from the model, which allows for consistency with the model's parametrisation schemes and the temporal evolution of the profiles. The LHN temperature increments are calculated from

$$\Delta T_{LHN} = (f - 1) \cdot \Delta T_{LH}^{mod} \tag{4.1}$$

where ΔT_{LH}^{mod} is the model latent heating calculated from processes that involve the phase changes of water. $f = RR_{ana}/RR_{mod}$ is the scaling factor determined from the ratio of an analysed rain rate RR_{ana} and the model rain rate RR_{mod}. The minus one takes into account the model latent heating added in the previous time step. The analysed rain rate is a weighted sum of the radar-estimated and the model rain rate:

$$RR_{ana} = w \cdot RR_{rad} + (1 - w) \cdot RR_{mod}. \tag{4.2}$$

At gridpoints where the model rain rate RR_{mod} is less than RR_{ana}/α_{up} (including the no rain case), no appropriate model latent heating profile is available at that point for the calculation of the assimilation increment and a more appropriate profile is searched for at surrounding gridpoints and used for the scaling. If the search is not successful, a climatological profile is taken. In the case of an overestimation of the model rain rate, the scaling factor is limited to $1/\alpha_{down}$ in order to prevent the scheme from removing too much heat from the model. LR05 found that a careful tuning of the LHN scheme is necessary for application in a convective system. Therefore we use their scheme settings for this study: α_{up} and α_{down} are set to a value of 2, RR_{ana} and RR_{mod} are filtered before the calculation of f and the subcloud part of the model latent heating profile is not used for the scaling.

The observation weight $w = w(x, y, t) \in [0, 1]$ allows for a treatment of the radar

quality. For $w = 1$ the analysed rain rate is equal to the radar-estimated rain rate, where for $w = 0$ the observations are disregarded and the analysed rain rate equals the model rain rate. Jones and Macpherson (1997) proposed a simple function dependent only on the distance to the next radar station, accounting for the beam broadening error of the radar which increases with distance. Macpherson et al. (2001) improved the weight by additionally considering the time dependent number of radar stations contributing to the composite and, more important, the uncertainty of radar measurements extrapolated to the surface from above the freezing level.

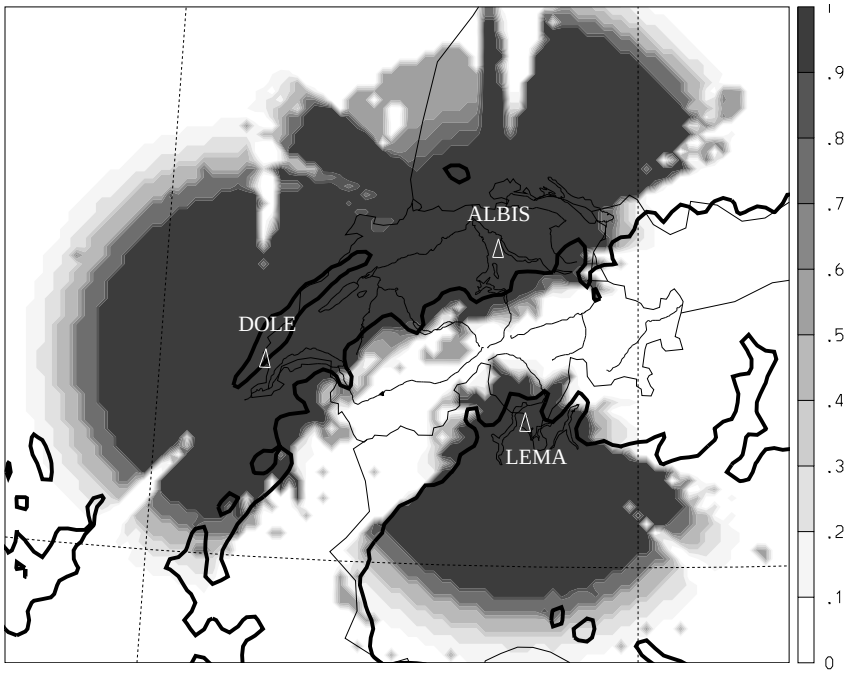

Figure 4.2: Observation weights used in the LHN scheme as derived from radar data quality indicators of the SRN composite interpolated onto the 7 km model grid. Dark shading denotes high quality, bright values low quality. The bold solid line outlines the 1000 m contour of the model topography . The white triangles mark the locations of the three SRN radar sites. Note, that the weight is high for the area of development of the examined cases.

As in mountainous terrain shielding and partial shielding by the orography are among the dominant error sources (see section 4.2.1) we propose a new weighting function based on a visibility map. A good first guess of the radar visibility can be obtained by a geometrical simulation in which the visibility is calculated ray by ray by combining a digital terrain model and the radar beam propagation properties. The height above sea level of the lowest radar measurement contributing the corresponding surface precipitation value is obtained for each radar pixel. Low values mark high surface QPE quality, high values less reliable measurements. Moreover, since a wet observation is more likely to be accurate than a dry observation (in a yes/no sense), wet observations are assigned a higher quality for the same visibility. The visibility values are mapped to the observation weight as follows: Visibility values less than 2000 m result in a maximum weight of 1. Between 2000 m and 4000 m the weight decreases linearly to $w = 0.5$ for wet observations

and to $w = 0$ for dry observations. A similar relation was used by Jones and Macpherson (1997) to calculate the weight from the distance to the nearest radar. Figure 4.2 shows the observation weighting function w interpolated to the model grid ($\Delta x = 7\,\text{km}$) for the SRN composite. Dark shading results in areas of good radar visibility and denotes high quality with associated large weights. On the other hand, bright shading denotes lower quality with correspondingly lower weights, resulting from areas where the radar beam is blocked by elevated terrain (see 1000 m contour) and at long ranges. If just one or two radar stations contribute to the composite, the weight is adjusted accordingly, resulting in a time dependent quality function. This weight could be easily extended to take into account other quality information, like clutter maps or vertical reflectivity profile corrections, once such is available.

The LHN scheme allows, as an option, an adjustment of the humidity in addition to the latent heating. This is accomplished by retaining the relative humidity during the LHN temperature adjustment. At gridpoints where a positive (negative) temperature increment is applied, this results in an increase (decrease) of the water vapour q_v. At locations were $f > 1$ (i.e. where precipitation should be enhanced in the model), q_v is additionally nudged towards saturation. A similar humidity adjustment was proposed by Manobianco et al. (1994). In this study, the humidity adjustment was found to be beneficial and was applied in all simulations.

LR05a demonstrated that the LHN scheme was highly sensitive to the insertion frequency in the case of a fast moving, coherent system in an unstable atmosphere. Therefore, radar data is provided at the frequency of the Radar Network, i.e. every 5 min.

4.2.4 Evaluation methods

Quantitative verification of precipitation is a difficult task, especially at the convective scale. Small precipitation systems may be only partially captured or even missed by rain gauges because of the large variability of rainfall in time and space (e.g. Germann and Joss, 2001). On the other hand, radar-derived precipitation is afflicted with large uncertainties (see section 4.2.1). We therefore evaluate the simulated rainfall both subjectively and quantitatively with radar QPEs exercising the necessary care.

For the quantitative precipitation verification we use radar data interpolated to the respective model grid (7 km or 2.2 km) and only consider those gridpoints, where observations are available. The areal mean precipitation is defined by

$$\overline{O} = \frac{1}{N}\sum_{i=1}^{N} O_i \qquad \overline{P} = \frac{1}{N}\sum_{i=1}^{N} P_i, \tag{4.3}$$

where N is the number of gridpoints and O and P refer to the observed and predicted rainfall values, respectively. Moreover, based on 2×2 contingency tables (Table 4.1) for different thresholds, the equitable threat score (ETS) (see e.g. Joliffe and Stephenson, 2003) has been calculated using

$$ETS = \frac{a - a_r}{a - a_r + b + c}, \qquad a_r = \frac{(a+b)(a+c)}{a+b+c+d}, \tag{4.4}$$

with a, b, c, d denoting the values of the contingency table and a_r the number of hits expected due to chance.

The equitable threat score is the percentage of hits (a in Table 4.1) that are not forecast due to chance ($a - a_r$), i.e. it measures the performance relative to a random forecast. A perfect forecast yields $ETS = 1$, a random forecast $ETS = 0$, while a forecast that is systematically worse than chance $ETS < 0$. It has the following appealing properties and is therefore widely used for precipitation verification: It is equitable (i.e. constant forecasts of 0 or 1 give $ETS = 0$), does not overly weight correct rejections (d in Table 4.1) (since those typically occur very frequently) and does not strongly depend on the precipitation probability $(a + c)/(a + b + c + d)$. The ETS does account for localisation errors and is therefore subject to a double penalty in case of phase errors. In order to mitigate this effect we calculate the ETS only for rainfall accumulations (3h, 6h or 12h) filtered with a 3-gridpoint box filter.

An independent verification of the model simulations can be obtained from surface observations from the network of MeteoSwiss (ANETZ). The stations have a mean spatial resolution of $30 - 40$ km and provide a variety of meteorological parameters every 10 min. We use 10 m maximum wind gusts measured during the last 10 min, 2 m temperature, 2 m relative humidity and station surface pressure of 15 selected stations, all being located on the Swiss Plateau below 800 m above sea level. For comparison the model gridpoint closest to the station is selected, resulting in a maximum location mismatch between model and observation of 1.5 km for the 2.2 km grid. In order to account for the difference between the station height and the corresponding height of the model gridpoint the model values of 2 m-temperature are corrected using a lapse rate of 0.6 K/100 m and the model surface pressure is corrected with the barometric formula. The maximum height difference between a model gridpoint and the corresponding station amounts to 85 m for the 2.2 km grid. All other model variables are not corrected.

	Observation $\geqslant$ threshold	Observation $<$ threshold
Forecast $\geqslant$ threshold	a	b
Forecast $<$ threshold	c	d

Table 4.1: Schematic contingency table for the definition of the ETS

4.3 The case studies

For the purposes of this study, two cases of severe convection over the Swiss Plateau have been analysed in some detail, one on 8 May 2003 (hereafter CASE 1) and the other on 20/21 August 2000 (CASE 2). Both cases exhibited radar echoes above 47 dBZ in the systems mature stages and thus can be categorised as mesoscale convective systems (MCS) following the definition of Schiesser et al. (1995). Such systems occur frequently in the northern foreland of the Alps during summer and can cause severe local flooding and/or damage through hail and strong winds. In both cases a cold front was involved in triggering the convection.

4.3.1 CASE 1 (8 May 2003)

On 1200 UTC 8 May 2003, a meridionally oriented upper-level trough was located over Spain. The associated southerly flow impinging on the Alps attained values of 30 knots

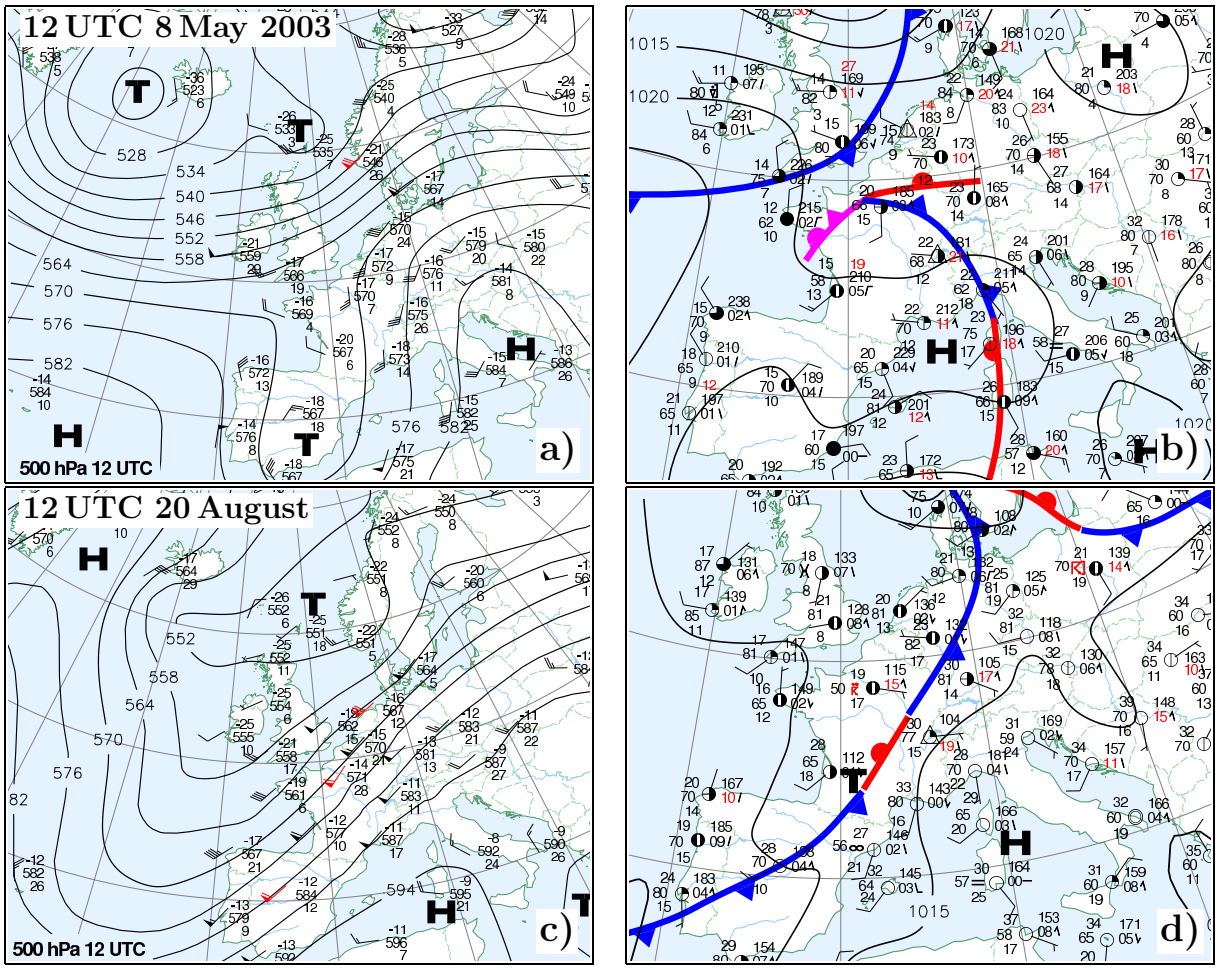

Figure 4.3: MeteoSwiss analyses of the 500 hPa geopotential height (left panels, in dm), and mean sea level pressure including surface fronts (right panels) for CASE 1 (upper panels) and CASE 2 (lower panels).

at 500 hPa (Fig. 4.3a). A cold front connected to a surface low located over Spain a day before, has reached Switzerland from the South-west (Fig. 4.3b). Ahead of it, warm and moist air was advected at low levels from the Mediterranean bringing unstable air to the region of interest. The 12 UTC sounding of Payerne of 8 May 2003, shows a conditionally unstable profile with CAPE values of 600 J/kg[1] (Fig. 4.4a). A weak inversion at 850 hPa prevented the air from spontaneous overturning (Convective inhibition (CIN) of 10 J/kg). Profiles of this type are known to be favourable for severe convective storms, especially in connection with large wind shears (e.g. Emanuel, 1994). A Bulk Richardson Number (Ri) [2] of 18 is obtained (wind shear of 21 m/s in the lowest 6000 m, clockwise turning with height).

At 1400 UTC the first radar signals appeared over the western part of the Jura mountains and the western part of the foothills of the Alps, both being preferred locations of thunderstorm formation (Linder et al., 1999; Morel and Senesi, 2002). Several cells formed along the foothills, quickly resulting in radar echoes of over 55 dBZ and moving

[1] calculated using an air parcel with a mean temperature and humidity of the lowest 50 hPa

[2] defined by Weisman and Klemp (1982) as the ratio of the CAPE and the square of the mean shear of the wind speed in the lower troposphere

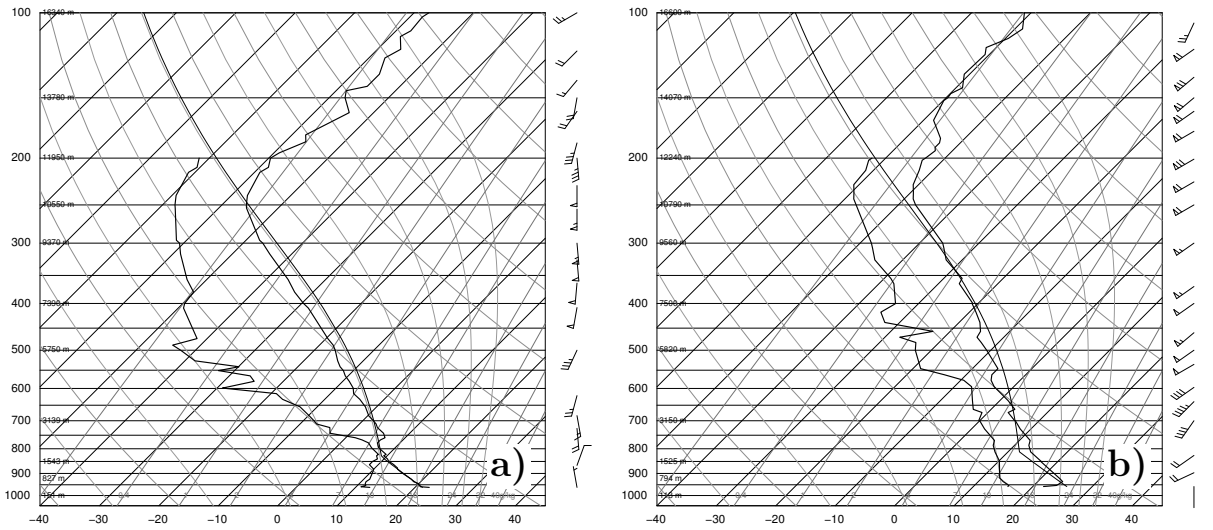

1200 UTC 8 May 2003		**0000 UTC 21 August 2000**	
CAPE (J/kg)	600	CAPE (J/kg)	226
CIN (J/kg)	10	CIN (J/kg)	97
LCL (m)	1700	LCL (m)	1900
LFC (m)	2100	LFC (m)	3100
BRN	18	BRN	2.6

Figure 4.4: SkewT-logP diagrams along with some thermodynamic quantities derived from radiosoundes of Payerne launched at 1200 UTC 8 May 2003 (panel a), and 0000 UTC 21 August 2000 (panel b).

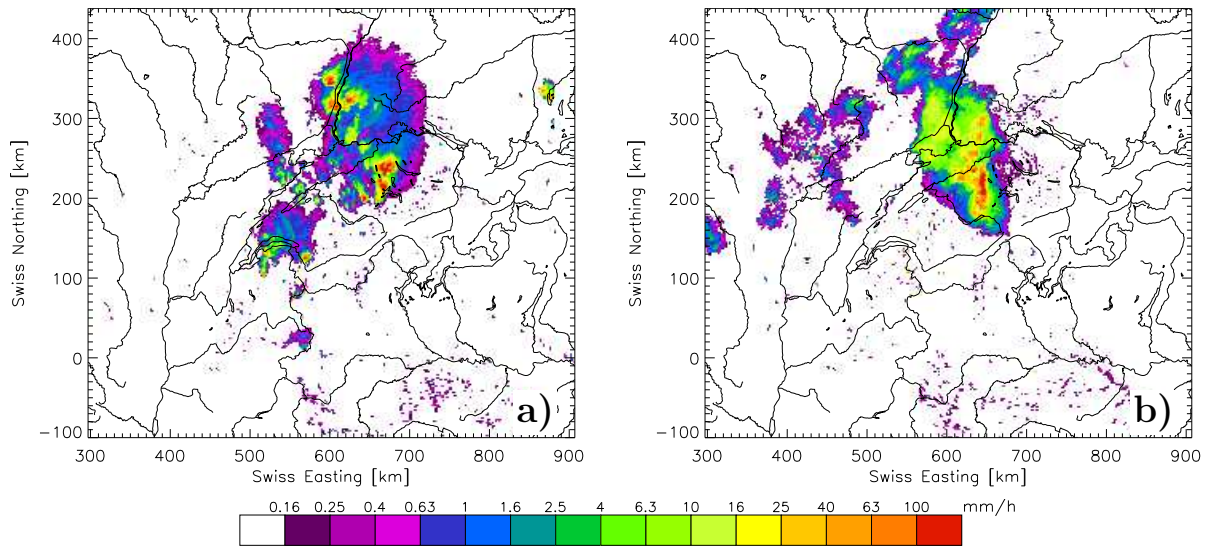

Figure 4.5: SRN QPE composite image (mm/h) derived from maximum reflectivity valid at 1800 UTC 08 May 2003 (panel a) and 0300 UTC 21 August 2000 (panel b).

with the mean wind in North-easterly direction. At 1600 UTC and 1700 UTC two large cells developed in the central part of the foothills near the surface stations used for the sounding correction. Both cells produced hail (with diameters of up to 5 cm), exhibited a movement to the right of the mean wind, and Doppler winds indicated the presence of a mesocyclone, both indications that the main cell exhibited supercell characteristics (e.g. Schmid et al., 1997). The two hail cells merged at 1830 UTC and continued their way to the North-east towards Southern Germany. The whole MCS extent, as derived from the 25 dBZ reflectivity contour, continuously increased and reached more than 300 × 200 km before leaving the SRN domain. Figure 4.5a) shows the SRN composite maximum reflectivity revealing the two main cells at 1800 UTC. Behind the main cells new convection was continuously formed along the foothills until 0000 UTC 9 May and subsequently crossed the Swiss Plateau.

The CAPE and the Ri obtained from this sounding appears to be too low considering the intensity of the storm. Thus, a pseudo sounding is constructed by replacing the temperature and dewpoint temperature values of the sounding with measurements from six ANETZ stations at heights ranging from 456 m to 2490 m. The locations of these stations are some 100 km to the east of the radio sounding of Payerne and may thus be more representative for the airmass in which the main convection was triggered. A similar correction has been done by Houze et al. (1993) for a climatological description of the environments connected with hailstorms in Switzerland. The pseudo sounding from 1500 UTC yields a CAPE value of 1600 J/kg and a Ri (using the uncorrected wind profile) of 32. According to Weisman and Klemp (1982, 1984), supercell and multicell type storms may concomitantly occur for these values. 12h-rainfall totals recorded by the ANETZ were very variable with a maximum value of 37 mm. However, since the intense cells were not very large, the ANETZ surface stations probably did not capture the most intense rainfall properly. Where precipitation fell in the form of hail, rain gauge measurements probably underestimated the precipitation, while radar overestimated it. Wind gusts connected with the outflow reached maximum values of 18 m/s. This MCS caused a hail damage of 3.5 million Swiss Francs.

4.3.2 CASE 2 (21 August 2000)

On 1200 UTC 20 August 2000 a well developed, elongated, quasi-stationary upper-level trough was situated over the British Isles, featuring wind speeds of up to 50 knots on 500 hPa (Fig. 4.3c) with the associated surface cold front located over central France (Fig. 4.3d). Temperatures of 30°C were reached at several surface stations in Switzerland.

During this day several systems of deep convection formed ahead of the cold front, one particular system was orographically triggered around 2230 UTC over the French Massif Central, well known as a favoured location for MCS triggering (Morel and Senesi, 2002). It developed into a distinct band of strong southwesterly winds and continued its way towards Switzerland, where it was reinforced several times by orography. The thermodynamic profile as measured by the Payerne radiosonde ascent of 0000 UTC 21 August reveals a weakly unstable atmosphere with a CAPE of 226 J/kg (Fig. 4.4b). This sounding is judged to be representative for the storm environment, as the system passed Payerne only 1.5 hours after its release and was confirmed by the ANETZ pseudo sounding. Around 2300 UTC the system entered the domain of the SRN. While sweeping across the Swiss Plateau with an average speed of about 22 m/s it gained strength and was accompanied by violent wind gusts (up to 33.6 m/s) which caused severe damage of more than 1 million

Swiss Francs in Switzerland. The rainfall totals measured by the ANETZ surface stations were not very high, with a maximum value of 24 mm.

The MCS can be classified as 'continuous line cell complex' according to Schiesser et al. (1995). Several convective cells with maximum reflectivity values up to 55 dBZ formed a line more or less perpendicular to their propagation direction during more than four hours. The system extended on an area (derived from the 25 dBZ reflectivity contour) of about 250 × 90 km during its mature stage. Such line-shaped MCSs are known to cause particularly strong windgusts in Switzerland (Schiesser et al., 1995). Figure 4.5b) shows a snapshot of the SRN composite maximum reflectivity at 0300 UTC. After leaving the SRN domain, it quickly decayed over Southern Germany.

4.3.3 The numerical simulations

Simulations of the two cases have been performed using the Local Model (LM) in MeteoSwiss' operational setup (mesh size of 7 km on a domain covering central Europe), and a high-resolution version of LM (mesh size of 2.2 km) on a smaller domain (see Fig. 4.6). For the high-resolution version, no cumulus parametrisation scheme is applied. The 7 km simulations are driven by the operational analyses of the continuous mesoscale nudging assimilation cycle of MeteoSwiss (LMAna, see Schraff and Hess, 2003) which includes conventional observations as upper-air wind, temperature and humidity from radiosondes, wind and temperature from aircrafts and pressure, wind and humidity from surface stations. Alternatively, interpolated analyses of the global model of the German Weather Service (GME) and the ECMWF's global model are used. The fine-scale simulations are one-way nested into the 7 km simulations. CTRL simulations denote free forecasts started from analyses, while ANA simulations start from the same initial conditions (IC) and are driven with the same boundary conditions (BC) as CTRL, but continuously assimilate radar data through LHN. The latter are used to study the performance and the dynamical impact of the LHN scheme during the assimilation period. Finally, FC simulations are free forecasts started from the LHN analyses at different times and give insight on the LHN's ability to improve upon forecast by virtue of a better initial state.

The simulations of CASE 1 are initialised at 1200 UTC 8 May 2003, two hours before the first radar signals appear, and are integrated for 12 hours. IC and BC are taken from LMAna. 7 km simulations include a CTRL (CTRL7), an ANA (ANA7), and a FC simulation started at 1800 UTC (FC718). The same strategy is used for the 2 km simulations but two additional forecasts are started at 1700 UTC (FC217) and 1600 UTC (FC216). In order to test the sensitivity to a reduced forcing, additional LHN ANA simulations were performed with a reduced weight of the LHN in the prognostic temperature equation (ANA2_RI), with corrected target precipitation (ANA2_RO), and a combination of both (ANA2_RIO).

The simulations related to CASE 2 are initialised at 0000 UTC 21 August 2000, when the convective system has already moved inside the SRN domain, and are integrated for 6 hours. IC and BC are taken from interpolated GME analyses. The same simulation strategy and notation as in CASE 1 is adopted, but the free forecasts are started at 0300 UTC (FC203/FC703). See also Tab. 4.2 for an overview of the simulations.

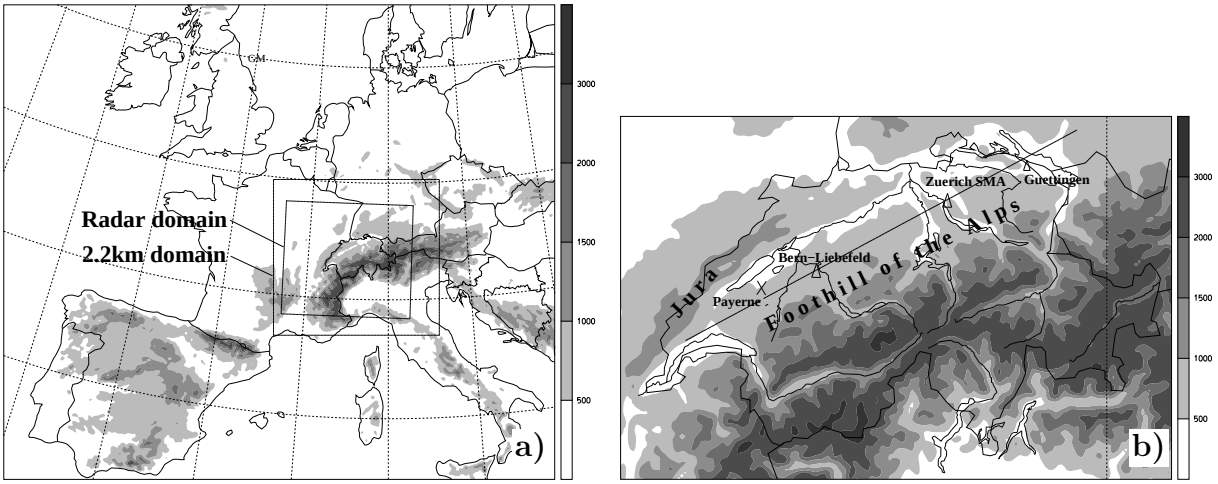

Figure 4.6: Left panel: definition of the 2.2 km LM and Swiss Radar Network domain (rectangles) in the 7 km LM domain (entire map) including topography height (in m) in grey shading. Right panel: Zoom over Switzerland. Triangles mark selected surface stations and the cross denotes the location of the Payerne radiosonde station. The location of the cross-section used in Fig. 4.12 is indicated with a line.

4.4 Results

4.4.1 CASE 1 (8 May 2003)

Performance of CTRL simulations

First the performance of the CTRL simulations in capturing the convective event is evaluated. At 1200 UTC the initial states of the CTRL simulations are characterised by a conditionally unstable atmosphere over central Switzerland with widespread CAPE values of 600 J/kg, locally reaching up to 1000 J/kg. This is consistent with the value obtained by the radiosonde Payerne from 1200 UTC (Fig. 4.4), but too low when comparing with the pseudo sounding. A convergence line associated with the cold front was developed by the model and triggered widespread convection. Figure 4.7 reveals that the overall low to medium amplitude pattern of the 12h accumulated precipitation is reasonably well predicted by both the CTRL7 and CTRL2 forecasts but not the strong signal of the main cell, which is visible in the radar QPE (Fig. 4.7c,f). CTRL2 gives more precipitation North-east of Switzerland, an indication that CTRL2 captures the later stage of the system better than CTRL7. The temporal evolution of the domain-averaged precipitation (Fig. 4.8) confirms that CTRL2 simulated well the overall timing of the event but missed the main cell, active from 1600 to 2000 UTC, resulting in an underestimation by roughly a factor of 2 during this period. A comparison of CTRL2 with surface observations of 15 ANETZ stations was carried out. Figure 4.9 shows time series of stations Bern-Liebefeld and Fig. 4.10 of Guettingen. Station Guettingen is hit by the main cell, while Bern-Liebefeld is more representative for the convection that developed before and after the main cell. CTRL2 (black, dashed lines) depicts well the convergence line associated with the main cell, as can be seen from the timing and amplitude of the wind peak at Guettingen (Fig. 4.10). Also the strength of the cold pool (temperature drop of roughly 5 K)

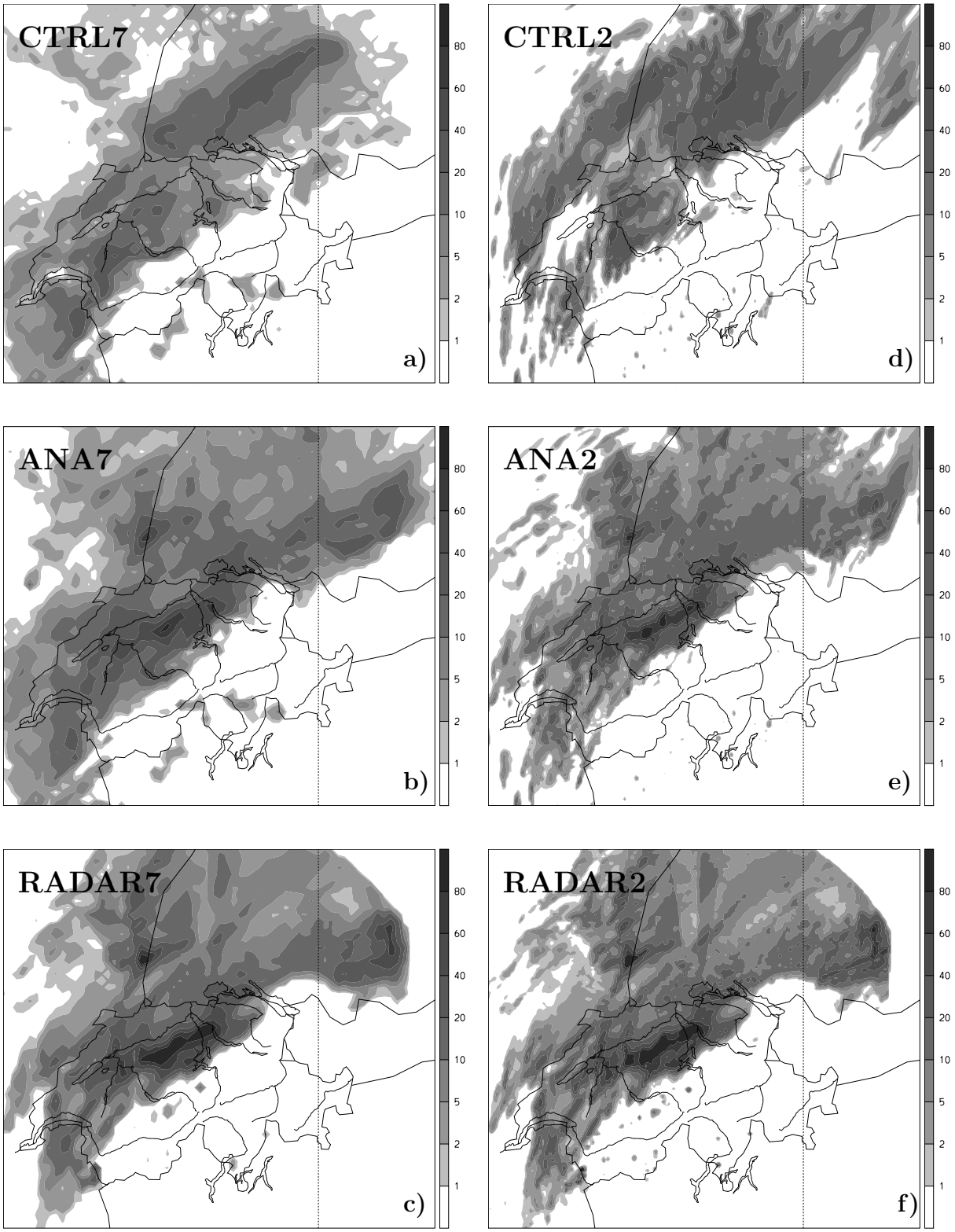

Figure 4.7: 12h-accumulated precipitation (mm) from 1200-2400 UTC 8 May 2003: a) CTRL7, b) ANA7, c) SRN radar observations interpolated onto the 7 km LM grid, d) CTRL2, e) ANA2, f) SRN radar observations interpolated onto the 2.2 km LM grid.

CASE 1 (8 May 2003)			Simulation period: 1200-2400 UTC			
Name	Grid length	IC	BC	LHN (UTC)	LHN weight	radar correction
CTRL7	7 km	LMAna	LMAna	-	-	-
ANA7	7 km	LMAna	LMAna	1200-2400	1	-
FC718	7 km	LMAna	LMAna	1200-1800	1	-
CTRL2	2.2 km	CTRL7	CTRL7	-	-	-
ANA2	2.2 km	CTRL7	CTRL7	1200-2400	1	-
FC218	2.2 km	CTRL7	CTRL7	1200-1800	1	-
FC217	2.2 km	CTRL7	CTRL7	1200-1700	1	-
FC216	2.2 km	CTRL7	CTRL7	1200-1600	1	-
ANA2_RI	2.2 km	CTRL7	CTRL7	1200-2400	0.5	-
ANA2_RO	2.2 km	CTRL7	CTRL7	1200-2400	-	1/3
ANA2_RIO	2.2 km	CTRL7	CTRL7	1200-2400	0.5	1/3
CASE 2 (21 August 2003)			Simulation period: 0000-0600 UTC			
Name	Grid length	IC	BC	LHN (UTC)	LHN weight	radar correction
CTRL7	7 km	GME	GME	-	-	-
ANA7	7 km	GME	GME	0000-0600	1	-
FC703	7 km	GME	GME	0000-0300	1	-
CTRL2	2.2 km	CTRL7	CTRL7	-	-	-
ANA2	2.2 km	CTRL7	CTRL7	0000-0600	1	-
FC203	2.2 km	CTRL7	CTRL7	0000-0300	1	-

Table 4.2: Characteristics of the different sets of numerical experiments

and the surface pressure surge after the passage of the system is well captured. The underestimated relative humidity indicates that the pre-storm low-level environment is too dry in the model. The simulated surface signals at Bern-Liebefeld also show good overall agreement with the observations, but a phase error of 60 min in the wind, temperature and relative humidity is evident at 1600 UTC, when a convective cell passed the station (Fig. 4.9).

Performance of the LHN analysis

After the first appearance of radar signals, the LHN scheme triggers convection in the model at the appropriate location within some tens of minutes and closely adjusts the model precipitation to the target precipitation. This results in a 12h accumulated precipitation well in line with the observations (Fig. 4.7e). The swath of high precipitation amplitudes connected with the main cell is clearly visible in ANA2 but the intensity is somewhat lower than observed by the radar (Fig. 4.7f). To a lesser extent the intense signals were also captured in ANA7 simulation (Fig. 4.7b), but the shape of the swath is degraded when compared with ANA2. The temporal evolution of the event is very well

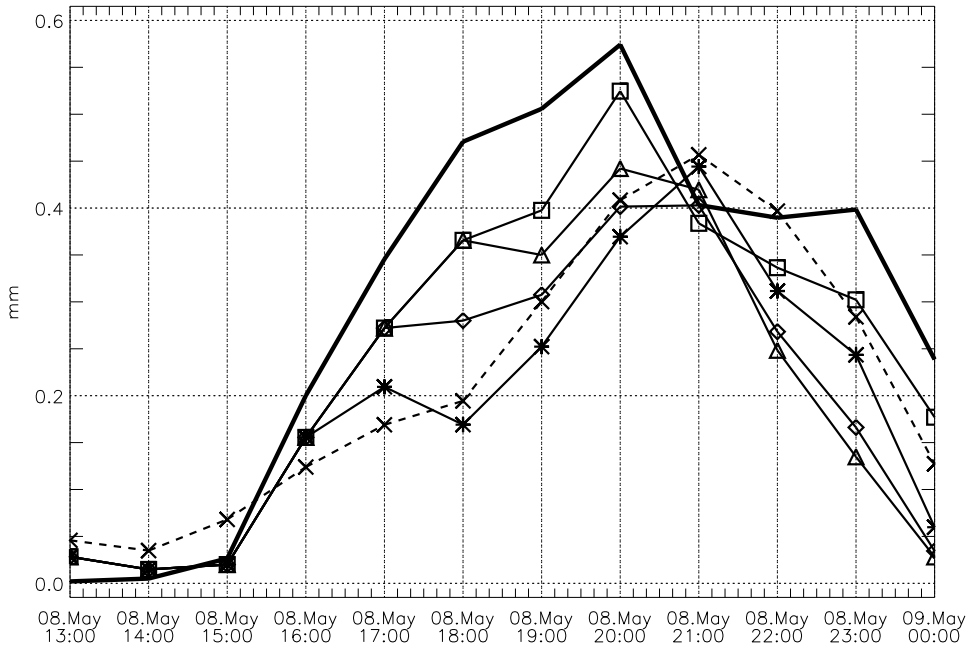

Figure 4.8: Time series of domain averaged precipitation of CASE 1 simulations compared against radar-derived QPE. The bold solid line denotes the radar QPE, the dashed line CTRL2, while squares denote ANA2, stars FC216, diamonds FC217, and triangles FC218.

reproduced in ANA2, as can be seen in Fig. 4.8 (square symbols). The LHN is able to correct the slight precipitation overestimation of the CTRL2 (dashed line) from 1300 to 1500 UTC and introduce the main cell from 1600 to 2000 UTC, QPE yielding amplitudes close to the radar observations.

Inspection of the mid-level rotation of the assimilated main cell reveals that the LHN-forced updrafts in ANA2 are able to tilt horizontal vorticity of the environmental wind into vertical vorticity (see e.g. Klemp, 1987) yielding a distinct vortex signature collocated with the most intense radar signal (Fig. 4.11b), which is confirmed by Doppler wind observations (not shown). CTRL2, on the other hand, did not produce such a vortex signature.

In order to characterise the response of the model dynamics to the continuous rainfall assimilation the outflow and the strength of the surface cold pool connected with the forced storm is examined. A comparison of the modeled surface temperatures with their observed counterparts indicates that ANA2 overestimates the low-level cooling by up to 3K at those stations influenced by the main cell (Fig. 4.9, red lines). Moreover, the drop in temperature and dewpoint depression, as well as the surge in the surface pressure occurs some $20 - 30$ min too early suggesting a phase error in the propagation of the simulated cold pool. This phase shift is even more pronounced (up to 80 min) in the ANA2 wind peak. The phase shift is constant for stations lying in the path of the cell, indicating that the convergence line does not propagate too fast, but is just placed too far downstream. The wind gusts at Guettingen are overestimated by up to 65% (28 m/s instead of 17 m/s) and live too long in the assimilation. The shift in the gust front is further illustrated with a vertical cross-section of potential temperature and relative humidity through the centre of the main cell valid at 1800 UTC (Fig. 4.12). The ANETZ stations Bern-Liebefeld and

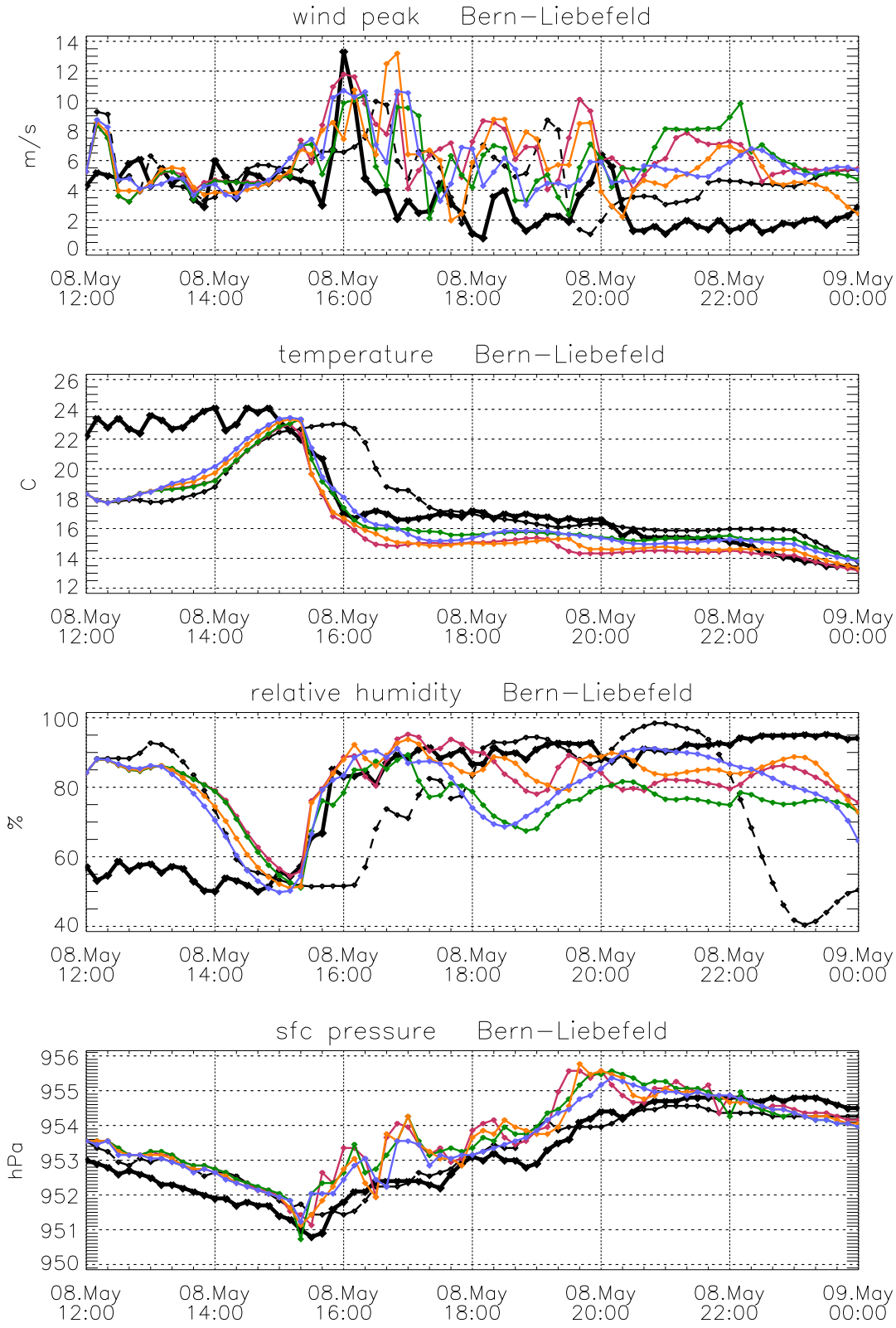

Figure 4.9: Comparison of CASE 1 simulations against surface observations of ANETZ station Bern-Liebefeld. Variables are (from top to bottom) peak 10 m wind speed during last 10 min, 2 m temperature, relative humidity, and surface pressure at station height. Black, bold, solid lines denote observations, black dashed lines CTRL2, red lines ANA2, green lines ANA2_RI, orange lines ANA2_RO, and blue lines ANA2_RIO.

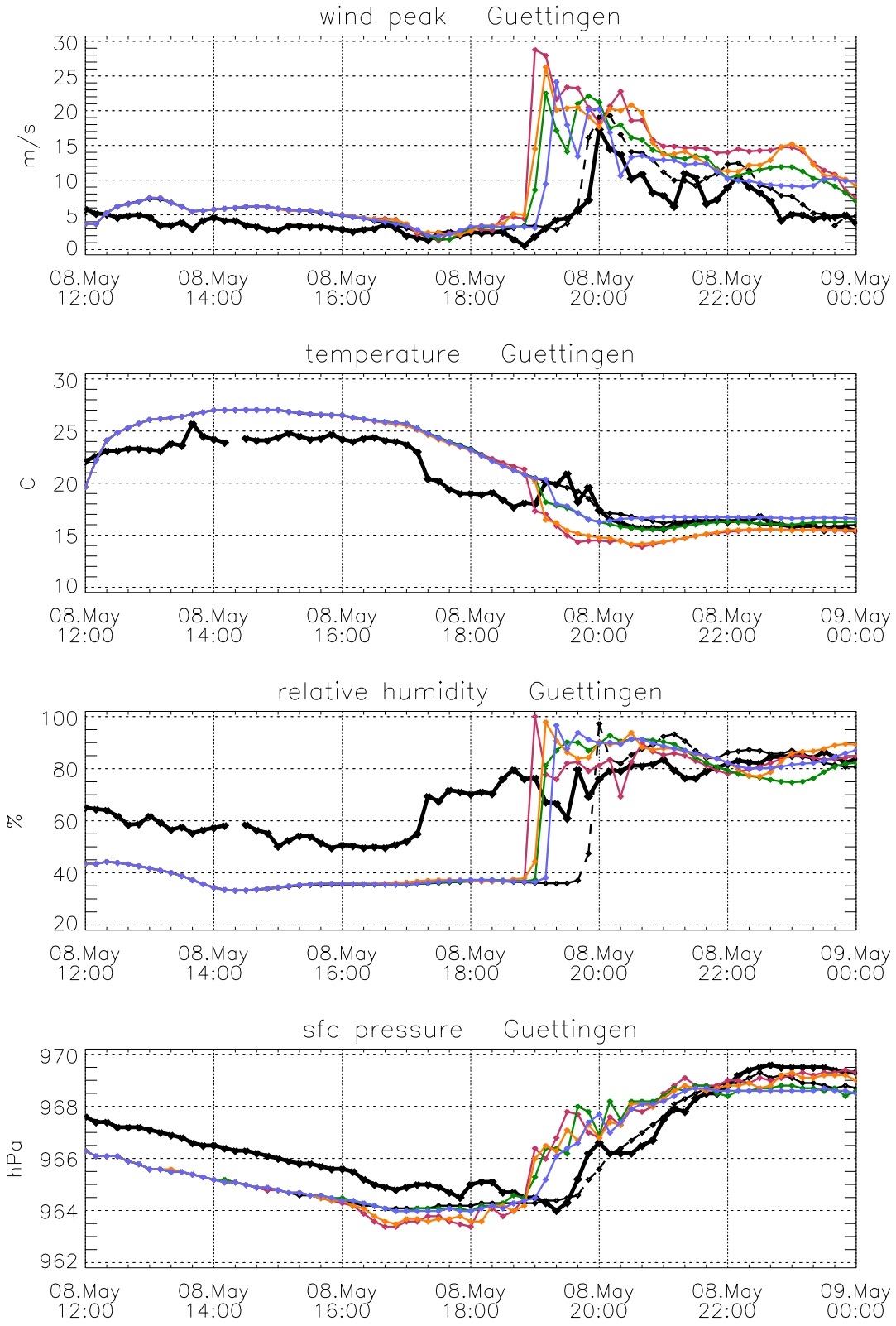

Figure 4.10: Same as Fig. 4.9, but for station Guettingen.

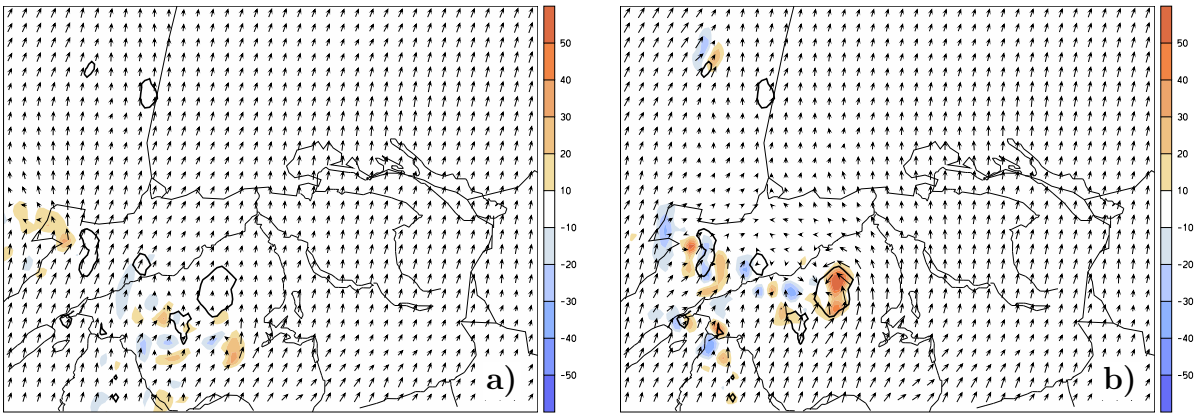

Figure 4.11: Vertical vorticity (in units of $10^{-4}\,s^{-1}$) at 5000 m (shaded), radar-derived rainrate (50 mm/h contour), and wind at 5000 m of CTRL2 (panel a) and ANA2 (panel b) valid at 1700 UTC 8 May 2003.

Guettingen are both located on this cross-section (see also Fig. 4.6b) for its position). The surface gust front, marked by the strong potential temperature gradient collocated with the interface between dry and moist air, is shifted some 40 km downstream (i.e. to the Northeast) in ANA2 (Fig. 4.12b) compared to CTRL2 (Fig. 4.12a). The shift is also evidenced in Fig. 4.13a,c), showing the position of the convergence line (bold, red contours) at 1800 UTC of CTRL2 and ANA2, respectively. The simulated surface parameters of ANA2 at Bern-Liebefeld, on the other hand, agree better with the observations than in the CTRL2 experiment. The timing in the signal associated with the convection is very well captured, indicating that the radar assimilation has a positive impact in this area. However, the cold pool is overestimated also at this station. These results indicate that the main cell cannot be accurately be captured by the model, but the surrounding convection is reasonably well simulated. An examination of the updrafts resulting from the assimilation indicates that ANA2 exhibits a stronger vertical circulation than that produced in CTRL2. The domain maximum vertical velocity of CTRL2 amounts to 13 m/s around 1800 UTC while values of up to 30 m/s result from the LHN forcing. As a result the convective system in ANA2 penetrates deeper into the stratosphere than that in the CTRL2 simulation (Fig. 4.12). Although the cell in CTRL2 is not situated at the same place as the forced (correctly located) cell in ANA2, it is considered representative for the updrafts produced in this simulation.

The stronger circulation in the ANA2 simulation yields a more pronounced stabilisation of the atmosphere than in CTRL2 as can be seen in the CAPE fields presented in Fig. 4.13. At locations upstream of the convergence line (i.e. where the storm has already passed) almost no CAPE is left in ANA2 while in the CTRL2 values of up to 1000 J/kg are analysed suggesting that a substantial amount of instability remains after the passage of the convective system.

Performance of the forecasts

The performance of the free forecasts started from LHN analyses at 1800 UTC (i.e. at a time where the main cell had been fully developed) is first discussed in terms of 6h accumulated precipitation fields (1800-2400 UTC) shown in Fig. 4.14. Neither the 7 km

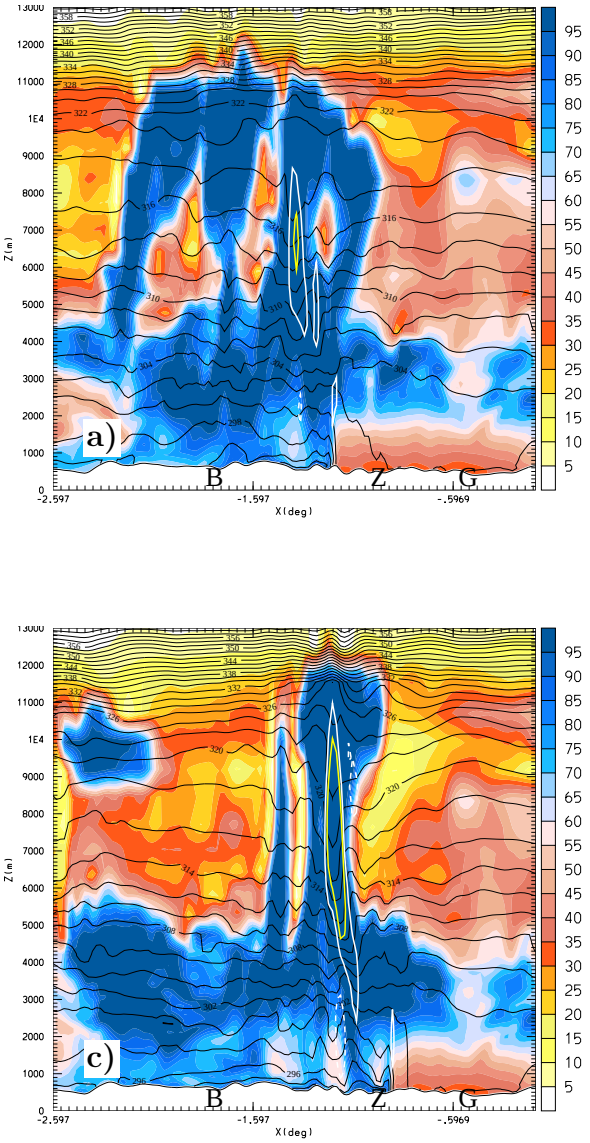

Figure 4.12: Vertical cross-sections (see Fig. 4.6 for the location) through the centre of the main convective cell at 1800 UTC 8 May 2003. Color shading denotes relative humidity (%), thin black contours potential temperature (contour interval 2 K), and thick contours vertical velocity (white 5 m/s contour and yellow 10 m/s contour, dashed contours denote downdrafts) for CTRL2 (panel a), ANA2 (panel b), and ANA2_RO (panel c). The labels 'B', 'Z', and 'G' indicate the locations of the ANETZ stations Bern-Liebefeld, Zuerich SMA, and Guettingen, respectively.

(FC718) nor the 2.2 km (FC218) forecast is able to retain the strong precipitation signal related to the main convective cell visible in the radar observations (Fig. 4.14c,f), indicating that the forced cell rapidly loses strength during the initial stage of the forecast. However, the lower to medium amplitudes are well predicted in both the CTRL and the FC simulations, where FC is slightly better over eastern Switzerland and over the Vosges but underestimates precipitation more than CTRL in western Switzerland. This underestimation is consistent with the more stable post-convective environment in the FC simulation compared to CTRL, which inhibits the development of new convection behind the main system. The effect is more pronounced in the 7 km simulations than in the 2.2 km simulations. A more quantitative evaluation of the simulated 6h precipitation accumulations has been done using objective scores for the different simulations. Fig. 4.15 presents Equitable Threat Scores (ETS) of the 6h accumulated precipitation (1800-2400 UTC) for different thresholds. The forecast started from the LHN analysis (FC218) (dotted lines with square symbols) performs slightly better than CTRL2 (dashed lines with square symbols) for the 1 mm threshold, but slightly worse for the medium thresholds, suggesting that the assimilation of radar data has a slightly detrimental effect in this case, since CTRL already had the main ingredients (instability and low-level convergence) necessary

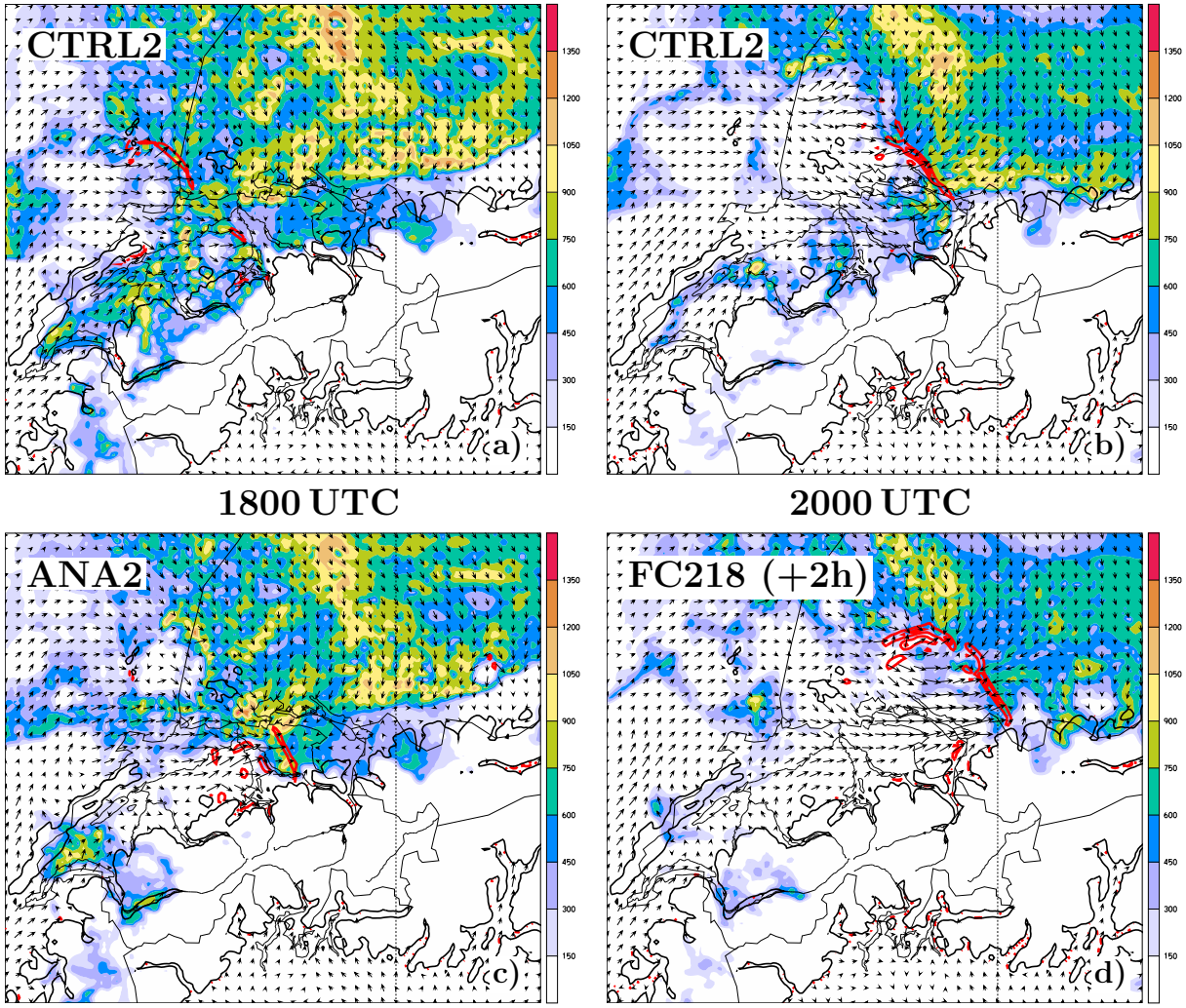

Figure 4.13: CAPE (J/kg, color shading), horizontal convergence (bold red lines, contour interval $0.002\,s^{-1}$), and horizontal wind field at 1000 m for CTRL2 (panels a and b), ANA2 (panel c), and FC218 (panel d), valid at 1800 UTC (left panels) and 2000 UTC (right panels). Wind arrows are plotted every 5th gridpoint (maximum vector 20 m/s).

to predict the overall structure of the convective system. The large intensities connected with the main cell are captured neither by FC218 nor by CTRL2. As expected, ANA2 (solid line with square symbols) is much closer to the observations, resulting in an ETS of 0.75 for light rain, gradually decreasing to 0.25 for large intensities.

The phase error of the convergence line, introduced during the radar assimilation, is retained in the free forecast. After 2h into the forecast time, the line is still shifted some 40 km to the North-east compared with CTRL2 (Fig. 4.13b,d). New convection is subsequently triggered at its leading edge, resulting in a phase shift of the whole convective system during the free forecast (Fig. 4.16). In the post-convective region (central Switzerland) the development of new convection is underestimated from CTRL2 and even more from FC218. In order to see if the evolution of the main cell in the free forecast is dependent on the initialisation time, two additional free forecasts have been performed, starting at 1700 UTC (FC217) and 1600 UTC (FC216). None of these simulations were able to retain the high precipitation intensity introduced during the LHN assimilation,

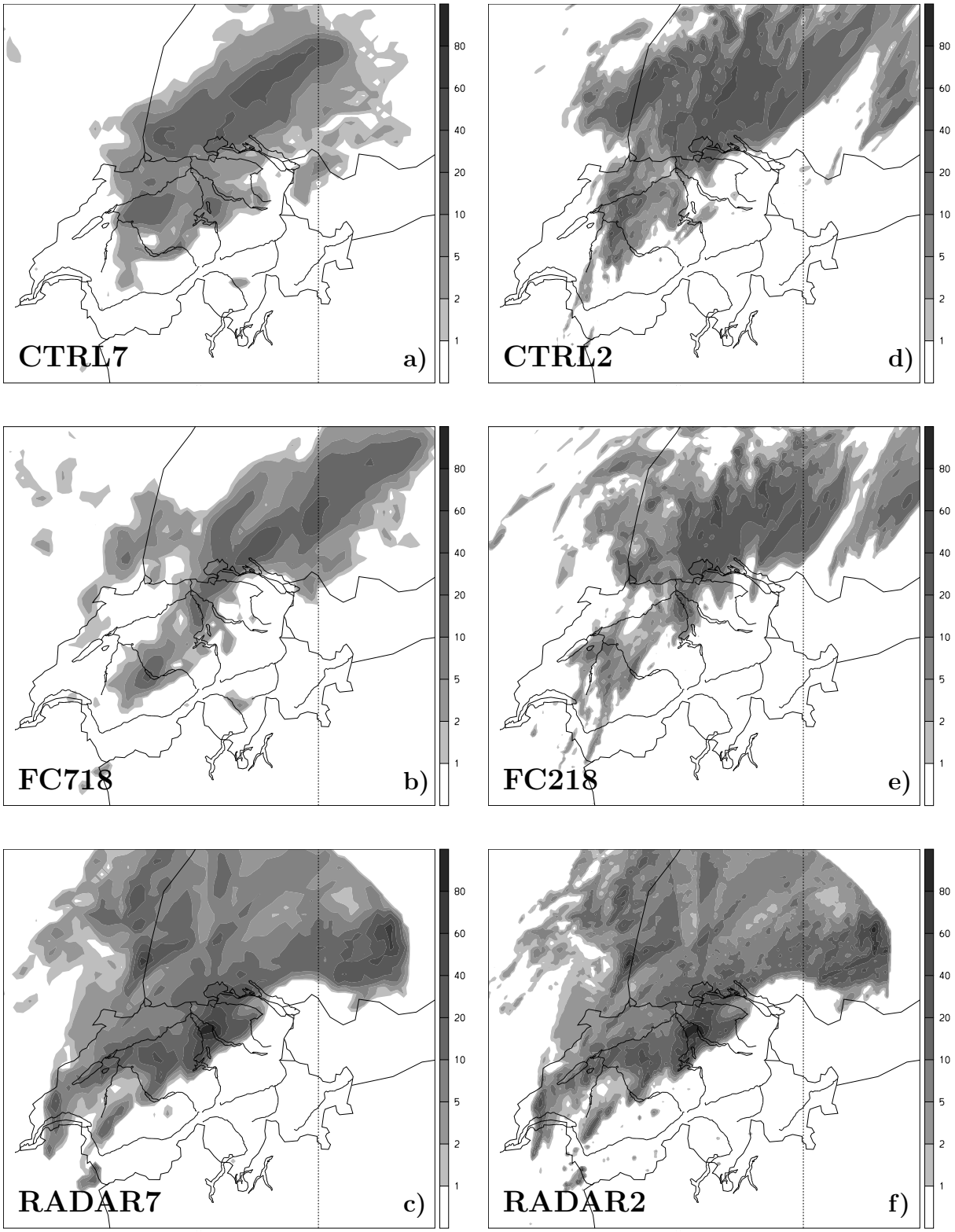

Figure 4.14: 6h-accumulated precipitation (mm) for 1800-2400 UTC 8 May 2003: a) CTRL7, b) FC718, c) SRN QPE interpolated onto the 7 km LM grid, d) CTRL2, e) FC218, f) SRN QPE interpolated onto the 2.2 km LM grid.

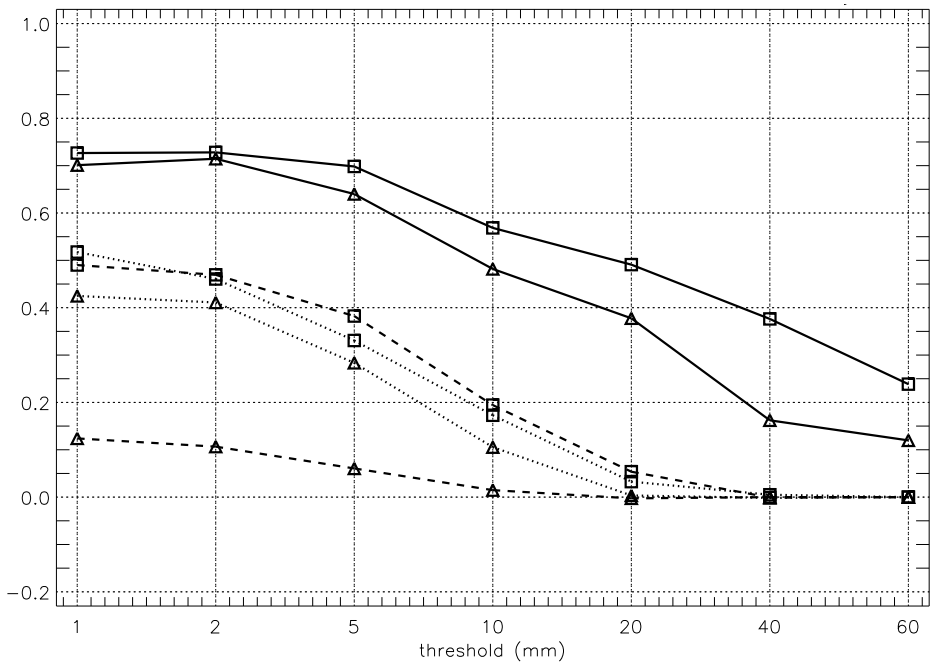

Figure 4.15: ETS for simulated 6h precipitation sums from 1800-2400 UTC 8 May 2003 compared against radar QPE. Dashed lines denote CTRL2, thin solid lines ANA2, thin dotted lines FC218. Squares stand for simulations driven by 7 km mesoscale LM analyses, and triangles for simulations driven by interpolated ECMWF analyses.

but the convective system could be kept in the model during the free forecast, irrespective of its initial time (Fig. 4.8).

Sensitivity to reduced increments and corrected radar data

Since the comparison of the simulated surface variables with the observations suggests that the LHN generates too strong a circulation in connection with the main cell (i.e. an overestimated cold pool, a too strong outflow and a phase shift in the convergence line at its leading edge), additional LHN simulations were conducted with a reduced forcing. This was accomplished by i) reducing the weight of the LHN increments in the prognostic temperature equation from 1 to 0.5 (ANA2_RI simulation) and ii) dividing the amplitude of the radar rainfall observations (i.e. the target precipitation) by a factor of 3 (ANA2_RO simulation). The choice of this factor was motivated by the rough comparison of the radar QPE with gauges (see section 4.2.1) that indicated an overestimation of the former by this amount. Note that the two methods of correction do not have the same effect: i) only reduces the amount of heating/cooling in one timestep, whereas ii) reduces the target precipitation.

Both modifications lead to improved simulated surface variables at Guettingen. Decreasing the LHN weight produces slightly lower wind gusts and reduces the phase shift of the convergence line by up to 10 min (Fig. 4.10, orange lines), but is not able to correct for the overestimated cold pool. Reducing the target precipitation has a stronger effect on the surface variables in that, in comparison with ANA2_RI, the wind gusts are weaker, the phase shift of the outflow is slightly smaller, and the cold pool is substantially improved (up to 3 K in Guettingen, Fig. 4.10, green lines). The maximum areal updrafts

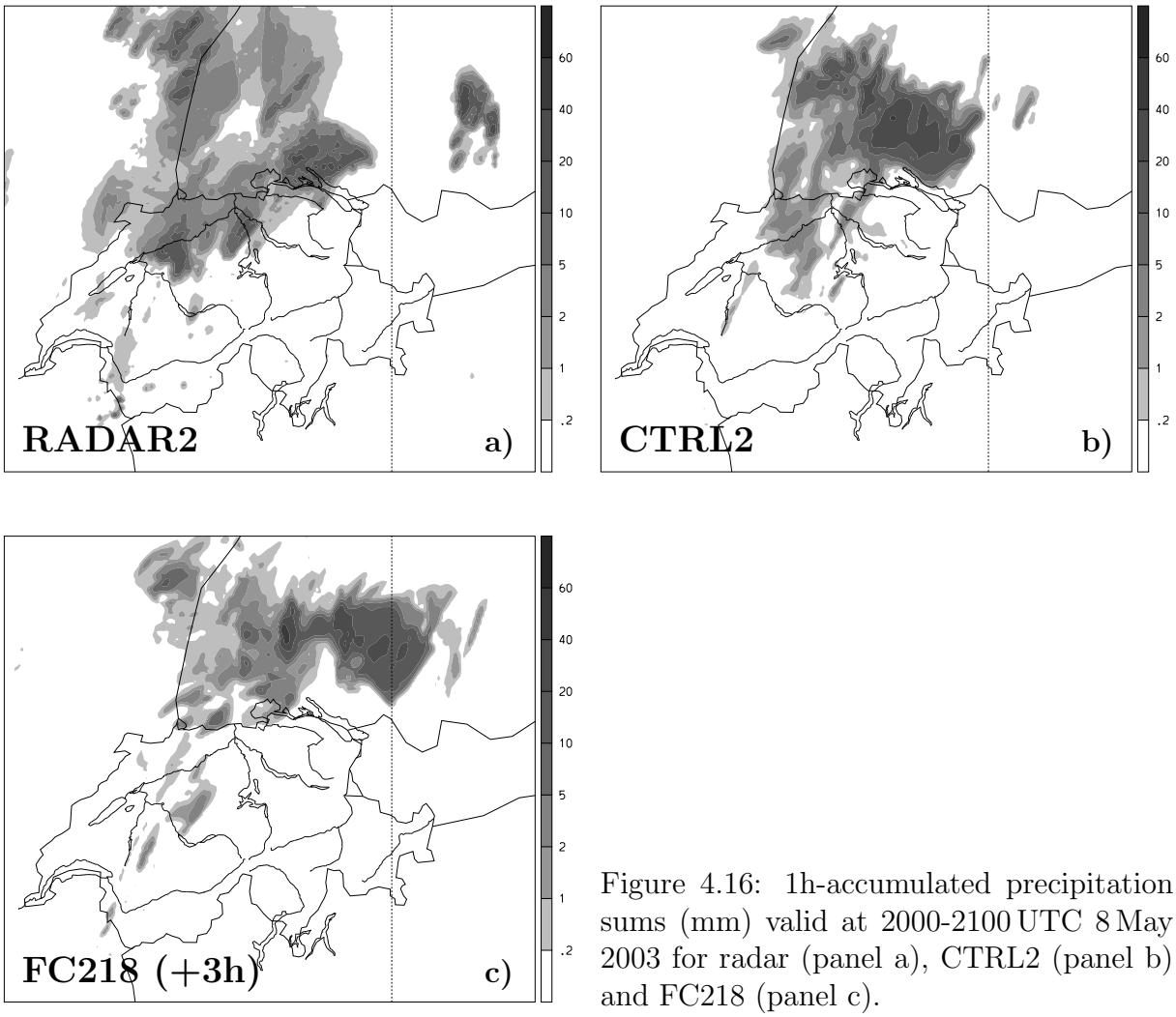

Figure 4.16: 1h-accumulated precipitation sums (mm) valid at 2000-2100 UTC 8 May 2003 for radar (panel a), CTRL2 (panel b) and FC218 (panel c).

around 1800 UTC amount to 15 m/s and are thus roughly half those obtained in ANA2 and the forced main cell shows a smaller vertical extent (Fig. 4.12c). A combination of modifications i) and ii) (ANA2_RIO, Fig. 4.9,4.10, blue lines) further improves the surface variables, suggesting that a weaker LHN forcing indeed produces a more realistic low-level cold pool. Furthermore, comparison with radiosonde measurements from Payerne 0000 UTC 9 May 2003 indicates, that the vertical structure of the post-convective atmosphere is best captured by the ANA2_RO simulation (not shown). At the station of Bern-Liebefeld, the benefit of a reduced forcing is most pronounced in the reduction of the overestimated cold pool but less evident in the other parameters. Finally, a simulation with a bias correction by a factor of 9 (not shown) further improved the errors in the surface variables, notably the phase error of the gust front.

Simulations driven by interpolated ECMWF analyses

A second set of simulations has been carried out using initial and boundary conditions from interpolated ECMWF analyses instead of the mesoscale LM analyses. These analyses differ substantially from the latter, in that the CTRL simulation driven therefrom does not develop prefrontal convergence line and fails to trigger the convective system. However, the atmosphere exhibited a similar instability in terms of CAPE as in CTRL.

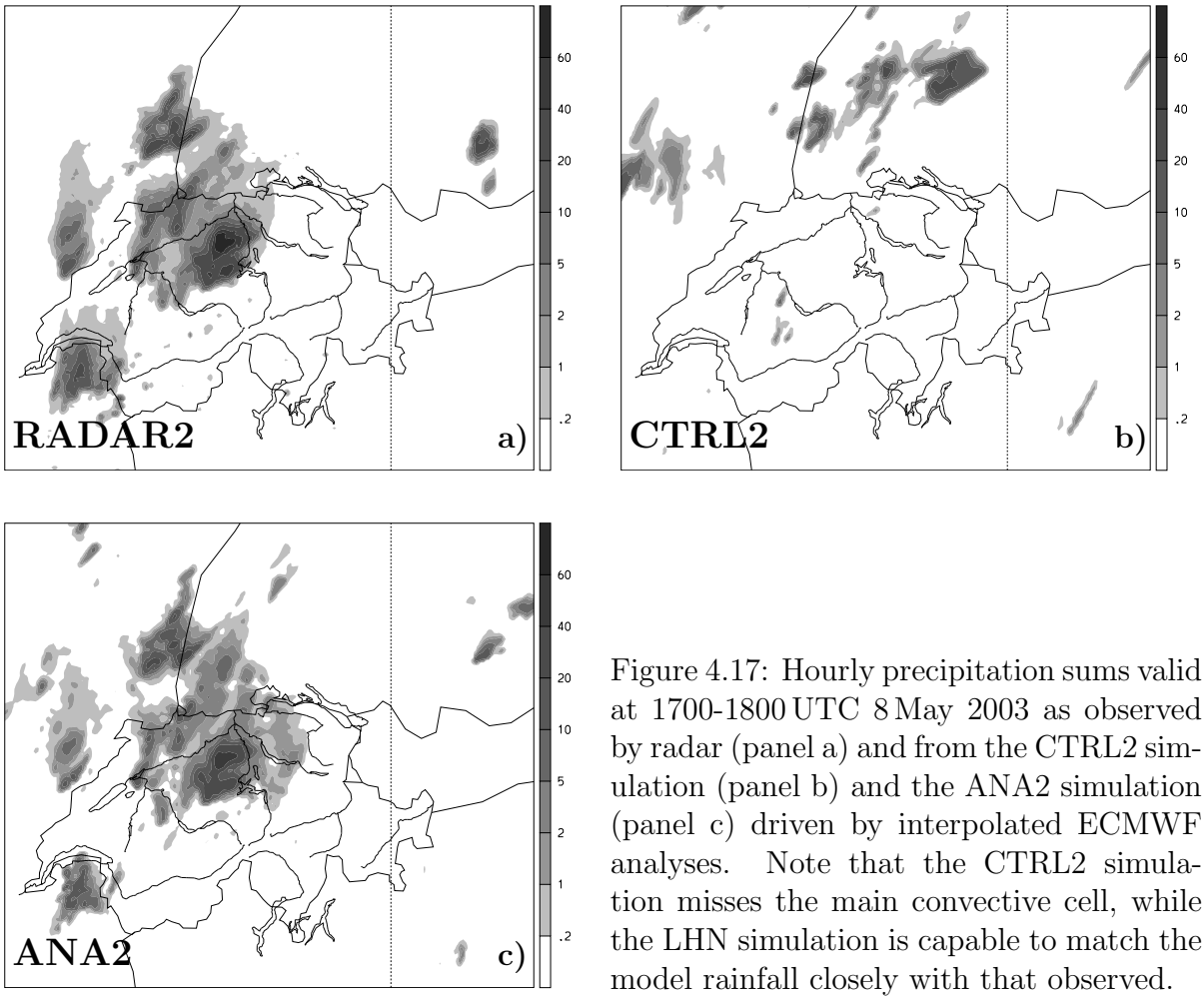

Figure 4.17: Hourly precipitation sums valid at 1700-1800 UTC 8 May 2003 as observed by radar (panel a) and from the CTRL2 simulation (panel b) and the ANA2 simulation (panel c) driven by interpolated ECMWF analyses. Note that the CTRL2 simulation misses the main convective cell, while the LHN simulation is capable to match the model rainfall closely with that observed.

The simulations CTRL7, CTRL2 as well as ANA2 and FC218 have been repeated substituting the LMAna with the ECMWF analyses to explore if the convective system can be captured with the LHN scheme. Figure 4.17 shows hourly precipitation sums valid at 1700-1800 UTC 8 May 2003 from the CTRL2 simulation (panel b) and the ANA2 simulation (panel c) driven by interpolated ECMWF analyses and radar QPE (panel a). The CTRL2 run obviously misses the main convective cell while LHN is well able to match the model rainfall closely with that observed.

ETS scores of 6h accumulated precipitation from 1800-2400 UTC have been calculated for the different simulations and are compared to those obtained with the simulations driven by the LMAna analyses in Fig. 4.15. The CTRL2 (dashed line with triangle symbols) obviously did not capture the event resulting in a low ETS for all intensities. The ANA2 simulation (solid line with triangle symbol) succeeded in assimilating the storm but did not perform as well for the higher intensities as the ANA2 simulation driven by the LM analysis. The FC218 forecast (dotted line with triangle symbols) retained the convective system, introduced by the LHN scheme during the pre-forecast period and clearly outperforms the corresponding CTRL2 simulation, showing that the radar assimilation was highly beneficial in this case. All simulations driven by the LM analyses, however, are more skillful in terms of ETS than the corresponding simulations driven by the ECMWF analyses, demonstrating the positive impact of the additional information introduced by the mesoscale data assimilation.

4.4.2 CASE 2 (21 August 2000)

Performance of CTRL

The initial environment of the CTRL simulations is slightly unstable with CAPE values generally below 300 J/kg, as is expected given the value of 226 J/kg obtained from the Payerne radiosonde. Neither the CTRL7 nor the CTRL2 developed the convective system, but both produced a distinct band of stratiform precipitation to the West of Switzerland (Fig. 4.18a,d) which is clearly misplaced and overestimated compared with the radar observations (Fig. 4.18c,f). A comparison with the ANETZ surface observations confirms the lack of any severe wind gust in the CTRL2 simulation (Fig. 4.19,4.20, black, dashed lines). The pre-frontal low-level environment is too dry and too warm in the model.

Performance of LHN Analysis

As in CASE 1 the LHN scheme is able to trigger the convective system and closely matches the precipitation with the target, as can be seen from the 6h accumulated precipitation in Fig. 4.18b,e). Moreover, it effectively inhibits the misplaced stratiform precipitation band by removing humidity and generating a stabilising downward circulation at the appropriate location. A vertical cross-section (see Fig. 4.18d) for its location) along the path of the convection reveals the deep convection triggered by the LHN scheme (Fig. 4.21) in which a tower of saturated air reaches up to 12 km and a sharp gradient of low-level potential temperature at its leading edge anticipates the presence of a gust front. Indeed, the ANA2 simulation produces a distinct signal of high surface winds at all ANETZ stations (Fig. 4.19,4.20, green lines). The peak values are underestimated by 27% (24%) and occur only 10 min later than observed in Zuerich SMA (Guettingen). The temperature, relative humidity and surface pressure fluctuations connected with the passage of the system are reproduced much better than in the CTRL simulation, demonstrating that the LHN scheme is able to capture the convective system with realistic dynamical and thermodynamical low-level structure. The impact of the radar data is clearly positive for all stations and all low-level variables.

Performance of forecasts

A free forecast starting from the ANA simulations at 0300 UTC has been performed in order to see if and how long the information introduced during the LHN assimilation can be retained in the model. The simulated 3h precipitation accumulations from 0300-0600 UTC (Fig. 4.22a,b) reveal, that the FC simulations partially reproduce precipitation patterns similar to those observed by the radar, generally underestimating the amounts in Eastern Switzerland. Inspection of the CAPE field at 0300 UTC (not shown) indicates that the convective system could be retained longer in regions of enhanced instability, but rapidly starved in the stable areas. The 2.2 km forecast triggers small-scale, strong convective cells which contribute to an overestimation in the northern part of Switzerland, where the 7 km forecast did not develop such strong cells. The positive impact from LHN assimilation with regard to precipitation forecasting is limited to 3h in this case, the predicted convective system no longer being visible after 3 hours into the free forecast. The surface variables at Zuerich SMA and Guettingen were still well predicted by the free forecast, the wind gust being slightly lower than in LHN-forced simulation (Fig. 4.19,4.20, red lines).

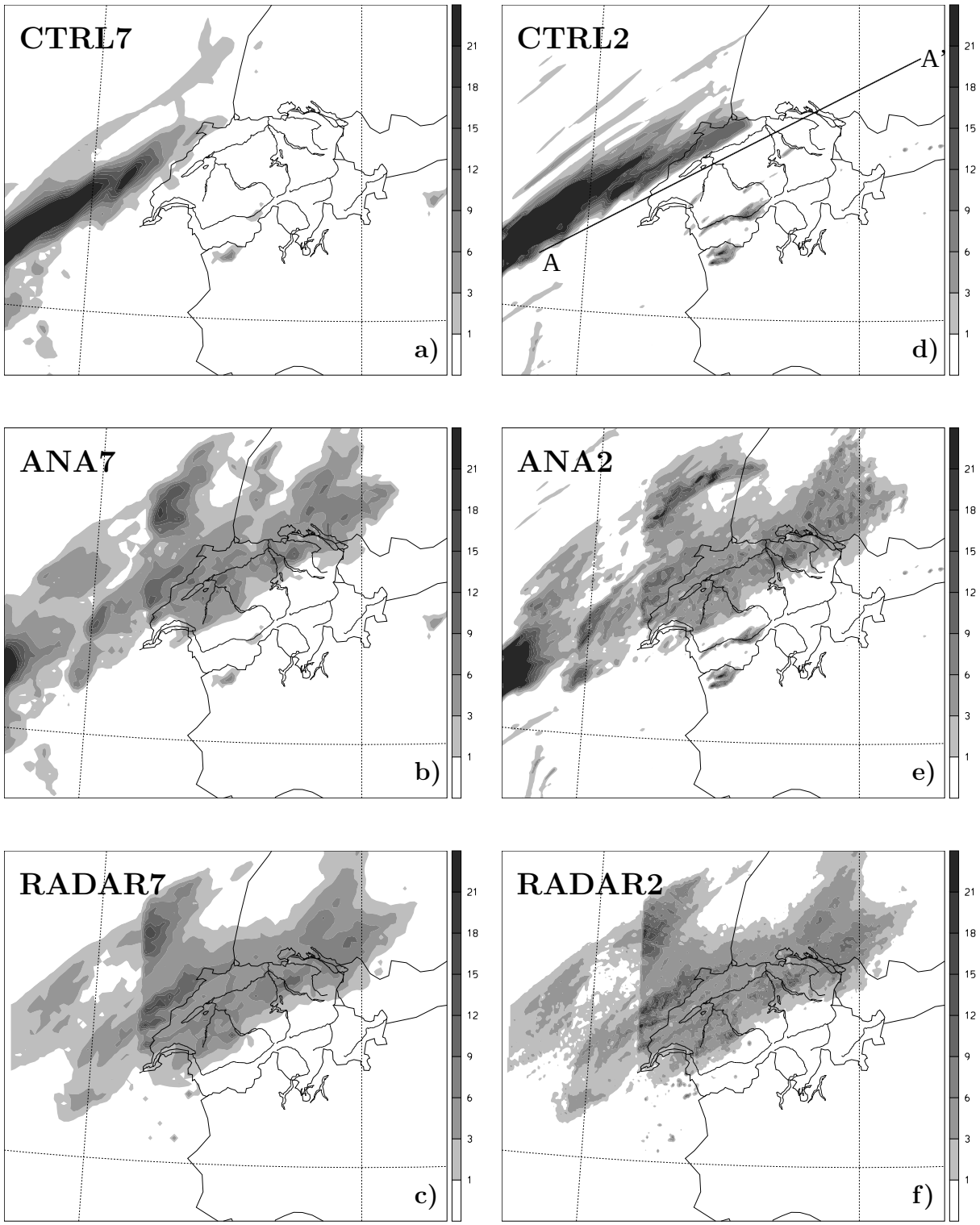

Figure 4.18: 6h-accumulated precipitation (mm) for 0000-0600 UTC 21 August 2000, a) CTRL7, b) ANA7, c) SRN QPE interpolated onto the 7 km LM grid, d) CTRL2, e) ANA2, f) SRN QPE interpolated onto the 2.2 km LM grid.

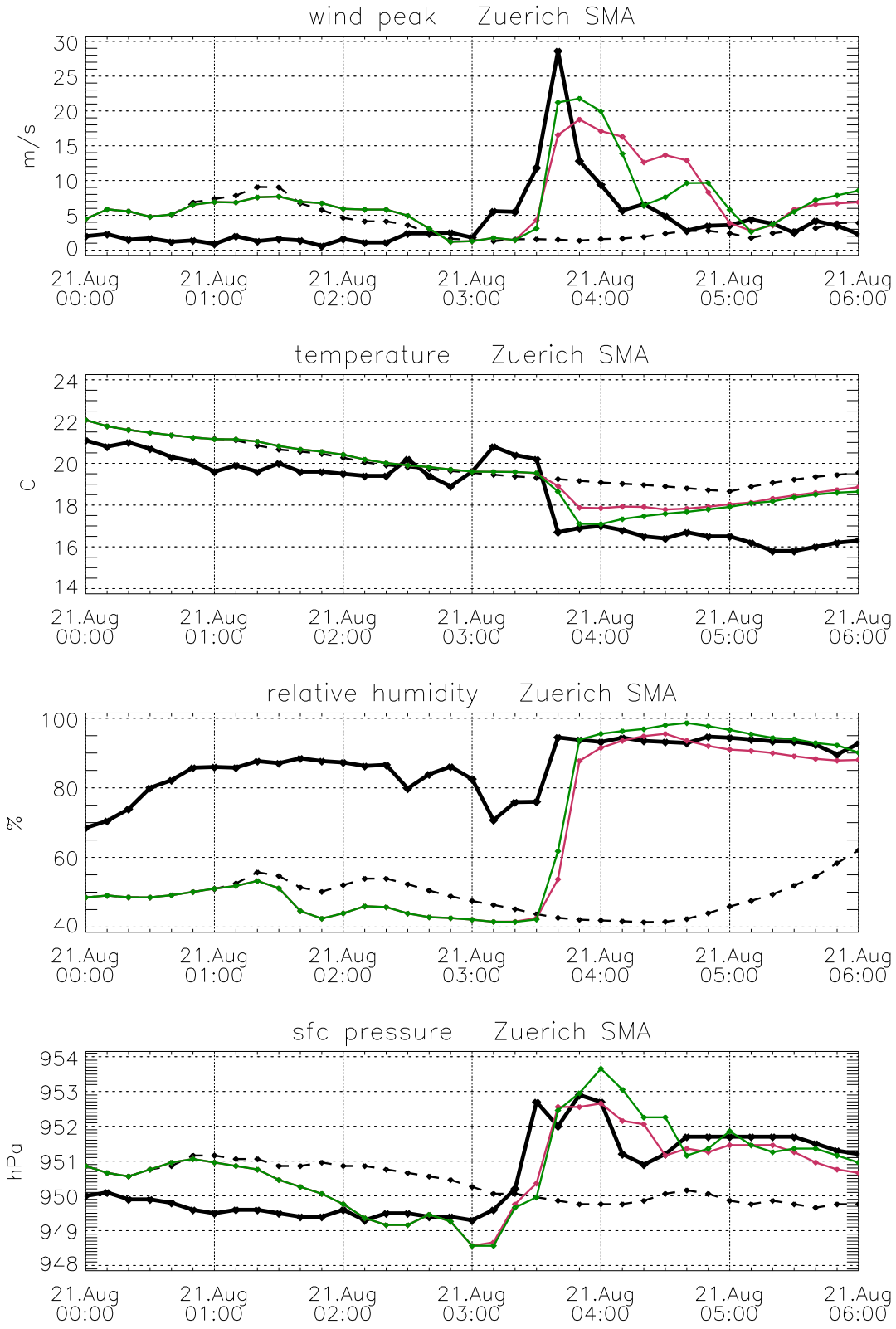

Figure 4.19: Comparison of 21 Aug 2000 simulations against surface observations of ANETZ station Zuerich-SMA. Variables are (from top to bottom) peak 10 m wind speed during last 10 min, temperature, relative humidity, and surface pressure at station height. Black, bold, solid lines denote observations, black dashed lines CTRL2, red lines ANA2, and green lines FC203.

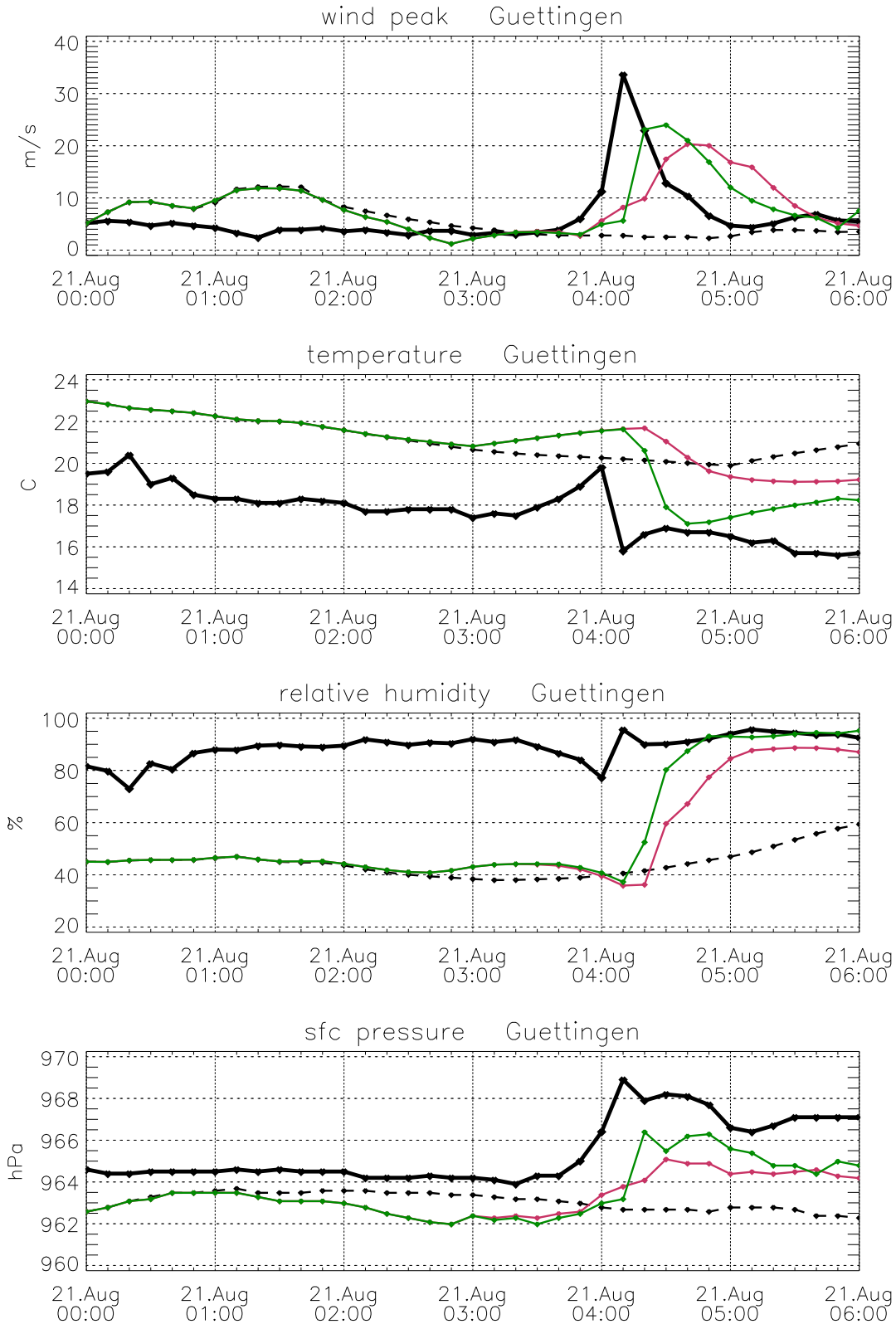

Figure 4.20: Same as Fig. 4.19, but for station Guettingen.

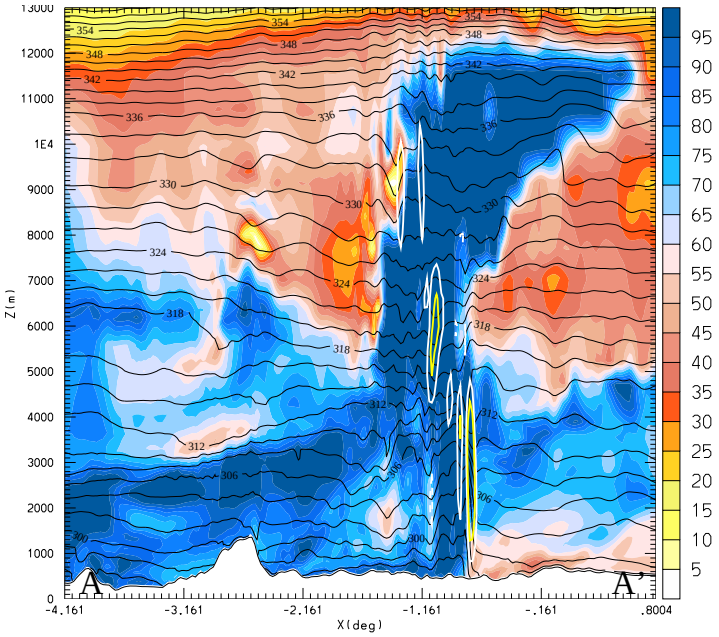

Figure 4.21: Vertical cross-section (see Fig. 4.18d for its location) of relative humidity (%, shaded) potential temperature (thin contours, contour interval 2 K), and vertical velocity (white 1 m/s contour and yellow 2 m/s contour) of ANA2, valid at 0400 UTC 21 Aug 2000.

Simulations driven by LM analyses or interpolated ECMWF analyses could not prolong the positive impact of the radar assimilation in this case, both driving fields exhibiting an environment of similar stability and therefore not supporting a longer life of the storm in the free forecast.

4.5 Summary and discussion

In this study, the applicability of the Latent Heat Nudging precipitation assimilation method on the meso-γ scale has been investigated. To this end, two cases of severe convection over Switzerland have been simulated using the operational model of MeteoSwiss in a high-resolution setup. Simulations with radar assimilation and forecasts started therefrom have been performed and validated against radar-derived precipitation and independent surface observations. The CASE 1 was characterised by a multicell storm triggered by a frontal low-level convergence line. The main cell exhibited supercell characteristics and was accompanied by damaging hail. The convective system of CASE 2 developed over France, propagated into Switzerland and produced violent wind gusts. The following main results have been found in this study:

- Although large-scale forcing was present in both cases, the simulations without radar assimilation had significant problems in predicting the convective systems. The overall evolution of the convective system of CASE 1 could be simulated, when started from a mesoscale analysis, but the right intensity and the details of the precipitating cells were not captured. When starting from interpolated global analyses the system was entirely missed. The system of CASE 2 was missed even when the model was driven by mesoscale analyses.

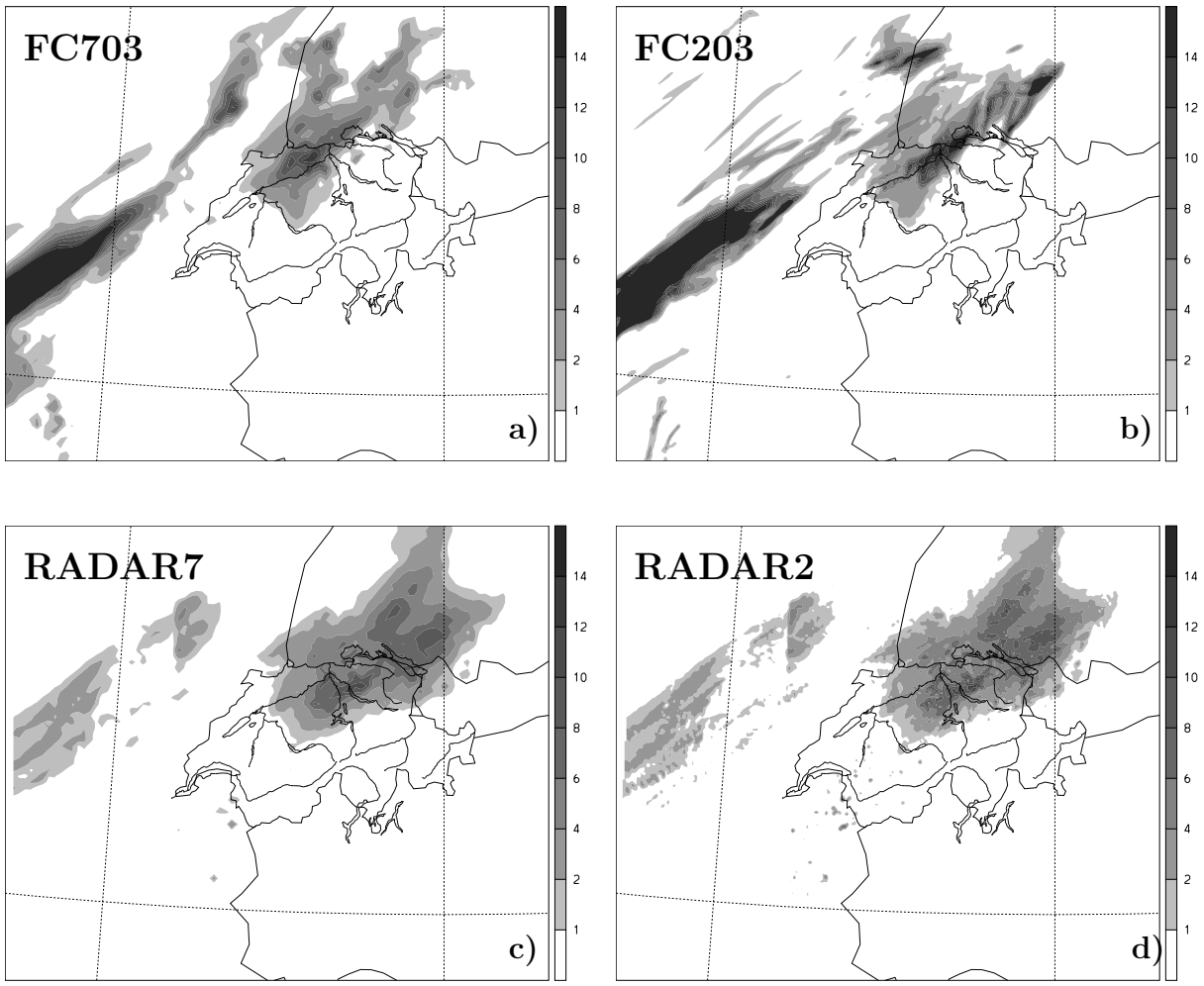

Figure 4.22: 3h-accumulated precipitation (mm) for 0300-0600 UTC 21 August 2000 for a) FC7, b) FC2, c) SRN radar observations interpolated onto the 7 km model grid, d) SRN QPE interpolated onto the 2.2 km LM grid.

- The LHN method was found to be able to capture the details of the convective cells and matched the model precipitation closely with the target precipitation derived from radar. This can not be expected a priori because of the continuous, highly variable forcing, the fact that only a rough proxy of precipitation (i.e. the latent heating) is assimilated into the model, and because of the complex interactions between the dynamical, thermodynamical and microphysical model variables. Moreover, LHN was able to assimilate the vortex structure related to the main cell of CASE 1 at the appropriate location.

- Comparison of simulated surface variables with observations at 15 mesonet stations revealed that the low-level mesoscale structure of the atmosphere can be significantly improved with radar assimilation. In CASE 2 the severe wind gusts, entirely missed without LHN, are well introduced, both in timing and amplitude at most of the stations, this holds true even for a 1h free forecast started from the LHN analysis. In CASE 1 the benefit of LHN in simulating the low-level structure of the convective system was found to be dependent on the location. Whereas the impact

was clearly positive at some stations in simulating the convective outflow structure (i.e. propagation and intensity of the cold pool and the associated gust front), other stations showed an overestimation of the cold pool and the introduction of a position error in the low-level convergence connected with the main convective cell.

- In both cases, the detailed structure and intensity of the forced storm could not be retained in the model for a long time. The supercellular structure introduced in CASE 1 immediately vanished, indicating that the modelled cell was not in balance with the environment and probably not correctly represented by the simple microphysics in the LM. The cell moved not along the observed path, but instead, new convection was triggered at the leading edge of the outflow, located some 40 km downstream of the observed system and propagated with a phase error. The overall system, however, could be retained in the free forecast for several hours as sufficient instability was present on its path of propagation. In CASE 2 a positive impact of the radar assimilation could be observed up to three hours into the free forecast. The severe low-level windgust connected with its outflow was clearly present one hour after initialisation. A too stable environment is thought to have prevented a longer life of the storm.

- The assimilation of conventional observations can improve the environment of a convective event and, as in CASE 1, can even provide the trigger, e.g. in form of a low-level convergence line. In this case the additional information from the radar observations did not improve the precipitation forecasts. However, when the trigger was not provided from the driving model, as in the simulations where the initial and boundary conditions were obtained from downscaled global analyses, the assimilation of radar data was found to be highly beneficial in that a positive impact on QPF could be observed during the entire lifetime of the convective system.

- The LHN scheme was found to be sensitive to the amplitude of the target precipitation in that it produced a too cold and overestimated outflow during the assimilation period when using rainfall observations with a positive bias. Dividing the rainfall by a factor of three resulted in an improvement of the simulated low-level temperatures, and, to a lesser extent, in a reduction of the error in strength and position of the outflow.

The rapid cessation of the CASE 2 storm in the free forecast can be compared to the results of the sensitivity simulations in LR05a. They reported a gradual decay of the convective storm after the assimilation of idealised rainfall in a drier and more stable environment than used in the reference simulation, although the model rainfall matched well with the forcing during the assimilation period. LR05a also found a strong sensitivity of the LHN to the insertion frequency of the rainfall data. In our case studies, this sensitivity might be less pronounced. In CASE 1 the storm propagation velocity is somewhat slower than in the idealised case (approximatively 9 m/s instead of 14 m/s) which may allow a larger observation interval. The storm of CASE 2 propagated faster (22 m/s) but the model environment was much stabler and less humid than that in LR05a. In such an environment, convection triggered by a too large forcing area (resulting from a inadequate temporal interpolation between two subsequent coherent radar signals) might be less amplified. However, the sensitivity to the insertion frequency in the case studies remains to be tested by assimilating data e.g. only every 15 minutes. LR05a further demonstrated

that a mismatch in the propagation speed of the forcing and the environmental wind can result in distorted storm dynamics, eventually leading to a decoupling of the updrafts from the low-level moisture inflow. One reason for the cessation of the supercell in the free forecast of CASE 1 could be such a mismatch between the radar velocity propagation and the model wind speed and direction.

Our results confirm the results of previous studies (e.g. Ducrocq et al., 2002) in that the success of radar data assimilation depends on the environment into which the convection is assimilated. In the absence of favourable conditions (e.g. sufficient instability) the assimilated signal may rapidly vanish. This points to the need for additional observations in the mesoscale and small-scale assimilation, such as humidity and cloud information from satellites, surface observations or new remote-sensing observations such as LIDAR (Light Detection and Ranging) or microwave radiometers.

This study suffers from several limitations. In particular, our operational NWP model does not account for the advection of precipitation and uses simplified microphysical parametrisations (e.g. graupel and hail not treated, simplified representation of turbulence). The advection of precipitation is in contrast with one of the approximations used in the LHN scheme, i.e. that the vertically integrated latent heating is proportional to the surface rain rate at each grid point, and needs further addressing in the context of high-resolution models. Despite these limitations, our study confirms the importance of cloud-scale assimilation and demonstrates the potential of the LHN scheme on the meso-γ scale.

Chapter 5

The Sensitivity of the LHN Scheme to Non-Rain Echoes

Abstract

Radar-derived quantitative precipitation estimates (QPE) are becoming an increasingly important element in high-resolution numerical weather prediction (NWP). As such they complement conventional data like surface or upper-air observations. Unlike the latter, radar data exhibit a highly variable quality, in that they are affected by a number of factors that limit their accuracy in estimating precipitation at the surface. In the context of assimilating radar-derived QPE in high-res NWP models this poses two salient questions, i.e. how is a specific assimilation scheme affected by errors in the observations, and how can such variable quality be accounted for?

This paper addresses the first question and presents a sensitivity study of the Latent Heat Nudging (LHN) scheme in a meso-γ scale NWP model to gross errors in the radar data, notably non-rain echoes. It was found that, non-rain, or clutter, echoes as small as one model pixel can trigger the release of convective instabilities when forced by the LHN scheme, with resulting precipitation that is large compared to the original signal, where factors 3 up to 50 have been found for moderate to high value of CAPE and low to medium intensity clutter signals. Furthermore, the response of the model atmosphere to the forcing was found to be very quick, i.e. on the time scale of convection (less than ten minutes for strong forcing to a couple of hours for moderate forcing). Large, coherent areas of non-rain echoes seemed to suffer more severely from such error amplification than gridbox-sized signals. Finally, non-rain echoes resulting from anomalous propagation of the radar beam, by virtue of the usually very stable conditions associated, are not conducive to rainfall amplification. However, a strong spurious vertical circulation, along with undesired mixing, may be induced and adversely impact the mesoscale circulation.

5.1 Introduction

One of the major benefits of using high-resolution Numerical Weather Prediction (NWP) models is expected at short to very short ranges, say, one day to one hour. Coherent, quickly evolving, small-scale precipitation systems have a lifetime of a few hours, thus requiring forecasts to be delivered to the forecasters and customers in no more than an hour after real time and, possibly, updated every few hours. In order to meet these

tight time constraints a very efficient observation acquisition, assimilation, and forecast system is essential. Moreover, the dynamics of these precipitation systems, mostly of a convective nature, are not sufficiently resolved by conventional surface or upper-air observing systems. Such resolution requirements demand new, adequate types of high-resolution observations, both for initialisation and verification purposes.

Doppler radars are able to provide this kind of information and have become an increasingly important complement to conventional observations for these purposes, and currently receive much attention in many research actions around the world (e.g. the COST 717 Action 'On the Use of Radar Information in Hydrological and NWP Models', Rossa, 2000). Doppler radar wind and precipitation data deliver spatial resolutions of a few kilometres and temporal resolutions of a few minutes, sufficient to capture the essence of convective scale precipitation-related phenomena.

Estimating surface rain rates from radar observations is a challenging task, especially in complex terrain. There are a number of problems involved in the quantitative precipitation estimation (QPE) at the surface, notably strong ground clutter including anomalous propagation, (partial) shielding combined with the vertical reflectivity profile, beam-broadening and partial beam-filling, variations in the reflectivity-rainfall (Z-R) relationship and beam attenuation, especially in cases with intense precipitation (Germann and Joss, 2004). At MeteoSwiss, these issues have been coherently addressed over the past decade resulting in a product of best QPE at the surface over Switzerland. For instance, the clutter detection algorithm implemented in 1999 removes, on average, 98% of the ground clutter.

The recently completed COST 717 Action undertook a major effort to produce a comprehensive inventory on the quality control and characterisation of weather radar data in Europe (Michelson et al., 2004). It includes a compilation of sensitivities of hydrological and meteorological models to radar data errors, but notes that the treatment of observation error in assimilation of radar data is at a relatively immature stage, and that, as assimilation schemes improve, they become more vulnerable to bad data. Moreover, the sensitivity to certain errors may depend on the specific application, and, in the case of NWP models, on the current atmospheric situation.

Simple, economical schemes for cloud-scale radar data assimilation, one of which is Latent Heat Nudging (LHN), have recently received considerable attention, and were reported to produce beneficial results. In particular, while for large-scale NWP systems four-dimensional variational (4D-Var) methods have proven to be superior, established procedures for assimilating cloud-scale observations have yet to emerge (see e.g. Macpherson et al., 2004; Park and Zupanski, 2003, for recent reviews).

LHN seeks to adjust the model's buoyancy in order to match the observed precipitation intensity and, therefore, seems to be a natural candidate for the assimilation of convective weather systems. Allowing for a timely insertion of high-frequency observations at low computational costs, LHN features the basic prerequisites for real-time assimilation of convective phenomena. On the other hand, the forcing exerted by LHN is local and does not depend but on the difference between the modeled and observed precipitation. This may render the LHN scheme particularly vulnerable to erroneous observations, such as non-rain echoes, for instance. Systematic studies addressing the error sensitivities of rainfall assimilation schemes have not yet been widely published in the literature. Chang and Holt (1994) and Manobianco et al. (1994) have found that the LHN scheme was more sensitive to position than amplitude errors. In the assimilation of TRMM data into the ECMWF model (Marécal and Mahfouf, 2002), tests were conducted on the

sensitivity to the assumed rain rate error of the TRMM TMI data. When it was increased from 25% to 50% of the observed rainrate, the assimilation scheme showed only a weak response.

In a recent study Leuenberger and Rossa (2005a,b) systematically investigated the performance of the LHN scheme at meso-γ scale, both in an idealised setup and in the context of real cases. They found that LHN has considerable potential at the convective scale in that for an idealised supercell it successfully initialised the storm in a perfect environment and - to a lesser extent - in non-perfect environments in which low-level humidity or wind fields were altered. For the real case convective systems, a supercell and a squall line case, LHN was able to capture the salient features of the storms. Persistence of the assimilated systems in the subsequent free forecasts appeared to depend much on the instability of the environment into which the observed systems were forced.

Leuenberger and Rossa (2005a) included a study of the sensitivity of the LHN scheme to errors in the radar data within the framework of an idealised supercell storm. In an identical twin experiment they found the LHN scheme to be able to reproduce the supercell in terms of dynamical structure and correct rainfall amount, while the scheme was found to exhibit a distinct sensitivity to errors in the observations. They confirmed that errors in position and structure seem to be more serious than amplitude errors. Amplitude errors were modeled by halving and doubling the reference precipitation rate, a very rough estimate of the radar rainfall accuracy over well covered terrain Germann et al. (2004). The LHN scheme managed to dampen these errors yielding total precipitation accumulations of 88% and 133%, respectively, while preserving much of the spatial pattern, given a perfect environment.

For quickly moving precipitation systems the observation acquisition period becomes an issue, as the LHN scheme interpolates observations linearly between two subsequent observation times. This causes the assimilated precipitation to be spread over an increasingly larger area as the interval between two observation times increases. The resulting effect on the storm assimilation is negative and can be detrimental. For an acquisition period of 10 min, for example, the resulting total rainfall accumulations almost triples relative to the reference simulation, exhibiting precipitation swathe which is of more than doubled width compared to the reference. In addition, a substantially distorted dynamical structure results, an alteration from which the model is not able to recover in a subsequent free forecast. Obviously, this problem is accentuated in more unstable environments.

This paper is intended to complement LR05a and LR05b as it systematically explores the sensitivity of the LHN scheme to non-rain echoes in the radar data errors. These include ground clutter returns and spurious signals due to anomalous propagation of the radar beam. Consideration is given to the dynamical response of the model to the continuous forcing of such signals during assimilation time, and to the performance of free forecasts started from the LHN analyses. The simple radar data error model, the numerical model and assimilation scheme as well as the evaluation methods used in this study are described in section 5.2. The results of the simulations, along with a real case example, are presented in section 5.3 and discussed in the final section 5.4.

5.2 Methodology

5.2.1 The numerical model

All numerical simulations in this paper are conducted with the Lokal Modell (LM) developed within the Consortium for Small Scale Modelling (COSMO) and deployed operationally at five European National Weather Services. The model solves the three-dimensional, fully elastic and nonhydrostatic atmospheric equations on an Arakawa-C grid using the split-explicit technique described by Klemp and Wilhelmson (1978). Prognostic variables include the three Cartesian velocity components (u, v and w), temperature (T), pressure perturbation (p') and mass fractions of water vapour (q_v) and cloud water (q_c). The parametrisation for grid-scale precipitation accounts for four categories of water (water vapour, cloud water, rain and snow). The mass fractions of rain water (q_r) and snow (q_s) are treated diagnostically for reasons of efficiency. Vertical subgrid turbulence is parametrised following Mellor and Yamada (1982) and the surface flux formulation is based on a roughness-length specifying the drag-coefficients for turbulent momentum and heat exchange with the ground. For a more complete description of the model we refer to Doms and Schättler (2002) and Steppeler et al. (2003).

All model integrations were uniformly performed on a 50×50 gridpoint domain. In the vertical, a stretched, terrain-following grid after Gal-Chen and Sommerville (1975) is employed composed of 60 levels and separated by 67 m near the ground and 2000 m near the model top at 23500 m. Above 11000 m a Rayleigh damping layer is used to absorb vertically propagating waves. In order to damp grid-scale noise, fourth-order numerical diffusion is applied. All simulations are integrated to 2 hours.

5.2.2 Assimilation method

The Latent Heat Nudging (LHN) scheme used in this study is based on that developed by Manobianco et al. (1994) for the assimilation of satellite-derived rainfall observations into a large-scale model, adopted by Jones and Macpherson (1997) for the use with radar QPE, and described in some detail in LR05b. In essence, for each model profile the scheme acts to change its buoyancy in order to match the modeled to the observed precipitation. This is done for each gridpoint individually and constitutes, therefore, a purely local forcing. LR05b enhanced a quality function primarily based on range introduced by Jones and Macpherson (1997) to include the adverse effects of complex terrain on the quality of radar data. The weighting function is based on a visibility map, which, to a good first approximation, is obtained by a geometrical calculation of the lowest visibility height of the radar beam. Values of less than 2000 m result in a maximum weight of 1. Between 2000 m and 4000 m the weight decreases linearly to $w = 0.5$ for wet observations and to $w = 0$ for dry observations. This weighting function could, in principle, include more factors describing the radar data quality, e.g. clutter maps.

5.2.3 Setup of the sensitivity experiments

The basic atmospheric environment for the sensitivity experiments was chosen as in LR05a and following Weisman and Klemp (1982) for the study of splitting supercell storms (Fig. 5.1). They used a conditionally unstable thermodynamical profile and a moist, well mixed boundary layer with constant water vapour mixing ratio r with a reference value of

$r = 12\,\mathrm{g/kg}$, yielding a lifting condensation level of ∼1500 m, a level of free convection of ∼1900 m, a level of neutral buoyancy of ∼10000 m and a Convective Available Potential Energy (CAPE) of 1200 J/kg. As a simplification for the present study the environmental wind was set to zero for most experiments. For selected experiments, the wind profile was set to exhibit a vertical shear of 20 m/s over the lowest 4000 m and constant wind aloft with no variations of the wind direction with height ($V = 0$). The lateral boundaries are relaxed towards the initial state throughout the whole simulation.

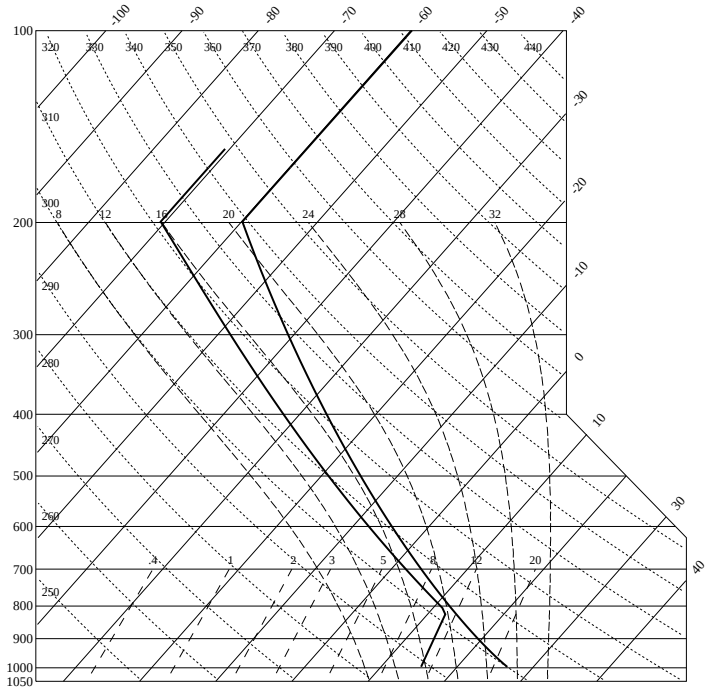

Figure 5.1: Reference sounding following Weisman and Klemp (1982) used for the clutter experiments. The instability was varied by varying the boundary layer humidity. Here the profile for a maximum mixing ratio of 11 g/kg (resulting in a CAPE of 800 J/kg) is displayed.

Ground clutter can be considered as one of the most important source of non-rain echoes, most of which is eliminated by appropriate clutter filters. However, in order to minimise eliminating real rain echoes, MeteoSwiss' clutter filter, for instance, leaves some 2% of the non-rain echoes in the data. This residual clutter often manifests as small scale, quasi-static, medium to high intensity signals. On the basis of this, ground clutter is modeled for the purposes of this study as isolated, one-pixel signals of varying intensities I_f. These signals are assimilatied during forcing times of various length (t_f). The boundary layer humidity was varied to obtain environments of various degrees of instability (see Tab. 5.1). An NWP model's numerical diffusion scheme is designed to act strongly upon one-pixel signals so that results obtained by these experiments can be taken as lower limits of the respective impact. I.e. in reality, and for larger non-rain echo areas, the impacts are expected to be more pronounced than what results from these experiments.

A large number of of experiments, i.e. 125, have been conducted, varying the clutter intensity I_f = 2, 5, 10, 20, 30, 50, 60 mm/h, the forcing times t_f from 2 min up to 3 hours. The varying the degree of instability with the boundary layer moisture content

results in differing lifting condensation levels and levels of free convection. Often, these levels are lower for environments of larger instabilities.

r_{max} (g/kg)	CAPE (J/kg)	LCL (m)	LFC (m)
10	400	1630	2840
11	800	1450	2400
12	1200	1290	2040
13	1700	1130	1730
14	2200	990	1470

Table 5.1: Specifications of the environments used for the numerical experiments. Values include the maximum water vapour mixing ratio in the boundary layer, CAPE, lifting condensation level and level of free convection.

5.3 Results

5.3.1 Description of a single experiment

Figure 5.2 summarises the outcome of two individual experiments both conducted in a 1700 J/kg CAPE atmosphere, with a 10 mm/h clutter forced during 20 min. (solid lines in panel a) and 6 min (dashed line). The model response to the applied forcing is depicted in terms of maximum up- and downdraft (panel a) and total accumulated precipitation (panel b). The larger forcing causes an updraft which reaches a strength of 1 m/s after about 7 min. Continuing the forcing out to 20 min. does not increase the vertical velocity, but keeps it at this level even though a slight modulation is visible, indicating an interaction between the forcing and the developing model dynamics. However, after having switched off the forcing air parcels seem to have reached the level of free convection sometime between 20 and 30 min. Once this level is reached the instability present in the basic state is released, exhibiting values of the vertical velocity up to 13 m/s at $t = 52$ min. Substantial rain falls out beginning at $t = 41$ min. and stops when the system relaxes at $t = 60$ min. Total rainfall accumulates close to $0.1 \cdot 10^6$ m^3 whereas the precipitation equivalent of the forcing amounts to $0.01 \cdot 10^6$ m^3, i.e. the error given by the non-rain echo has been amplified by the assimilation scheme by a factor of close to 10. Note, that in this experiment downdrafts form of several m/s in response to the convectively driven updraft.

The second experiment in Fig. 5.2, on the other hand, is an example in which the initial erroneous forcing is not sufficient to lift air parcels to their level of free convection. Hence the initially triggered vertical velocity gradually decreases without producing any precipitation and downdrafts.

5.3.2 Evaluation of the idealised clutter experiments

The impact of a particular non-rain echo on the assimilation and the subsequent forecast in an individual experiment can be measured as the ratio of the resulting model-produced

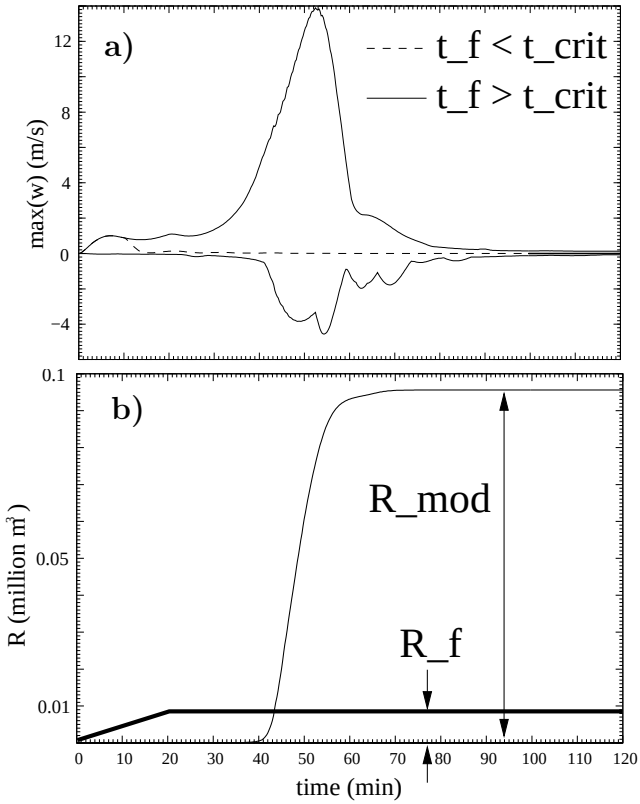

Figure 5.2: Panel a displays the time evolution of the maximum up- and downdraft (m/s) during an individual assimilation and subsequent forecast experiment. The solid (dashed) line denotes an experiment in which the convective instability was (not) released (i.e. the forcing time is larger (smaller) than the critical forcing time). Panel b shows the corresponding cumulated forcing (R_f) and resulting model precipitation (R_mod) (mm) for an experiment in which the convective instability is released with a corresponding ratio of roughly 10.

precipitation R_mod and the precipitation equivalent of the total forcing R_f calculated from the product of the forcing time t_f and the clutter amplitude I_f (Fig. 5.2 b). If the ratio R_mod/R_f is zero or much smaller than one, the effect of the spurious signal on the assimilation is negligible. If, however, the ratio is larger than one, the assimilation has amplified the error in the radar data. In the former case, the conditional instability present in the environment was not released by the applied forcing, i.e. it is too small to lift an air parcel to reach the level of free convection. For the latter, however, this level is eventually reached and the instability released. Consequently, the model-produced rain can be much larger than the forcing equivalent. The instability is accompanied by significant values of vertical velocity of the order of several tens of m/s as illustrated in Fig. 5.2 a).

The ensemble of one-pixel clutter experiments with zero wind is evaluated in terms of the resulting amplification factors which are summarised in Fig. 5.3. It becomes evident that even medium-intensity ground clutter signals can be dramatically amplified in unstable environments and, therefore, hamper the precipitation assimilation substantially. This occurs when the forcing induced by the spurious echo is sufficient to lift air parcels to their level of free convection. For instance, a clutter signal of 20 mm/h nudged dur-

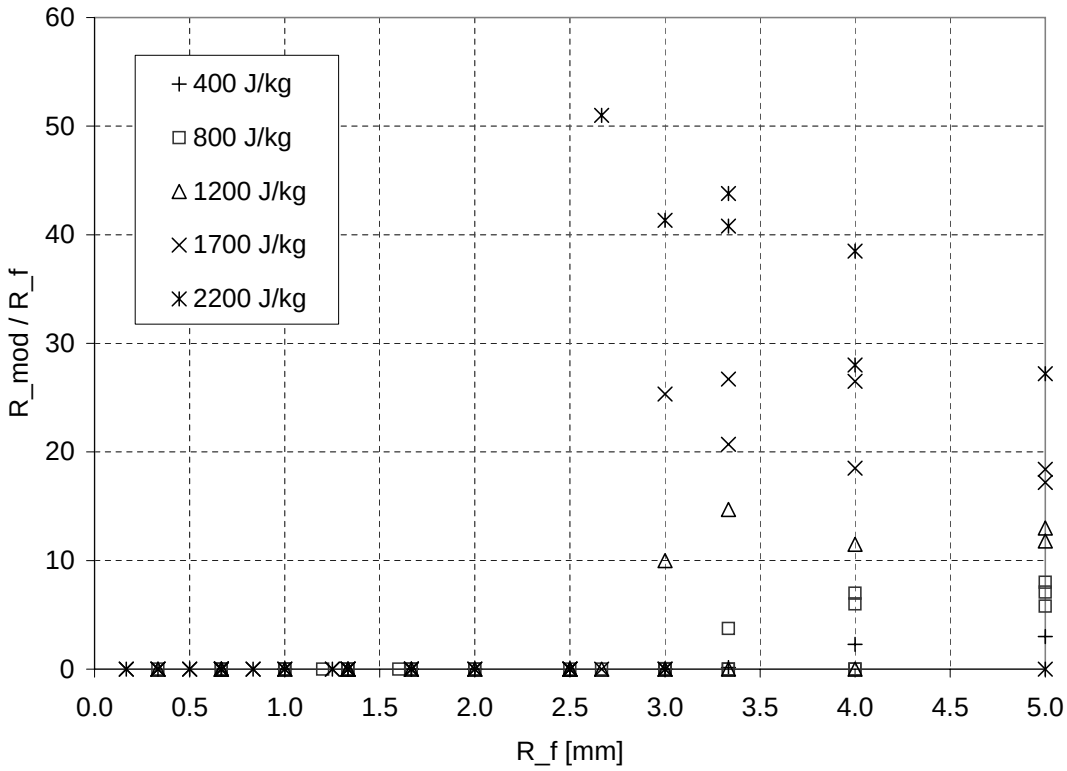

Figure 5.3: Sensitivity of the Latent Heat Nudging scheme to ground clutter-like non-rain echoes (refer to section 5.3.2). The symbols denote individual experiments in which a single-pixel forcing was applied during various periods of time in atmospheres of various instabilities. The x-axis denotes the total applied forcing (i.e. the product of intensity of the echo times the time over which it is applied), the y-axis the ratio of the resulting total model precipitation and the total forcing. Note, that even for relatively moderate instabilities amplification of the signal (i.e. ratio larger than 1) takes place after modest forcing.

ing 10 min into an environment with a CAPE of 1200 J/kg, is amplified by a factor of 15, while in a 400 J/kg environment a 50 mm/h clutter amplifies by a factor of 3 after 8 minutes, i.e. even for relatively moderate instabilities amplification of the signal (ratio larger than 1) takes place after modest total forcing. Accompanying updrafts easily reach values between 10 and 20 m/s. This scatter plot suggests the existence of a threshold forcing, for the present configuration at R_f between 2.5 and 3 mm, above which air parcels do reach their level of free convection, and the instability is released. However, there are cases with a larger total forcing, e.g. 10 mm resulting from a combination of small clutter intensity and long forcing time, in which the level of free convection is not attained. This may partly be due to an interference of the LHN forcing with the model dynamics (such as numerical diffusion), when the convective system starts to develop in the model. Investigation of this is beyond the scope of the present study.

A slightly different way of representation is given in Fig. 5.4, in which the critical forcing time t_crit, i.e. the minimum time for a given amplitude to reach amplification, is depicted for several degrees of instability. Again, for unstable environments even very small amplitude signals are amplified given sufficient forcing time. For high-amplitude

signals dramatic error amplification is almost immediate, i.e. takes place after as little as a few minutes. For smaller values of CAPE and clutter amplitude, however, the assimilation scheme is able to dampen the error.

In the light of these results and given that real ground clutter amplitudes often reach, or even exceed, such amplitudes, a thorough clutter elimination in convectively unstable situations seems to be fundamental.

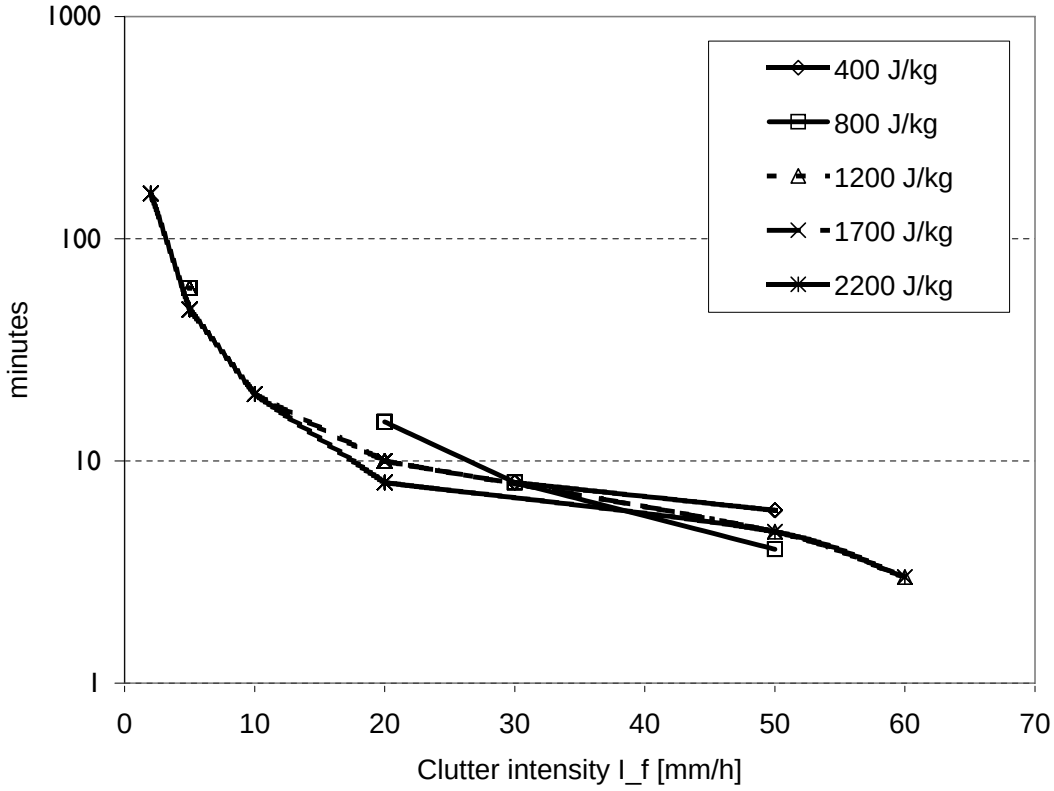

Figure 5.4: Minimum time needed for the Latent Heat Nudging scheme to amplify a ground clutter-like non-rain echo for various instabilities (denoted by different symbols (refer to section 5.3.2). The x-axis represents the clutter amplitude (mm/h), while the y-axis the critical forcing time (min) in logarithmic scale. Note, that for the higher clutter amplitudes it takes only a few minutes of forcing for the amplification to take place.

5.3.3 Real case example

In order to illustrate what can happen in real cases of clutter, Swiss Radar Network (SRN) data for a non-rain day are assimilated for a six hour period into the experimental setup of this study using the reference profile with CAPE=800 J/kg (Fig. 5.1). The simulation was performed with the setting used by LR05, i.e. a model domain of 361×333 horizontal grid points, with a mesh size of 2.2 km and 45 vertical levels. The six hour accumulation of the resulting model precipitation (Fig. 5.5 b) exhibits dramatic amplification of the original clutter signals. It is evident that regions of large coherent clutter amplify to larger intensities than pixel-sized signals, as the former are less dampened by the model's numerical diffusion scheme that acts primarily on the structures with sizes of the order

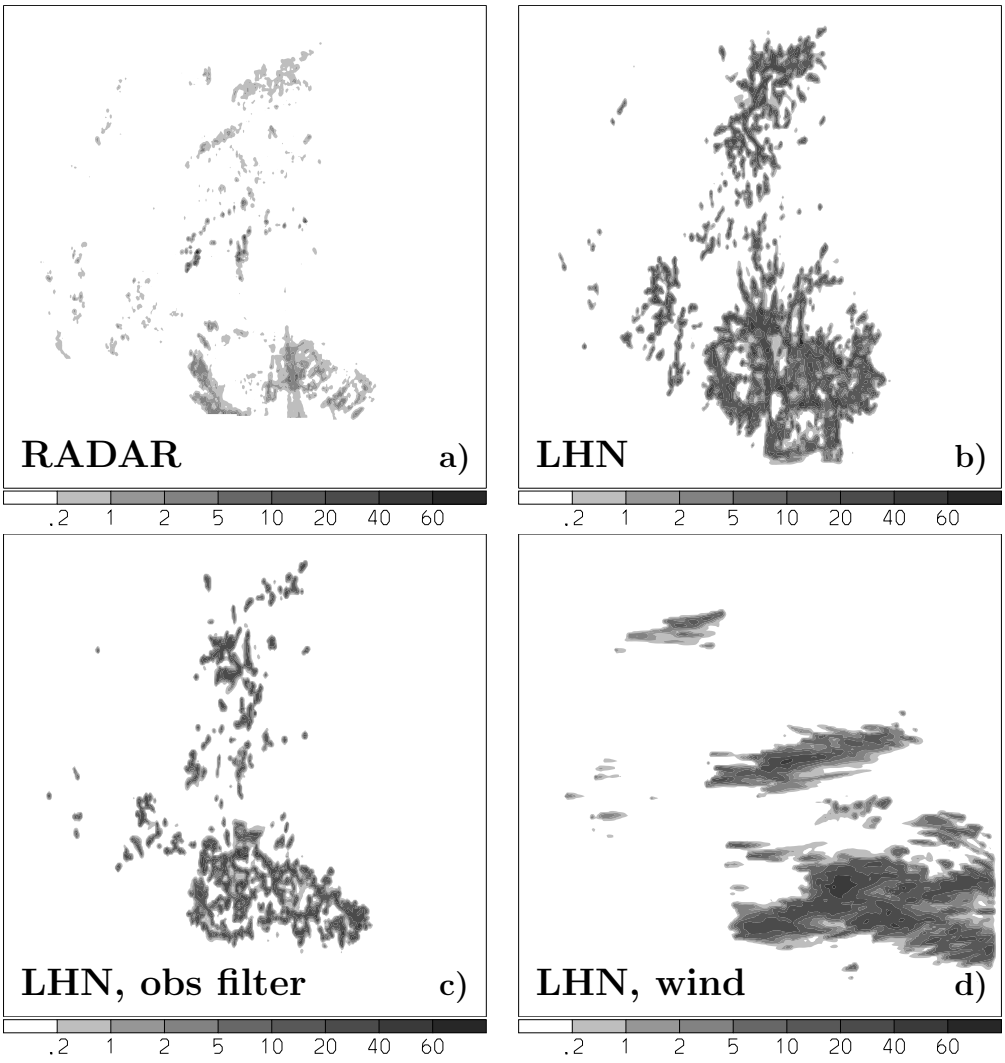

Figure 5.5: Examples for the assimilation of real clutter in a convectively unstable situation. Panel a) shows a six-hour accumulation (mm/h) of the Swiss Radar Network for a non-rain day, and panel b) displays the model precipitation resulting from a continuous forcing of the clutter by LHN. Panel c) is as b) except that the observed clutter is filtered. Finally, panel d) is as b) except that wind is added in the basic state. The domain has a size of 730×800 km.

of the gridlength. The problem is somewhat mitigated if the SRN data are run through a Shapiro type observation filter with length 4 (Shapiro, 1975) (Fig. 5.5c). In addition, the presence of appreciable wind causes the precipitation resulting from the clutter assimilation to be exported to neighbouring regions, in which new convection can be triggered (Fig. 5.5d).

5.3.4 Anomalous propagation conditions

The signal resulting from anomalous propagation of the radar beam is another important source of non-rain echoes (e.g. Koistinen et al., 2004). In contrast to regular ground clutter, anomalous propagation clutter can be more coherent in space but more intermittent

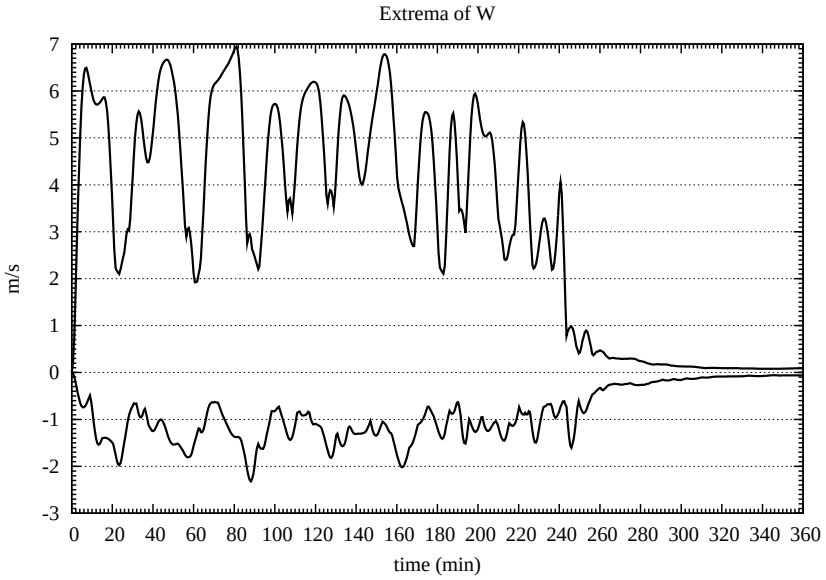

Figure 5.6: Time evolution of the maximum up- and downdraft (m/s) during the assimilation experiment in conditions conducive to anomalous propagation of the radar beam. Positive values denote updrafts, negative values downdrafts. The forcing is applied during 4 hours.

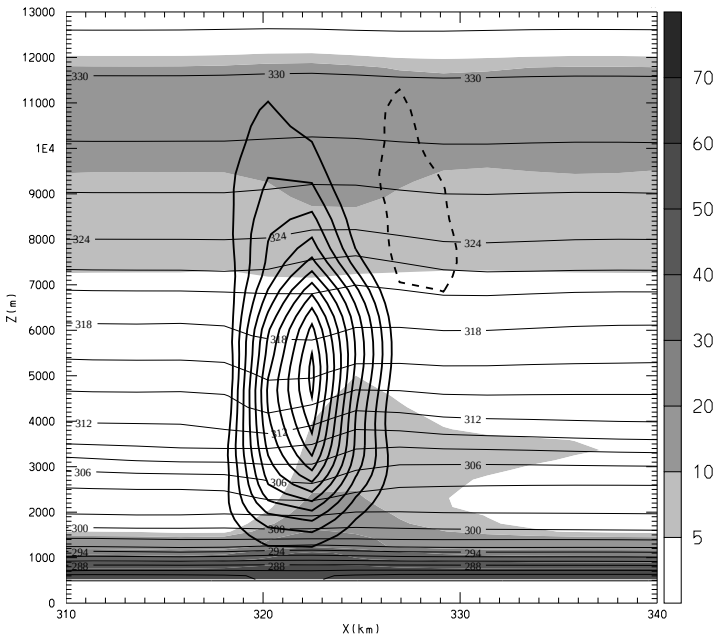

Figure 5.7: Vertical cross-section through maximum updraft of the anaprop experiment at 2h into simulation time. Displayed are RH (in %, shaded), potential temperature (2K contour interval, thin lines) and vertical velocity (0.5 m/s contour interval, bold lines, solid updrafts, dashed downdrafts).

in time. In Switzerland, conditions conducive to anomalous propagation are characterized by very stable conditions and often occur in concomittance with low-stratus, in which often very dry upper-level air tops the planetary boundary layer and the thermal inversion, thus giving rise to strong vertical refractivity gradients. Consequently, assimilating such clutter signals does not usually result in precipitation amplification, due to the absence of convective instability and sufficient moisture. However, the LHN forces the model in trying to match the model precipitation with the input signal. As the model does not produce precipitation the forcing is continued and may yield significant vertical circulations throughout the troposphere. Values for up- downdrafts can reach 7 m/s and −2 m/s, respectively (Fig. 5.6). This spurious circulation may distort the dynamical fields locally and interact adversely with the mesoscale flow. In particular, substantial vertical mixing of the local model atmosphere can take place. Fig. 5.7 illustrates how more humid air of the boundary layer is generously mixed into the dryer air of the free troposphere. This effect would be undesired, for instance, in the context of air pollution modelling, as critical pollution episodes are usually tied to strong inversions. However, this issue was not pursued further in this study.

5.4 Summary and discussion

In this study the sensitivity of the Latent Heat Nudging (LHN) scheme to non-rain echoes was investigated by means of idealised experimentation with synthetic and real radar data. It constitutes one part of an effort to judge the LHN's aptness as an efficient and economic scheme for operational high-resolution rainfall assimilation. Leuenberger and Rossa (2005a) described that the scheme is able to reproduce an idealised supercell in terms of dynamical structure and correct rainfall amount, while it was found to exhibit a distinct sensitivity to errors in the observations where errors in position and structure proved to be more serious than amplitude errors, while Leuenberger and Rossa (2005b) successfully applied LHN for the assimilation of two cases of severe convection. The main findings of this study are:

- non-rain, or clutter, echoes as small as one pixel can trigger the release of convective instabilities when forced by the LHN scheme;
- the resulting precipitation can be large compared to the original signal, i.e. factors 3 up to 50 have been found for moderate to high value of CAPE;
- the response of the model atmosphere to the forcing is very quick, i.e. on the time scale of convection (less than ten minutes for strong forcing to a couple of hours for moderate forcing);
- large, coherent areas of non-rain echoes pose a more stringent problem;
- filtering the input data can significantly mitigate the problem;
- non-rain echoes resulting from anomalous propagation of the radar beam in a low-stratus case over Switzerland, by virtue of the usually stable and dry conditions associated, are not conducive to error amplification. However, a strong spurious vertical circulation, along with undesired mixing, may be induced and adversely impact the mesoscale circulation.

A limitation of the study is that the impact of non-rain echoes is investigated in isolation. The negative impact found may be less dramatic in situations, when clutter is embedded in real precipitation echoes.

Characterisation of the radar data quality for use in atmospheric data assimilation schemes is very important. It has been shown that errors can, in certain circumstances, be dramatically amplified and cause the QPF to deteriorate. Quality characterisation of radar data could, therefore, include at the pixel level some sort of probability for the signal to be rain in terms of a static clutter map of zero probability of rain and a dynamic estimate of varying amplitude. An assimilation scheme like LHN can include such information into a quality or weighting function as proposed by Jones and Macpherson (1997) and Leuenberger and Rossa (2005b). It is conceivable to make the assimilation of pixels with non-zero probabilities for being spurious conditional on the prevailing atmospheric conditions. For instance, a pixel with a 50% probability of being real rain would be assimilated in stable to neutral environments, while rejected in highly unstable situations. The dialog between radar data producer and users is absolutely vital in this context.

Chapter 6

Further Remarks

6.1 Synthesis of the results

In this study, the potential of the Latent Heat Nudging rainfall assimilation scheme on the convective scale has been explored. Experiments with simulated and radar-derived rainfall from severe convective systems have been carried out within an operational NWP model in a meso-γ scale configuration, similar to that which will be deployed in the near future. Further, the sensitivity of the LHN scheme to non-rain echoes in the radar observations has been addressed. The variety of findings are summarised and discussed at the end of the corresponding chapters 3, 4 and 5. Here, the main results are assembled and future perspectives are outlined.

- The LHN technique shows potential when applied to convective events, in that it is able to introduce precipitation into the model in close agreement with the observations within the time scale of convection, i.e. several tens of minutes.

- LHN is found to be able to provide the trigger for convection at the right position. In cases where the model does not develop mesoscale disturbances that lead to the onset of convection, the radar data assimilated with LHN can be of significant value and a positive impact can be observed during the whole lifetime of a convective storm.

- A generally realistic response of the model dynamics to the precipitation forcing is found during the assimilation period. In the idealised experiments dynamical and thermodynamical model fields show close resemblance to the reference simulation after an initial transient period of some tens of minutes, whereas in the real cases realistic low-level flow features, such as gust fronts and cold-pools can be introduced. This result points to the potential of LHN to produce high-resolution dynamically consistent analyses superior to those where only conventional observations are assimilated.

- The performance of free precipitation forecasts is found to strongly vary from case to case. The storm environment appears to play an important role in the evolution of the convection once the LHN forcing is stopped. In a perfect environment the idealised supercell storm follows very closely the reference storm, while in a case study where the environment exhibits low instability the storm ceases within

three hours. This result confirms findings of previous studies where the storm environment, in particular the humidity, was found to be of major importance for the development and evolution of convection (e.g. Ducrocq et al., 2002; Lascaux et al., 2004). However, not only does a lack of instability and low-level moisture prevent the convection from developing, also too much instability and an excess of moisture in the environment can render the precipitation forecast inaccurate, both in amplitude and position.

- The quality of the rainfall observations is important. The LHN scheme is found to be sensitive to the amplitude of the target precipitation in that it produces too cold and overestimated an outflow during the assimilation period when using rainfall observations with a positive bias (factor 3). Dividing the observations by a factor 3, results in an improvement of the simulated low-level temperatures, and, to a lesser extent, in a reduction of the error in strength and position of the outflow. A high sensitivity to the observation insertion frequency is found in the idealised experiments, pointing to the need of high update rates for the radar observations, particularly for cases with high propagation velocities.

- Synthetic non-rain echoes as small as one model pixel can be significantly amplified on a time scale of a few minutes to a couple of hours when assimilated into unstable atmospheres. Non-rain echoes resulting from anomalous propagation of the radar beam in a low-stratus case over Switzerland, by virtue of the usually stable and dry conditions associated, are not conducive to error amplification. However, a strong spurious vertical circulation, along with undesired mixing, may be induced and adversely impact the mesoscale circulation.

6.2 Future perspectives

The results of this study are not comprehensive but can be viewed as a first step towards the assessment of the LHN's suitability on the meso-γ scale. One limiting aspect is that the model used in this study does not account for the advection of precipitation. While this is justified for grid-spacings larger than about 10 km it can limit the skill of QPF on smaller scales. The advection of precipitation contrasts with one of the approximations used in the LHN scheme, i.e. that the vertically integrated latent heating is proportional to the surface rain rate at each grid point. There are indications that this can lead to problems when using the LHN scheme together with the advection of precipitation (Klink, 2004). This point will need attention in future developments of the scheme. It would be desirable to insert the latent heating at places where it is actually released. As the main contribution to latent heating comes from the phase transition from water vapour to cloud water, other remote sensing observations e.g. from satellites could help to specify its horizontal distribution.

A direct comparison of the LHN with other, more sophisticated but also more expensive assimilation schemes such as 4D-Var on a common case study would be needed in order to estimate the benefit of the schemes relative to their computational expense.

As the initiation and the evolution of convection depends heavily on its surrounding environment, efforts for an improved three-dimensional representation of moisture and temperature will be crucial for future improvements of QPF. Probabilistic approaches using ensemble methods, where a set of disturbed observations are assimilated, possibly

using model versions with different settings of physical parametrizations, are hoped to help specifying the uncertainty in the synoptic and mesoscale environment. This idea has already been followed in the Ensemble Kalman Filter method, but could be implemented using any assimilation scheme (e.g. Ensemble Nudging). Moreover, the assimilation of surface variables, such as temperature, humidity and wind, have proven to be helpful in simulating the initiation of convection (Ducrocq et al., 2000, 2002) since its location and strength are largely governed by near-surface dynamical and thermodynamical conditions. Doppler radial winds as a complement to reflectivity could also help in determining the fine-scale flow in the vicinity of precipitating systems. Also, the distribution of external parameters such as soil moisture appeared to be important in some cases (Bernardet et al., 2000; Cheng and Cotton, 2004). The correct specification of the soil moisture distribution is a largely unsolved problem and should receive more attention in the future.

The success of QPF is not only dependent on a proper specification of the atmospheric initial conditions. The skill of QPF can be affected by model components other than explicit microphysical parametrisations (e.g. the treatment of graupel and hail) (e.g. Richard et al., 2003) or boundary layer parametrisation schemes and numerical diffusion (Zängl, 2004a). Past experience has shown that improvements in NWP could only be achieved with a concerted effort in improving models, data assimilation methods and observing systems (Simmons and Hollingsworth, 2002). Field campaigns like the Mesoscale Alpine Programm (MAP) (Bougeault et al., 2001) or the International H_2O Project (IHOP) (Weckwerth et al., 2004) provide invaluable observation data sets to validate models and test data assimilation schemes. Future assimilation experiments should be conducted using such data sets.

6.3 Suitability and recommendation for operational use

The LHN scheme is planned to be employed operationally on the convective scale in the future at at least three European weather services, namely the Metoffice (UK), DWD (Germany) and MeteoSwiss (Switzerland). Extended tests and further developments of the scheme are under way to achieve that goal. The following recommendations based on the results of this study can be formulated:

- The LHN scheme has potential on the convective scale and deserves further attention.
- Extended tests and tuning of the scheme are necessary, particularly together with the advection of precipitation and on a larger set of cases including different weather situations.
- A strict quality control of the radar data, with particular respect to ground clutter and anaprop signals are important to prevent the LHN scheme from introducing spurious convection in unstable situations or strong vertical circulations in stable situations. The disadvantage of losing real rain information is judged to be less important than the negative impact of non-rain echoes.
- Efforts in the improvements of QPF should not focus to the assimilation of radar rainfall alone, but should include the assimilation of all available observations to

improve the environment of the precipitation systems. Near-surface observations as temperature, humidity and wind, as well as radar winds (VAD and radial components) are jugded as most important.

- When testing the LHN scheme on cases dominated by larger scale (e.g. frontal) systems, care has to be taken at the boundaries of the radar domain in order to provide a smooth blending from regions with to regions without observations. The impact of the radar domain size on the LHN performance should be tested, particularly in situations, where the radar domain is smaller than the precipitation systems to be assimilated.

References

Anderson, S. R., 2001: The impact of observations on mesoscale models forecasts of 3-hourly rainfall accumulations – updated results, Metoffice Forecasting Research Technical Report No. 385.

Benedetti, A., P. Lopez, P. Bauer, and E. Moreau, 2004: Experimental use of TRMM precipitation radar observations in 1D+4D-Var assimilation. ECMWF Technical Memorandum No. 448, Tech. rep.

Benoit, R., et al., 2002: The real-time ultrafinescale forecast support during the special observing period of the map. *Bull. Amer. Meteor. Soc.*, **83**, 85–109.

Bernardet, L. R., L. D. Grasso, J. E. Nachamin, C. A. Finley, and W. R. Cotton, 2000: Simulating convective events using a high-resolution mesoscale model. *Journal of Geophysical Research (Atmospheres)*, **105**, 14,963–14,982.

Bougeault, P., P. Binder, A. Buzzi, R. Dirks, J. Kuettner, R. Houze, R. B. Smith, R. Steinacker, and H. Volkert, 2001: The MAP special observing period. *Bull. Amer. Meteor. Soc.*, **82**, 433–462.

Bouttier, F., 2003: The Arome mesoscale project. *Proceedings, ECMWF Seminar on recent developments in data assimilation for atmosphere and ocean*, pp. 433–447.

Brewster, K., 1996: Application of a Bratseth analysis scheme including Doppler radar data. *Preprints, 15th Conference on Weather Analysis and Forecasting, Norfolk, Virginia*, AMS, pp. 92–95.

Brewster, K., 2003: Phase-correcting data assimilation and application to storm-scale numerical weather prediction. Part I: Method description and simulating testing. *Mon. Wea. Rev.*, **131**, 480–492.

Browning, K. A., 1964: Airflow and precipitation trajectories within severe local storms which travel to the right of the winds. *J. Atmos. Sci.*, **21**, 634–639.

Bryan, G. H., J. C. Wyngaard, and J. M. Fritsch, 2003: Resolution requirements for the simulation of deep moist convection. *Mon. Wea. Rev.*, **131**, 2394–2416.

Chang, S. W., and T. R. Holt, 1994: Impact of assimilating SSM/I rainfall rates on numerical prediction of winter cyclones. *Mon. Wea. Rev.*, **122**, 151–164.

Cheng, W. Y. Y., and W. R. Cotton, 2004: Sensitivity of a cloud-resolving simulation of the genesis of a mesoscale convective system to horizontal heterogeneities in soil moisture initialization. *Journal of Hydrometeorology*, **5**, 934–958.

Christidis, N., and B. Macpherson, 2004: Short-period precipitation forecasts: report from the mesoscale 'tiger team' project, Metoffice Forecasting Research Technical Report No. 436.

Cosma, S., E. Richard, and F. Miniscloux, 2002: The role of small-scale orographic features in the spatial distribution of precipiation. *Quart. J. Roy. Meteor. Soc.*, **128**, 75–92.

Cotton, W. R., and R. A. Anthes, 1989: *Storm and Cloud Dynamics*. Academic Press, New York, pp. 883.

Daley, R., 1991: *Atmospheric Data Analysis*. Cambridge University Press, pp. 456.

Davies, H. C., 1976: A lateral boundary formulation for multi-level prediction models. *Quart. J. Roy. Meteor. Soc.*, **102**, 405–418.

Davolio, S., and A. Buzzi, 2004: A nudging scheme for the assimilation of precipitation data into a mesoscale model. *Weather and Forecasting*, **19**, 855–871.

Doms, G., and J. Förstner, 2004: Development of a kilometer-scale NWP-system: LMK, COSMO Newsletter, No. 4, available from http://www.cosmo-model.org.

Doms, G., and U. Schättler, 2002: A description of the nonhydrostatic regional model LM: Part I: Dynamics and numerics, available from http://cosmo-model.org.

Doms, G., J. Förstner, E. Heise, H.-J. Herzog, M. Raschendorfer, R. Schrodin, T. Reinhardt, and G. Vogel, 2004: A description of the nonhydrostatic regional model LM: Part II: Physical parametrization, available from http://cosmo-model.org.

Dowell, D. C., F. Zhang, L. Wicker, C. Snyder, and A. Crook, 2004: Wind and temperature retrievals in the 17 may 1981 Arcadia, Oklahoma, supercell: Ensemble Kalman Filter experiments. *Mon. Wea. Rev.*, **132**, 1982–2005.

Ducrocq, V., J.-P. Lafore, J. Redelsberger, and F. Orain, 2000: Initialization of a fine-scale model for convective-system prediction: A case study. *Quart. J. Roy. Meteor. Soc.*, **126**, 3041–3065.

Ducrocq, V., D. Ricard, J.-P. Lafore, and F. Orain, 2002: Storm-scale numerical rainfall prediction for five precipitating events over France: On the importance of the initial humidity field. *Weather and Forecasting*, **17**, 1236–1256.

Ebert, E. E., U. Damrath, W. Wergen, and M. E. Baldwin, 2003: The WGNE assessment of short-term quantitative precipitation forecasts. *Bull. Amer. Meteor. Soc.*, **84**, 481–492.

Emanuel, K., 1994: *Atmospheric Convection*. Oxford University Press, pp. 580.

Evensen, G., 1994: Sequential data assimilation with a nonlinear quasi-geostrophic model using Monte Carlo methods to forecast error statistics. *Journal of Geophysical Research (Atmospheres)*, **99**, 10,143–10,162.

Falkovich, A., E. Kalnay, S. Lord, and M. B. Mathur, 2000: A new method of observed rainfall assimilation in forecast models. *J. of Appl. Meteor.*, **39**, 1282–1298.

Fiorino, M., and T. T. Warner, 1981: Incorporating surface winds and rainfall rates into the initialization of a mesoscale hurricane model. *Mon. Wea. Rev.*, **109**, 1915–1929.

Fritsch, J. M., and R. E. Carbone, 2004: Improving quantitative precipitation forecasts in the warm season: A USWRP research and development strategy. *Bull. Amer. Meteor. Soc.*, **85**, 955–965.

Gal-Chen, T., 1978: A method for the initialization of the anelastic equations: implications for matching models with observations. *Mon. Wea. Rev.*, **106**, 587–606.

Gal-Chen, T., and C.-J. Sommerville, 1975: On the use of a coordinate transformation for the solution of the Navier-Stokes equations. *Journal of Computational Physics*, **17**, 209–228.

Gassmann, A., 2004: An improved two-time-level split-explicit integration scheme for non-hydrostatic compressible models, accepted by *Meteorology and Atmospheric Physics*.

Germann, U., and J. Joss, 2001: Variograms of radar reflectivity to describe the spatial continuity of Alpine precipitation. *J. of Appl. Meteor.*, **40**, 1042–1059.

Germann, U., and J. Joss, 2004: Operational measurement of precipitation in mountainous terrain. *Weather Radar. Principles and Advanced Applications*, P. Meischner, Ed., Springer Verlag, pp. 52–75.

Germann, U., G. Galli, M. Boscacci, M. Bolliger, and M. Gabella, 2004: Quantitative precipitation estimation in the Alps: Where do we stand? *ERAD Publication Series Vol 2*, Copernicus GmbH, pp. 2–6.

Guo, Y.-R., Y.-H. Kuo, J. Dudhia, D. Parsons, and C. Rocken, 2000: Four-dimensional variational data assimilation of heterogeneous mesoscale observations for a strong convective case. *Mon. Wea. Rev.*, **128**, 619–643.

Haase, G., S. Crewell, C. Simmer, and W. Wergen, 2000: Assimilation of radar data in mesoscale models: Physical initialization and latent heat nudging. *Phys. Chem. Earth (B)*, **25**, 1237–1242.

Holm, E., E. Andresson, A. Beljaars, P. Lopez, J.-F. Mahfouf, A. Simmons, and J.-N. Thépaut, 2002: Assimilation and modelling of the hydrological cycle: ECMWF's status and plans, ECMWF Technical Memorandum No. 383.

Holton, J. R., 1992: *An introduction to dynamical meteorology*. Academic Press, New York, pp. 507.

Houze, R. A., W. Schmid, R. G. Fovell, and H. H. Schiesser, 1993: Hailstorms in Switzerland - left movers, right movers, and false hooks. *Mon. Wea. Rev.*, **121**, 3345–3370.

Huntrieser, H., 1995: Zur Bildung, Verteilung und Vorhersage von Gewittern in der Schweiz, Ph.D. thesis, Eidgenössische Technische Hochschule ETH, Dissertation Nr. 11020.

Ishikawa, Y., 2002: 'mesoscale analysis.', in: 'Outline of the Operational Numerical Weather Prediction at the Japan Meteorological Agency', JMA, pp. 26-31.

Joliffe, I., and D. B. Stephenson, 2003: *Forecast Verification: A Practitioner's Guide in Atmospheric Science*. John Wiley&Sons, Ltd, pp. 240.

Jones, C. D., and B. Macpherson, 1997: A latent heat nudging scheme for the assimilation of precipitation data into an operational mesoscale model. *Meteorol. Appl.*, **4**, 269–277.

Joss, J., et al., 1998: Operational use of radar for precipitation measurements in Switzerland. Final Report, NRP 31, vdf Hochschulverlag an der ETH Zuerich, 108 pp., ISBN 3 7281 2501 6, Tech. rep.

Kalnay, E., 2003: *Atmospheric Modelling, Data Assimilation and Predictability*. Cambridge University Press, pp. 431.

Klemp, J., 1987: Dynamics of tornadic thunderstorms. *Ann. Rev. Fluid Mech.*, **19**, 369–402.

Klemp, J. B., and R. B. Wilhelmson, 1978: The simulation of three-dimensional convective storm dynamics. *J. Atmos. Sci.*, **35**, 1070–1096.

Klink, S., 2004: personal communication.

Klink, S., and K. Stephan, 2004: Assimilation of radar data in the LM at DWD, COSMO Newsletter, No. 4, available from http://www.cosmo-model.org.

Koistinen, J., D. B. Michelson, H. Hohti, and M. Peura, 2004: Operational measurement of precipitation in cold climates. *Weather Radar. Principles and Advanced Applications*, P. Meischner, Ed., Springer Verlag, pp. 78–114.

Krishnamurti, T. N., J. Xue, H. S. Bedi, K. Ingles, and D. Oosterhof, 1991: Physical initialization for numerical weather prediction over the tropics. *Tellus*, **43AB**, 53–81.

Krishnamurti, T. N., H. S. Bedi, and K. Ingles, 1993: Physical initialization using SSM/I rain rates. *Tellus*, **45 A**, 247–269.

Lascaux, F., E. Richard, C. Keil, and O. Bock, 2004: Impact of the MAP reanalysis on the numerical simulation of the MAP-IOP2a convective system. *Meteorol. Z.*, **13**, 49–54.

Lemon, L. R., and C. A. Doswell, 1979: Severe thunderstorm evolution and mesocyclone structure as related to tornadogenesis. *Mon. Wea. Rev.*, **107**, 1184–1197.

Leuenberger, D., and A. Rossa, 2003: Assimilation of radar information in aLMo, COSMO Newsletter, No. 3, available from http://www.cosmo-model.org.

Leuenberger, D., and A. Rossa, 2005a: Revisiting the latent heat nudging scheme for the rainfall assimilation of a simulated convective storm, submitted to Meteorology and Atmospheric Physics.

Leuenberger, D., and A. Rossa, 2005b: Rainfall assimilation with latent heat nudging on the convective scale: Two case studies., to be submitted to Meteorological Applications.

Lin, Y., P. Ray, and K. W. Johnson, 1993: Initialization of a modeled convective storm using Doppler radar-derived fields. *Mon. Wea. Rev.*, **121**, 2757–2775.

Lin, Y., M. E. Baldwin, K. E. Mitchell, E. Rogers, and G. J. DiMego, 2001: Spring 2001 changes to NCEP ETA analysis and forecast system: Assimilation of observed precipitation data. *Preprints, 18th Conference on Weather Analysis and Forecasting, Ft. Lauderdale, Florida*, p. 4.

Linder, W., W. Schmid, and H. H. Schiesser, 1999: Surface winds and development of thunderstorms along southwestnortheast oriented mountain chains. *Weather and Forecasting*, **14**, 758–770.

Macpherson, B., 2001: Operational experience with assimilation of rainfall data in the Met Office mesoscale model. *Meteorol. Atmos. Phys.*, **76**, 3–8.

Macpherson, B., M. Lindskog, V. Ducrocq, M. Nuret, G. Gregoric, A. Rossa, G. Haase, I. Holleman, and P. P. Alberoni, 2004: Assimilation of radar data in numerical weather prediction (NWP) models. *Weather Radar. Principles and Advanced Applications*, P. Meischner, Ed., Springer Verlag, pp. 255–276.

Macpherson, B., et al., 2001: The operational mesoscale data assimilation system 1999-2001: Implementation of 3DVar and later upgrades, Metoffice Forecasting Research Technical Report No. 374.

Manobianco, J., S. Koch, V. M. Karyampudi, and A. J. Negri, 1994: The impact of assimilating satellite-derived precipitation rates on numerical simulations of the ERICA IOP4 cyclone. *Mon. Wea. Rev.*, **122**, 341–365.

Marécal, V., and J.-F. Mahfouf, 2002: Four-dimensional variational assimilation of total column water vapor in rainy areas. *Mon. Wea. Rev.*, **130**, 43–58.

Marécal, V., and J.-F. Mahfouf, 2003: Experiments on 4D-Var assimilation of rainfall data using an incremental formulation. *Quart. J. Roy. Meteor. Soc.*, **129**, 3137–3160.

Mass, C. F., D. Ovens, K. Westrick, and B. A. Colle, 2002: Does increasing horizontal resolution produce more skillful forecasts? *Bull. Amer. Meteor. Soc.*, **83**, 407–430.

Mellor, G., and T. Yamada, 1982: Development of a turbulence closure model for geophysical fluid dynamics. *Rev. Geophys. and Space Phys.*, **20**, 851–875.

Michalakes, J., S. Chen, J. Dudhia, L. Hart, J. Klemp, J. Middlecoff, and W. Skamarock, 2001: Development of a next generation regional weather research and forecast model. *Developments in Teracomputing: Proceedings of the ninth ECMWF workshop on the use of high performance computing in meteorology*, World Scientific, Singapore, pp. 269–276.

Michelson, D. B., T. Einfalt, I. Holleman, U. Gjertsen, K. Friedrich, G. Haase, and M. L. A. Jurczyk, 2004: Weather radar data quality in Europe: Quality control and characterization., COST Publication Series, 100 pp. (in press).

Moreau, E., P. Lopez, P. Bauer, A. M. Tompkins, M. Janiskova, and F. Chevallier, 2004: Variational retrieval of temperature and humidity profiles using rain rates versus microwave brightness temperatures. *Quart. J. Roy. Meteor. Soc.*, **130**, 827–852.

Morel, C., and S. Senesi, 2002: A climatology of mesoscale convective systems over Europe using satellite infrared imagery. II: Characteristics of European mesoscale convective systems. *Quart. J. Roy. Meteor. Soc.*, **128**, 1973–1995.

Orlanski, I., 1975: A rational subdivision of scales for atmospheric processes. *Bull. Amer. Meteor. Soc.*, **56**, 527–534.

Park, S. K., 1999: Nonlinearity and predictability of convective rainfall associated with water vapour perturbations in a numerically simulated storm. *Journal of Geophysical Research (Atmospheres)*, **104**, 31,575–31,587.

Park, S. K., and D. Zupanski, 2003: Four-dimensional variational data assimilation for mesoscale and storm-scale applications. *Meteorol. Atmos. Phys.*, **82**, 173–208.

Richard, E., S. Cosma, P. Tabary, J.-P. Pinty, and M. Hagen, 2003: High-resolution numerical simulations of the convective system observed in the Lago Maggiore area on 17 September 1999 (MAP IOP 2a). *Quart. J. Roy. Meteor. Soc.*, **129**, 543–564.

Richardson, L. F., 1922: Weather prediction by numerical process, Cambridge University Press.

Ritter, B., and J.-F. Geleyn, 1992: A comprehensive radiation scheme for numerical weather prediction models with potential applications in climate simulations. *Mon. Wea. Rev.*, **120**, 303–325.

Rogers, R. F., J. M. Fritsch, and W. C. Lambert, 2000: A simple technique for using radar data in the dynamic initialization of a mesoscale model. *Mon. Wea. Rev.*, **128**, 2560–2574.

Rossa, A., 1995: The impact of latent heat release on the dynamics of extratropical cyclogenesis, Ph.D. thesis, Eidgenössische Technische Hochschule ETH, Dissertation Nr. 11039.

Rossa, A., 2000: COST-717: Use of radar observations in hydrological and NWP models. *Phys. Chem. Earth (B)*, **25**, 1221–1224.

Schiesser, H. H., R. A. Houze, and H. Huntrieser, 1995: The mesoscale structure of severe precipitation systems in Switzerland. *Mon. Wea. Rev.*, **123**, 2070–2097.

Schmid, W., H.-H. Schiesser, and B. Bauer-Messmer, 1997: Supercell storms in Switzerland: Case studies and implications for nowcasting severe winds with Doppler radar. *Meteorol. Appl.*, **5**, 49–67.

Schraff, C., and R. Hess, 2003: A description of the nonhydrostatic regional model LM. Part III: Data assimilation, available from http://www.cosmo-model.org.

Seifert, A., 2002: Parametrisierung wolkenmikrophysikalischer Prozesse und Simulation konvektiver Mischwolken, Ph.D. thesis, Universität Karlsruhe.

Shapiro, R., 1975: Linear filtering. *Math. Comp.*, **29**, 1094–1097.

Simmons, A., and A. Hollingsworth, 2002: Some aspects of the improvement in skill of numerical weather prediction. *Quart. J. Roy. Meteor. Soc.*, **128**, 647–677.

Snyder, C., and F. Zhang, 2003: Assimilation of simulated Doppler radar observations with an Ensemble Kalman Filter. *Mon. Wea. Rev.*, **131**, 1663–1677.

Steppeler, J., G. Doms, U. Schättler, H.-W. Bitzer, A. Gassmann, U. Damrath, and G. Gregoric, 2003: Meso-gamma scale forecasts using the nonhydrostatic model LM. *Meteorol. Atmos. Phys.*, **82**, 75–96.

Sun, J., and N. A. Crook, 1997: Dynamical and microphysical retrieval from Doppler radar observations using a cloud model and its adjoint. Part I: Model development and simulated data experiments. *J. Atmos. Sci.*, **54**, 1642–1661.

Sun, J., and N. A. Crook, 1998: Dynamical and microphysical retrieval from Doppler radar observations using a cloud model and its adjoint. Part II: Retrieval experiments of an observed florida convective storm. *J. Atmos. Sci.*, **55**, 835–852.

Talagrand, O., 1997: Assimilation of observations, an introduction. *J. Meteor. Soc. Japan*, **75(1B)**, 191–209.

Tiedke, M., 1989: A comprehensive mass flux scheme for cumulus parametrization in large scale models. *Mon. Wea. Rev.*, **117**, 1779–1799.

Tong, M., and M. Xue, 2004: Ensemble Kalman Filter assimilation of Doppler radar data with a compressible nonhydrostatic model. *Preprints, 16th Conference on Numerical Weather Prediction, Seattle, Washington*, AMS, pp. 1–11.

Walser, A., D. Lüthi, and C. Schär, 2004: Predictability of precipitation in a cloud-resolving model. *Mon. Wea. Rev.*, **132**, 560–577.

Wang, W., and T. T. Warner, 1988: Use of four-dimensional data assimilation by newtonian relaxation and latent-heat forcing to improve a mesoscale-model precipitation forecast: A case study. *Mon. Wea. Rev.*, **116**, 2593–2613.

Weckwerth, T. M., et al., 2004: An overview of the international H_2O project (IHOP. *Bull. Amer. Meteor. Soc.*, **85**, 253–277.

Weisman, M. L., and J. B. Klemp, 1982: The dependence of numerically simulated convective storms on vertical wind shear and buoyancy. *Mon. Wea. Rev.*, **110**, 504–520.

Weisman, M. L., and J. B. Klemp, 1984: The structure and classification of numerically simulated convective storms in directionally varying wind shears. *Mon. Wea. Rev.*, **112**, 2479–2498.

Weisman, M. L., W. C. Skamarock, and J. B. Klemp, 1997: The resolution dependence of explicitly modeled convective systems. *Mon. Wea. Rev.*, **125**, 527–548.

Wilhelmson, R., and J. Klemp, 1978: A numerical study of storm splitting that leads to long-lived storms. *J. Atmos. Sci.*, **35**, 1974–1986.

Wilhelmson, R., and L. Wicker, 2001: Numerical modelling of severe local storms. *Severe Convective Storms*, C. Doswell III, Ed., vol. 28, AMS, pp. 123–166.

Wu, B., J. Verlinde, and J. Z. Sun, 2000: Dynamical and microphysical retrievals from Doppler radar observations of a deep convective cloud. *J. Atmos. Sci.*, **57**, 262–283.

Xue, M., D. Wang, D. Hou, K. Brewster, and K. K. Droegemeier, 1998: Prediction of the 7 May 1995 squall lines over the central US with intermittent data assimilation. *Preprints, 12th Conference on Numerical Weather Prediction, Phoenix, Arizona*, AMS, pp. 191–194.

Zängl, G., 2004a: The sensitivity of simulated orographic precipitation to model components other than cloud microphysics. *Quart. J. Roy. Meteor. Soc.*, **130**, 1857–1875.

Zängl, G., 2004b: Numerical simulations of the 12-13 August 2002 flooding event in eastern Germany. *Quart. J. Roy. Meteor. Soc.*, **130**, 1921–1940.

Zhang, F., C. Snyder, and J. Sun, 2004: Impact of initial estimate and observation availability on convective-scale data assimilation with an Ensemble Kalman Filter. *Mon. Wea. Rev.*, **132**, 1238–1253.

Zhang, J., 1999: Moisture and diabatic initialization based on radar and satellite observations, Ph.D. thesis, University of Oklahoma.

Zou, X., and Y.-H. Kuo, 1996: Rainfall assimilation through an optimal control of initial and boundary conditions in a limited area mesoscale model. *Mon. Wea. Rev.*, **124**, 2859–2882.

Zupanski, D., and F. Mesinger, 1995: Four-dimensional variational data assimilation of precipitation data. *Mon. Wea. Rev.*, **123**, 1112–1127.

Zupanski, D., M. Zupanski, E. Rogers, D. F. Parrish, and D. G. J., 2002: Fine-resolution 4DVAR data assimilation fort the great plains tornado outbreak of 3 May 1999. *Weather and Forecasting*, **17**, 506–525.

Acknowlegments

Writing this thesis was an exciting and demanding experience. Many people contributed to and supported my work in various ways. Here is the place to express my gratitude to the most important ones.

My first thanks address Prof. H. C. Davies for his willingness to accept me as Ph.D. student and to accompany my thesis. I very much appreciated motivating and inspiring discussions with him and admired his wise and kind supervision of my work.

I am deeply grateful to Andrea Rossa. He launched my Ph.D. project, which enabled me to work in the highly interesting interface of Numerical Weather Prediction and radar meteorology, to participate in many conferences and COST-717 meetings all over Europe and get to know numerous interesting people. Moreover, he continuously supported my work in a very positive and motivating way with many stimulating scientific discussions and a careful review of the draft of this thesis. It was with great pleasure that I shared with him three (!) different offices and enjoyed the wonderful diversity of Swiss dialects and the exotic tastes of tea ('secret garden'). Moreover, I was able to profit from numerous guitar lessons. His certainly most spectacular achievement was to nudge me towards buying finest, Goodyear welted shoes.

Many thanks go to Bruce Macpherson for being one of my co-examiners and his interest in my work. I was lucky to profit from his profound expertise and his thorough review of this thesis.

It is a pleasure to thank my MO colleagues for providing a superb working atmosphere and for their help in daily business, namely Marco Arpagaus, Jean-Marie Bettems, Matteo Buzzi, Pirmin Kaufmann, Guy de Morsier, Francis Schubiger, André Walser and Emanuele Zala. Special thanks go to the former and current head of the modelling group, Jean Quiby and Philippe Steiner for their support of my work. Thanks also to the colleagues of MeteoSwiss's NAZ satellite station Heike Kunz, Mark Liniger, Wolfgang Müller and Simon Scherrer.

A very big thank you to Urs Germann who introduced me to the mysteries of radar meteorology and QPE and provided many helpful tools for handling the radar data. I much enjoyed sharing the hotel room with him at several conferences and discussing all night long. Thanks also to Gianmario Galli, Marco Boscacci and Martin Bolliger for their support with the radar data.

All numerical simulations were carried out at the Swiss National Supercomputing Centre (CSCS) in Manno, Switzerland on a NEC SX5 supercomputer. Without the competent and reliable support from the CSCS staff, this work would not have been possible, thank you!

On the way of the COST-717 action I met some nice people, namely Günther Haase (thanks for introducing me to the LHN code!), Christian Keil, Daniel Michelson (I will never forget the very special dinner outside of Dublin!), Magnus Lindskog, Iwan Hollemann and Uta Gjertsen.

I would like to acknowledge many fruitful discussions with the following DWD colleagues: Stefan Klink, Werner Wergen and Christoph Schraff. My thoughts are with Günther Doms, who helped me a lot with the LM model and always showed great interest in my work.

My warmest thanks go to Petra for her love and understanding during the last three years. She never complained when I stayed away in the evening and over many weekends during the last months of writing, all the more it was shortly after our marriage. You are very precious to me.

I am indebted to my parents for giving me a very fine education, for their continued trust in me and for always making me feel at home. Thanks also to my brother Adrian for his cheerful nature and his friendship.

Last but not least a special thanks to all my friends who make life so amazing!

Curriculum Vitae

Daniel Marc Leuenberger
born in Bern, Switzerland, on 13 March 1974
citizen of Bern and Melchnau (BE), Switzerland

Education

09/2001 – 01/2005	PhD Student at the Institute of Atmospheric and Climate Science, ETH Zürich and MeteoSwiss under supervision of Prof. H. C. Davies, and Dr. A. Rossa
10/1997 – 03/2001	Study of Computational Science and Engineering at Dept. Mathematik, ETH Zürich with specialization in the field Atmospheric Science. *Diploma thesis under supervision of Prof. Ch. Schär at Institute of Atmospheric and Climate Science, ETH Zürich* **Dipl. Rech. Wiss. ETH**
09/1995 – 09/1997	Study of Electrical Engineering at Dept. Elektrotechnik, ETH Zürich **Pre-degree in Electrical Engineering**
1989 – 1994	Städt. Gymnasium, Bern-Neufeld **Matura Type C (Majors: Mathematics and Physics)**
1981 – 1989	Primary and secondary school in Ortschwaben and Meikirch (BE)

Professional Training

06/2001 –	Research scientist at MeteoSwiss, Zürich *Implementation of a new vertical coordinate* *Radar data assimilation*
2004 – 2005	Supervision of a diploma thesis
2002	ECMWF Meteorological Training Course "Data Assimilation and use of Satellite Data" (2 weeks)
1999	Assistant at Institute of Atmospheric and Climate Science, ETH Zürich, Software Development (3 Months)

1999	Practical training at MeteoSwiss (1 month)
1999	Assistant at Mesoscale Alpine Programme, Innsbruck (2 weeks)

International Conferences

09/2004	3^{rd} European Conference on Radar Meteorology, Visby, Sweden *Oral Presentation: "Revisiting the Latent Heat Nudging Scheme for the Rainfall Assimilation in Convective Systems"*
04/2004	COST-717 WG3 Meeting, Prague, Czech Republic *Oral Presentation: "Sensitivity of the LHN Scheme to Non-Rain Echoes in the Input Data"*
10/2003	Joint session of 10th SRNWP Meeting and COST-717 WG3 Meeting, Lisbon, Portugal *Oral Presentation: "Assimilation of Radar Information in the Alpine Model of MeteoSwiss"*
09/2003	5th COSMO General Meeting, Langen, Germany *Oral Presentation: "Latent Heat Nudging in aLMo: Experiments with Idealized Supercell Simulations"*
04/2003	LM-User Seminar, Langen, Germany *Oral Presentation: "Assimilation of Radar Observations in aLMo"*
11/2002	2^{nd} European Conference on Radar Meteorology, Delft, Netherlands *Poster Presentation: "Analysis of a severe Convection Case with Latent Heat Nudging"*
09/2001	Fourth SRNWP Workshop on Nonhydrostatic Modelling, Bad Orb, Germany *Poster Presentation: "A new Terrain-Following Vertical Coordinate for High-Resolution NWP Models"*
05/2001	MAP Meeting, Schliersee, Germany *Poster Presentation: "A new Terrain-Following Vertical Coordinate for High-Resolution NWP Models"*
05/1999	Workshop on Computational Sciences and Engineering, Ascona, Switzerland *Oral Presentation: "A numerical model for heat conduction in the soil"*

List of Publications

Leuenberger, D., 2002: The SLEVE Coordinate in LM, COSMO Newsletter, No. 2, available from http://www.cosmo-model.org.

Leuenberger, D., and A. Rossa, 2003: Assimilation of radar information in aLMo, COSMO Newsletter, No. 3, available from http://www.cosmo-model.org.

Leuenberger, D., and A. Rossa, 2004: Revisiting the latent heat nudging scheme for the rainfall assimilation in convective systems. *ERAD Publication Series Vol 2*, Copernicus GmbH, pp. 162–167.

Leuenberger, D., and A. Rossa, 2005a: Revisiting the latent heat nudging scheme for the rainfall assimilation of a simulated convective storm, submitted to Meteorology and Atmospheric Physics.

Leuenberger, D., and A. Rossa, 2005b: Rainfall assimilation with latent heat nudging on the convective scale: Two case studies., to be submitted to Meteorological Applications.

Rossa, A., and D. Leuenberger, 2005: The sensitivity of the LHN scheme to non-rain echoes, to be submitted.

Schär, C., D. Leuenberger, O. Fuhrer, D. Lüthi, and C. Girard, 2002: A new terrain-following vertical coordinate formulation for atmospheric prediction models. *Mon. Wea. Rev.*, **130**, 2459–2480.

Veröffentlichung

MeteoSchweiz

Veröffentlichungen der MeteoSchweiz

Kürzlich erschienen:

70 Müller G und Viatte P: 2005, The Swiss Contribution to the Global Atmosphere Watch Programme – Achievements of the First Decade and Future Prospects, 112pp, 83 Fr.

69 Müller WA: 2004, Analysis and Prediction of the European Winter Climate, 115pp, 34Fr.

68 Bader S: 2004, Das Schweizer Klima im Trend: Temperatur- und Niederschlagsentwicklung seit 1864, 48pp, 18 Fr.

67 Begert M, Seiz G, Schlegel T, Musa M, Baudraz G und Moesch M: 2003, Homogenisierung von Klimamessreihen der Schweiz und Bestimmung der Normwerte 1961-1990, Schlussbericht des Projektes NORM90, 170pp, 40 Fr.

66 Schär Christoph, Binder Peter, Richner Hans (Eds.): 2003, International Conference on Alpine Meteorology and MAP Meeting 2003, Extended Abstracts volumes A and B, 580pp, 100 Fr.

65 Stübi R: 2002, SONDEX / OZEX campaigns of dual ozone sondes flights: Report on the data analysis, 78pp, 27 Fr.

64 Bolliger M: 2002, On the characteristics of heavy precipitation systems observed by Meteosat-6 during the MAP-SOP**,** 116pp, 36 Fr.

63 Favaro G, Jeannet P, Stübi R: 2002, Re-evaluation and trend analysis of the Payerne ozone sounding, 99pp, 33 Fr.

62 Bettems JM: 2001, EUCOS impact study using the limited-area non-hydrostatic NWP model in operational use at MeteoSwiss, 17pp, 12 Fr.

61 Richner H, et al.: 1999, Grundlagen aerologischer Messungen speziell mittels der Schweizer Sonde SRS 400, 140pp, 42 Fr.

60 Gisler O: 1999, Zu r Methodik einer Beschreibung der Entwicklung des linearen Trends der Lufttemperatur über der Schweiz im Zeitabschnitt von 1864 bis 1990**,** 125pp**,** 36 Fr.

59 Bettems J-M**:** 1999, The impact of hypothetical wind profiler networks on numerical weather prediction in the Alpine region**,** 65pp, 25 Fr.

58 Baudenbacher, M: 1997**,** Homogenisierung langer Klimareihen, dargelegt am Beispiel der Lufttemperatur**,** 181pp**,** 50 Fr.

57 Bosshard, W: 1996, Homogenisierung klimatologischer Zeitreihen, dargelegt am Beispiel der relativen Sonnenscheindauer, 136pp, 38 Fr.

56 Schraff, C: 1996, Data Assimilation and Mesoscale Weather Prediction: A Study with a Forecast Model for the Alpine Region, 138pp, 38 Fr.

55 Wolfensberger, H: 1994, Chronik der Totalisatoren, Handbuch zu den Niederschlags-Totalisatoren, 390pp, 78 Fr.

54 Fankhauser, GA: 1993, Einfluss der Witterung auf den Ertrag und die Qualität von Zuckerrübenkulturen, 116pp, 36 Fr.

53 de Montmollin A: 1993, Comparaisons de différentes méthodes de calcul de la température journalière dans leurs influences sur les longues séries d'observations, 144pp, 41 Fr.

52 Brändli J: 1993, Niederschlag, Verdunstung und Wasserbilanz der Station Zürich SMA von 1901-1990, 109pp, 34 Fr.

Frühere *Veröffentlichungen* und *Arbeitsberichte* finden sich unter www.meteoschweiz.ch

Veröffentlichung

MeteoSchweiz

Arbeitsberichte der MeteoSchweiz

Kürzlich erschienen:

209 Schmutz C, Schmuki D, Duding O, Rohling S: 2004, Aeronautical Climatological Information Sion LSGS, 77pp, 25 Fr.

208 Schmuki D, Schmutz C, Rohling S: 2004, Aeronautical Climatological Information Grenchen LSZG, 73pp, 24 Fr.

207 Moesch M, Zelenka A: 2004, Globalstrahlungsmessungen 1981-2000 im ANETZ, 83pp, 26 Fr.

206 Schmutz C, Schmuki D, Rohling S: 2004, Aeronautical Climatological Information St.Gallen LSZR, 78pp, 25 Fr.

205 Schmutz C, Schmuki D, Ambrosetti P, Gaia M, Rohling S: 2004, Aeronautical Climatological Information Lugano LSZA, 81pp, 26 Fr.

204 Schmuki D, Schmutz C, Rohling S: 2004, Aeronautical Climatological Information Bern LSZB, 80pp, 25 Fr.

203 Duding O, Schmuki D, Schmutz C, Rohling S: 2004, Aeronautical Climatological Information Geneva LSGG, 104pp, 31 Fr.

202 Bader S: 2004, Tropische Wirbelstürme – Hurricanes –Typhoons – Cyclones, 40pp, 16 Fr.

201 Schmutz C, Schmuki D, Rohling S: 2004, Aeronautical Climatological Information Zurich LSZH, 110pp, 34 Fr.

200 Bader S: 2004, Die extreme Sommerhitze im aussergewöhnlichen Witterungsjahr 2003, 25pp, 14 Fr.

199 Frei T, Dössegger R, Galli G, Ruffieux D: 2002, Konzept Messsysteme 2010 von MeteoSchweiz, 100pp, 32 Fr.

198 Kaufmann P: 2002, Swiss Model Simulations for Extreme Rainfall Events on the South Side of the Alps, 40pp, 20 Fr.

197 WRC Davos (Ed): 2001**,** IPC - IX, 25.9. - 13.10.2000, Davos, Switzerland**,** 100pp, 32 Fr.

196 Hächler P et al.: 1999**,** Der Föhnfall vom April 1993**,** 139pp **,** 40 Fr.

195 Urfer Ch, Vogt R, 1999, Die Niederschlagsverhältnisse in Basel 1964-1998**,** 43pp**,** 40 Fr.

194 Courvoisier HW: 1998, Statistik der 24-stündigen Starkniederschläge in der Schweiz 1901 – 1996**,** 20pp, 11 Fr.

193 Defila C, Vonderach G: 1998**,** Todesfälle und Wetterlagen in Schaffhausen**,** 72pp**,** 25 Fr.

192 Maurer H: 1997, Frostprognose in der Schweiz: neue Methode mit automatischen Stationen**,** 38pp**,** 16 Fr.

191 Schönbächler M: 1996, Objektive Kontrolle der Textprognose SMA OPKO, 31pp, 14 Fr.

190 Brändli J: 1996, Statistische Auswertungen von täglichen und monatlichen Verdunstungswerten an 22 Standorten der Schweiz**,** 52pp, 19 Fr.

189 Schneiter D: 1994, SMI contribution to ETEX project in 1994, 24 Fr.

188 Fröhlich C: 1996, Internationaler Pyrheliometervergleich Comparison IPC VIII 25 September - 13 October 1995 Results and Symposium, 35 Fr.

187 Calame F: 1996, Evolution de la température de l'air et de la phénologie d'espèces végétales entre 1952 et 1992 dans la région genevoise et sur le Plateau Suisse, 19pp, 11 Fr.

186 Spinedi F, et al.: 1995, Le alluvioni del 1993 sul versante subalpino, 42pp, 20 Fr.

185 Held E: 1995, Radarmessung im Niederschlag und der Einfluss der Orographie, 98pp, 33 Fr.

Frühere *Veröffentlichungen* und *Arbeitsberichte* finden sich unter www.meteoschweiz.ch